

THE EFFECT OF ROCK PROPERTIES ON FRACTURE CONDUCTIVITY IN THE
MARCELLUS SHALE

A Thesis

by

PAOLA ALEJANDRA PEREZ PENA

Submitted to the Office of Graduate and Professional Studies of
Texas A&M University
in partial fulfillment of the requirements for the degree of

MASTER OF SCIENCE

Chair of Committee,	Ding Zhu
Co-Chair of Committee,	A. Daniel Hill
Committee Member,	Fredrick M. Chester
Head of Department,	A. Daniel Hill

December 2015

Major Subject: Petroleum Engineering

Copyright 2015 Paola Alejandra Perez Pena

ABSTRACT

Hydraulic fracturing is a stimulation technique that has made production from unconventional reservoirs such as shale formations economically feasible. This technique creates high conductivity paths that improve the communication between the reservoir and the wellbore. The success of this technique depends on the ability to fracture the rock and to maintain fracture conductivity. Therefore, in order to have a successful treatment, the effect of parameters such as formation properties, type of proppant and proppant concentration on fracture conductivity and fracture creation should be considered.

This work investigates the relationship between fracture conductivity and formation properties for two different locations in the Marcellus shale. Multiple cores from the locations were collected to ensure repeatability in the results. The core samples were fractured parallel and perpendicular to the bedding planes in order to analyze the effect of anisotropy in fracture conductivity. Additionally, compressive triaxial tests were performed to obtain the rock mechanical properties in the elastic region until permanent deformation was reached, and X-ray Diffraction analysis was used to obtain mineralogy composition.

The laboratory results were compared with previous fracture conductivity data and surface roughness data from the same Marcellus shale locations. The findings showed that the anisotropy effect is present for this formation and reflected in the fracture conductivity values, where samples parallel to the bedding plane seem to have

higher Young's Modulus. At proppant monolayer concentration the main mechanism for conductivity loss is proppant embedment, where due to the high localized stress, the rock-proppant interaction goes directly to permanent deformation of the rock. It was also observed that a higher Young's Modulus helps to maintain the fracture width which translates in lower rate of conductivity loss with increasing closure stress. Rock mechanical properties have impact on fracture conductivity. This effect is less pronounced if a multilayer proppant concentration is used, where the proppant pack characteristics become an important parameter in fracture conductivity.

DEDICATION

I would like to dedicate this work to my parents who have showed me the importance of education and persistence, and my grandparents who have been my motivation for any new step in my career.

ACKNOWLEDGEMENTS

I would like to express my gratitude to my advisers Dr. Ding Zhu and Dr. Daniel Hill for their guidance and support throughout the course of this research. I would also like to thank Dr. Fred Chester for his guidance and for accepting to be part of my graduate committee.

I would also like to thank Tim Jansen and Clotilde Chen for sharing their knowledge and experiences with the triaxial test apparatus. Thanks also go to Mark McGinley, Dante Guerra, Ashley Knorr, Jesse Guerra and Omar Enriquez for all the help and discussions we had. My sincere appreciations to John Maldonado, the facilities team, and IT group at the Department of Petroleum Engineering for their technical support while doing this research work, and also W.D. Von Gonten Laboratories for their help in the experimental part of this work.

I also want to extend my gratitude to the RPSEA for their financial support, and Baker Hughes Incorporated for supporting economically my graduate studies through the “Paula Erazo-Gonzalez” fellowship which was very helpful.

Finally, I would like to thank all my friends, especially Emanuel Ozuna for providing distraction and support when I needed it.

NOMENCLATURE

A	Area (mm ² , in ²)
$Bed - perp.$	Bed-perpendicular
$Bed - pl.$	Bed-parallel
BI	Brittleness Index (-)
E	Young's Modulus (psi or MPa)
E_B	Young's Modulus normalized (-)
F	Force (kN or lbf)
$k_f w_f$	Fracture Conductivity (md-ft)
l	Initial length (mm or in)
LVDT	Linear Variable Differential Transformers
Δl	Change in length (mm or in)
ν	Poisson's ratio
ν_B	Poisson's ratio normalized
σ	Stress (psi or MPa)
σ_1, σ_3	Principal Stresses (psi or MPa)
σ_c	Fracture closure stress (psi)
σ_D	Differential stress (psi or MPa)
ε	Strain (-)
ε_a	Axial Strain (-)
ε_l	Lateral or radial Strain (-)

r	Radius (mm or in)
Δr	Change in radius (mm or in)
λ	Conductivity decline rate (psi^{-1})

TABLE OF CONTENTS

	Page
ABSTRACT	ii
DEDICATION	iv
ACKNOWLEDGEMENTS	v
NOMENCLATURE	vi
TABLE OF CONTENTS	viii
LIST OF FIGURES	x
LIST OF TABLES	xiii
1. INTRODUCTION	1
1.1 Background	1
1.2 Marcellus Shale Overview	3
1.3 Literature Review	7
1.3.1 Fracture conductivity	7
1.3.2 Rock mechanics	9
1.4 Problem Description	13
1.5 Research Objectives	15
1.5.1 Rock mechanical properties and mineralogy composition of Marcellus Shale outcrop	16
1.5.2 Relationship between fracture conductivity and rock mechanics	16
2. LABORATORY APPARATUS AND EXPERIMENTAL PROCEDURE	17
2.1 Description of Laboratory Apparatus	17
2.2 Experimental Procedure	26
2.2.1 Sample collection	26
2.2.2 Sample preparation	28
2.2.3 Rock mechanical properties measurement	33
2.2.4 Elasticity	38
2.2.5 Permanent deformation	42
2.2.6 Anisotropy	44
2.3 X-Ray Diffraction Analysis	44
2.3.1 Sample preparation	45

2.3.2 XRD analysis.....	45
3. EXPERIMENTAL RESULTS AND DISCUSSION.....	47
3.1 Marcellus Shale (Elimsport) Results.....	47
3.1.1 Marcellus shale (Elimsport) rock mechanics	48
3.1.2 Marcellus shale (Elimsport) mineralogical composition	55
3.1.3 Surface roughness	56
3.1.4 Marcellus shale (Elimsport) fracture conductivity.....	57
3.2 Marcellus Shale (Allenwood) Results.....	59
3.2.1 Marcellus shale (Allenwood) rock mechanics	59
3.2.2 Marcellus shale (Allenwood) mineralogical composition	66
3.2.3 Surface roughness	67
3.2.4 Marcellus shale (Elimsport) fracture conductivity.....	68
3.3 Effect of Rock Properties on Fracture Conductivity	69
3.4 Effect of Rock Properties on Fracture Conductivity Loss	82
3.5 Mechanical Anisotropy	89
4. CONCLUSIONS AND RECOMMENDATIONS.....	91
4.1 Conclusions	91
4.2 Recommendations	92
REFERENCES.....	94
APPENDIX A	103
APPENDIX B	115

LIST OF FIGURES

	Page
Figure 1: Location of the Devonian Marcellus shale and the Mississippian Barnett shale (U.S Department of Energy, 2011).....	4
Figure 2: The Marcellus formation stratigraphy (modified from Lash and Engelder, 2011).....	5
Figure 3: Schematic of layered shale model parallel and perpendicular to the bedding plane (Sone, 2013).....	11
Figure 4: Fracture conductivity at 0.1lb/ft ² proppant concentration (Fredd, 2001)	14
Figure 5: Schematic of the basic components of triaxial test apparatus	19
Figure 6: Experimental set up for the GCTS RTX-1500 system	19
Figure 7: Triaxial cell photography.....	20
Figure 8: Top part of the triaxial cell	21
Figure 9: Cell pressure cabinet front (left) and oil reservoir (Right)	22
Figure 10: Sample ready to be tested (LVDT position can be seen).....	23
Figure 11: Metal supports for LVDT's	24
Figure 12: LVDT circumferential device.....	25
Figure 13: Location of Marcellus shale samples outcrop (Modified from US Geological Survey, 2011)	27
Figure 14: Research group at Elimспорт Quarry (McGinley, 2015)	28
Figure 15: Experimental set up to check cylindrical surface (ASTM, 2008)	31
Figure 16: System of stresses in a conventional triaxial test (Paterson and Wong, 2005).....	40
Figure 17: Different definitions of Young's modulus based on the stress-strain curve (Fjaer et. al, 2008).....	41
Figure 18: Stress-Strain diagram showing mechanics of brittle fracture (Undul et. al, 2015) Modified from Bieniawski (1997).....	43

Figure 19: Agate mortar and sieved used to get Marcellus powder	45
Figure 20: Core sample orientation	48
Figure 21: Stress-strain curve for a bed-perpendicular sample from ElimSPORT location	49
Figure 22: Stress-strain curve for a bed-parallel sample from ElimSPORT location	50
Figure 23: Radial-axial strain curve for a bed-perpendicular sample from ElimSPORT location	51
Figure 24: Radial-axial strain curve for a bed-parallel sample from ElimSPORT location.	52
Figure 25: Stress-strain curve for a bed-perpendicular sample from ElimSPORT location	53
Figure 26: Mineralogy composition ElimSPORT samples	55
Figure 27: Fracture surface of ElimSPORT bed-perpendicular sample	56
Figure 28: Fracture surface of ElimSPORT bed-parallel sample	57
Figure 29: Summary of the average conductivity behavior for ElimSPORT samples	59
Figure 30: ElimSPORT core with a calcite vein	60
Figure 31: Stress-strain curve for a bed-perpendicular sample from Allenwood location	61
Figure 32: Stress-strain curve for a bed-parallel sample from Allenwood location	61
Figure 33: Radial-axial strain curve for a bed-perpendicular sample from Allenwood location	62
Figure 34: Radial-axial strain curve for a bed-parallel sample from Allenwood location	63
Figure 35: Stress-strain curve for a bed-perpendicular sample from Allenwood location	64
Figure 36: Mineralogy composition Allenwood samples	66
Figure 37: Fracture surface of Allenwood bed-perpendicular sample	67
Figure 38: Fracture surface of Allenwood bed-parallel sample	67
Figure 39: Summary of the average conductivity behavior for Allenwood samples	69

Figure 40: Average mineralogy composition	71
Figure 41: Sample orientation comparison	72
Figure 42: Average conductivity behavior for Elimsport samples at 0.051 lb/ft ² proppant concentration	74
Figure 43: Summary of the average conductivity behavior at 0.051 lb/ft ² proppant concentration.....	75
Figure 44: Comparison between bed-perpendicular samples.....	77
Figure 45: Embedment for Elimsport samples at 1000 psi. (Left bed-perpendicular sample, right bed-parallel sample	79
Figure 46: Embedment for Allenwood samples at 1000 psi. (Left bed-perpendicular sample, right bed-parallel sample	80
Figure 47: Relationship between Young’s modulus and ultimate compressive strength	81
Figure 48: Elimsport average propped conductivity with the exponential fit.....	83
Figure 49: Allenwood average propped conductivity with the exponential fit.....	83
Figure 50: Relationship between Young’s modulus and conductivity decline curve at 0.051 lb/ft ² proppant	85
Figure 51: Relationship between ultimate compressive strength and conductivity decline rate.....	87

LIST OF TABLES

	Page
Table 1: Summary of Elimsport mechanical properties	54
Table 2: Summary surface roughness Elimsport samples	57
Table 3: Fracture conductivity experiments design	58
Table 4: Summary of Allenwood mechanical properties	65
Table 5: Summary surface roughness Allenwood samples	68
Table 6: Allenwood fracture conductivity experiments design.....	68
Table 7: Summary of mechanical properties.....	70
Table 8: Brittleness index for Elimsport and Allenwood samples.....	78
Table 9: Summary of anisotropy and conductivity decline rate values	89

1. INTRODUCTION

1.1 Background

Hydraulic fracturing is a stimulation technique that has been in the petroleum industry for decades to surpass effects of formation damage and low permeability rocks in order to enhance the reservoir productivity (Economides & Nolte, 2000). This technique has made production from unconventional shale reservoirs economically possible. Shale reservoirs are low permeability reservoirs with significant hydrocarbon resources that could not be extracted without well stimulation.

The main purpose of hydraulic fracturing is to create conductive paths that will improve the communication between the wellbore and the reservoir. During the hydraulic fracture treatment a fluid mix is pumped with a high pressure through the wellbore into the reservoir. If the pressure overcomes the fracture initiation pressure, the rock breaks, creating a fracture that propagates perpendicular to the direction of minimum stress. Proppant are commonly pumped along with the injected fluid to avoid the fracture from closing when pumping is stopped. Proppant can be ceramic spheres for high pressure environments or sand grains which are lower cost and commonly used in the industry. During production, the fluid will flow through the fracture towards the wellbore and the success of a fracture treatment will be measured by fracture conductivity, the capacity of the fluid to flow through the fracture.

Fracture conductivity is defined as the product of fracture permeability and fracture width, and it is directly related to the well productivity (Economides et al.,

2012). Therefore, it is one of the key parameters to design a successful fracture treatment. To enhance well production from these reservoirs, it is necessary to maintain sufficient fracture conductivity through the life of the well. This could be challenging especially in ductile formations (Alramahi et al., 2012) where the proppant is easier to be embedded into the formation rock. Many factors affecting the fracture conductivity have been reported in the literature. Fracture surface roughness, rock mechanical properties and closure stress affect the fracture conductivity when in the absence of proppant (Barton et al., 1985). Additionally, proppant strength, proppant concentration and closure stress affect propped fracture conductivity (Fredd et al., 2000). The analysis of how these parameters affect hydraulic fracturing have been the result of a tried-and-true method used over the past few years for the stimulation of different basins.

Starting in 1997, the first commercial shale gas play, the Barnett shale, moved from cross-linked gelled fracturing fluid with high proppant concentration to slickwater treatment with low proppant concentration. This change was successful due to the decrease in costs and the slight increase in production; slickwater was successful in the Barnett shale, but it may not have the same effect for other shale basin being explored (Matthews et al., 2007). Based on the success of the Barnett Shale, the Eagle Ford shale was also stimulated with slickwater, but the production rate was lower than expected (Mullen et al., 2010). Later analysis found that one of the reasons for this is that the Eagle Ford shale is more ductile (clay-rich limestone and low quartz content) than the Barnett shale, making it harder to keep the fracture open due to proppant embedment. Therefore, higher concentrations of large mesh proppant placed with a hybrid liquid is

used for a successful fracture treatment (Borstmayer et al., 2011). In the case of the Marcellus shale, many of the drilling and stimulation techniques developed in the Barnett were successfully used; in terms of geology and mineralogy these two formations are very similar, which could explain the success of the same technique for both plays. However, a few modifications were made to the Barnett fracture designs for use in the Marcellus: smaller volumes of fresh water, lower proppant concentration, and lower pumping rates (U.S Department of Energy, 2011). The stimulation technique varies for each case, making shale formations unique and difficult to explore and produce.

The cost of a hydraulic fracture treatment is usually very high and it might affect the economic viability of production from a specific formation. Therefore using the optimal stimulation technique becomes imperative. This requires, a full understanding of the relationship between the rock properties and the fracture conductivity behavior, especially, the proppant-rock interaction to keep the fracture open must be studied in depth.

1.2 Marcellus Shale Overview

The Marcellus shale is a Devonian unconventional reservoir that is part of the Hamilton group, and it is located in Pennsylvania, New York, Ohio, West Virginia, Virginia, Maryland, Ontario with a covered area of approximately 75,000 square miles (U.S Department of Energy, 2011). From geological standpoint, the Barnett and the Marcellus are similar. Figure 1 shows the Devonian Marcellus shale and the Barnett

location. The Marcellus has a history of gas production since 1821 when it was considered as source rock for the conventional upper Devonian and Lower Mississippian reservoirs. In 2004 Range Resources started the Marcellus exploration using the production techniques developed for the Barnett shale in Texas. The main production area is located where the formation surpasses 50 feet thickness which it is considered the zone with the best potential with an estimate of 500 Trillion Cubic Feet (tcf) of gas in place and 50 Tcf recoverable; this area is approximately 50,000 square miles and includes Pennsylvania, West Virginia and New York (Engelder and Lash, 2008).



Figure 1: Location of the Devonian Marcellus shale and the Mississippian Barnett shale (U.S Department of Energy, 2011).

The Marcellus shale is a brittle, soft, black, and carbonaceous shale with beds of limestone and carbonate solidifications and a high Pyrite content. This formation was stratigraphically divided into three members originally. The Union Springs, or Lower member, is thinly layered and organic rich with thicknesses between 60ft-150ft in Pennsylvania. The middle member or Cherry Valley which is also considered part of the lower Marcellus, is a skeletal limestone. The Upper member, or the Oatka Creek, is mainly gray shale and with black shale in the lower area; this interval is usually less radioactive than the interval of the Union Spring Member (Engelder and Lash, 2011). The Marcellus shale has been divided stratigraphically in different ways based on location and differentiation of similar geological units. However, in this study, we are going to adopt the stratigraphy classification already mentioned. Figure 2 shows a comparison of the Marcellus formation stratigraphy used in this study with the one proposed by Straeten and Brett (2006).

central and western New York and eastern Ohio			eastern New York			central and eastern Pennsylvania			this study		
Marcellus Subgroup	Oatka Creek Formation	Berne Member	Marcellus Subgroup	Mount Marion Formation	Solsville and Pecksport members	Marcellus Formation	Dalmatia (Fisher Ridge) Member	Marcellus Formation	Oatka Creek Member	Upper	
		Cherry Valley Member Hurley Member			Berne Member						Cherry Valley Member Hurley Member
Union Springs Formation	Bakoven Member		Union Springs Formation	Stony Hollow Member Bakoven Member		Shamokin Member	Marcellus Formation	Union Springs Member	Lower		

Figure 2: The Marcellus formation stratigraphy (modified from Lash and Engelder, 2011)

The potential of the source-rock in the lower Marcellus is outstanding, especially in the southwestern part of Pennsylvania and northern West Virginia. This member has a low clay content, a high quartz content and a total organic carbon (TOC) which ranges between 1-9%. It is characterized by its organic richness, which is the greatest in the area where the member has a thickness of 50 ft (Engelder, 2008a). This makes the Lower Marcellus a good candidate for production. The development of this formation has been very successful because its layers of silicious are brittle, which makes it easy to fracture, and because of its natural fractures or joints (Sumi, 2008). There are two different types of natural fractures present in the Marcellus shale: J1 fractures with a strike of 60-75° and J2 fractures with a strike of 315-345°. These both increase the fracture network through hydraulic fracturing. A typical fracture treatment in the Marcellus includes large amount of slickwater that utilizes 2,500-20,000 bbl water and low proppant (sand) concentration at a pumping rate of 30 to 100 bbl per minute (Gottschling, 2007). This fracture design can vary due to the natural fracture orientation and the heterogeneous nature of the Marcellus shale which means that there could be some differences in the formation properties based on location, layers orientation and properties of the rock. For this reason, the differences in rock characteristics based on bedding planes orientation and their impact in fracture conductivity were the scope of this project.

1.3 Literature Review

1.3.1 Fracture conductivity

To economically produce hydrocarbons from tight reservoirs such as shale, hydraulic fracture treatment is necessary to create the fracture networks in the reservoir, therefore increasing the contact area with the wellbore. Additionally, a high conductive path is necessary for an effective flow from the reservoir to increase well productivity. To create these conductive paths, large volumes of proppants are pumped into the fracture to keep it open. However, during production the reservoir pressure decreases, increasing the probability of proppants embedment into the fracture surface due to the direct interaction between proppant and rock, based on the hardness of the formation. This embedment effect decreases the fracture width and conductivity. Therefore, it is clear that this phenomenon plays an important role in the success of hydraulic fracturing stimulation (Gao, 2012). However, this is not the only factor affecting fracture conductivity; parameters such as closure stress, mineral composition, rock properties, fracture roughness, asperity size, proppant characteristics (strength and size), proppant concentration, fracture displacement and rock-fluid interaction have been studied for years in the industry in order to find the parameters that can improve the production from tight reservoirs (Fredd et al., 2001, Akrad et al., 2011).

There have been many studies related to fracture conductivity and the parameters affecting its performance. Lacy et al. (1997) did experimental research on embedment and fracture conductivity in soft formations. They learned that embedment is affected

mainly by rock type, closure stress, proppant size, strength, concentration and distribution. Penny (1987) studied the conductivity using Ohio sandstone and steel with a 2lb/ft^2 areal concentration of 20/40 sand. He found that proppant embedment was the main factor in conductivity lost. Guo et al. (2008) agrees with these statements; he also found that softer core would have greater proppant embedment than stiffer cores.

Due to the high cost of hydraulic fracture treatment, the industry has put a lot of effort to find a way to low the cost of this technique. Mayerhofer et al. (1998) evaluated the performance of 50 water-fracturing treatments in the Cotton valley and compared with the traditional fracturing treatments. They found that waterfracs performed similar to the traditional method in low permeability reservoirs with a lower cost. Based on these findings, several studies were conducted with low proppant concentration in order to understand the mechanism by which these treatments create conductivity. Fred et al. (2000) did experimental research on Texas Cotton Valley sandstone cores using low proppant concentration of 1lb/ft^2 and 0.1lb/ft^2 and rough surfaces. They found that conductivity can be proppant-dominated or asperity-dominated based on rock properties, proppant strength and proppant concentration. When low concentrations of low-strength proppant are used, the formation properties such as rock mechanics and asperity characteristics control the conductivity. However, if a high strength proppant is used with a high proppant concentration, the effects of formation properties are reduced. The formation of multiple layers of proppant on the fracture is likely to happen even though low proppant concentration is used, due to the poor transport capability of the fluids used in this treatment. Low viscosity liquids are unable to carry proppants deep into the

formation which generates a fracture with a multilayer bed at the bottom (dune) where the proppant pack characteristics will control conductivity, and unpropped fracture conductivity where the formation properties will control conductivity (Warpinski 2009).

1.3.2 Rock mechanics

These fracture treatments with slickwater might not be applicable to every formation because every shale play is unique, and requires a unique stimulation treatment. Even though there have been many studies on fracture treatments with low proppant concentration and water, this might not be successful for every shale. The formation properties should be taken into account in order to understand how the reservoir should be completed. Rickman et al. (2008) explains how the mechanical rock properties and the mineralogy of the formation need to be considered when selecting which fracture treatment to execute. They state that a brittle reservoir is more likely to react well to a hydraulic fracture treatment due to the natural fractures present in this type of rock, they propose that in order to have brittle behavior a high Young moduli and low Poisson's ratio are favorable, the former to keep the fracture open and the latter to actually fracture the rock or fail under stress. Additionally, the mineralogy of the rock will help to predict the formation's reaction to different fracture fluids that can deteriorate the properties of the rock. This can be different from well to well in the same shale formation. Hot et al. (2011) discuss how fracturing fluids can increase the plasticity of shale formations which lead to a more difficult fracture job. They also suggest that several factors such as confining pressure, temperature, shale anisotropy and

pore pressure can change the brittleness of a rock. Achalpurkar et al. (2013) agrees with Hot et al. (2011) about the factors that affect the proper selection of the stimulation fluids. They state that rock mechanics properties should be carefully evaluated, taking into account shale anisotropy to sample the cores in the correct orientation, in order to test a true representative sample, and in that way select the best fracturing fluids.

Sone et al. (2013) performed experimental research on the mechanical properties of shale-gas reservoir rocks. They studied the static and dynamic elastic properties from the Barnett, Haynesville, Eagle Ford and Fort St. John shale through laboratory experiments where samples were cut perpendicular and parallel to the bedding planes in order to take account of the mechanical anisotropy. They found that elastic properties fluctuate considerably between reservoirs and also inside the reservoir due to material composition and fabric of the rock. They confirmed that there is a significant anisotropic behavior based on sample orientation where the samples parallel to the bedding plane were stiffer than the perpendicular to the bedding planes. A similar behavior was seen in the Poisson's ratio where parallel samples presented higher values consistently; to explain this phenomenon, they use a simple model which represents anisotropic behavior through a rock of soft and stiff layers, where "soft" represents clay and organic matter, and "stiff" represents the other components but mainly quartz and calcite (Figure 3). They also found that the degree of anisotropy in this rock is correlated with clay and organic content, as well as with rock fabric. Cui et al. (2014) agrees with Sone et al. that samples parallel to the bedding plane are stiffer than samples perpendicular to the bedding plane. They did an experimental research using 31 cores from the Lower

Nordegg Member in the Western Canada Sedimentary Basin. Their work also included some simulations. They found that the elastic and plastic properties are difficult to correlate with depth, organic content or clay content. They also found based on the mechanical properties of the rocks and some simulations that in a rock-proppant interaction all the sand embedment is accommodated by plastic deformation which is the behavior dominating the deformation in the rock fracture face.

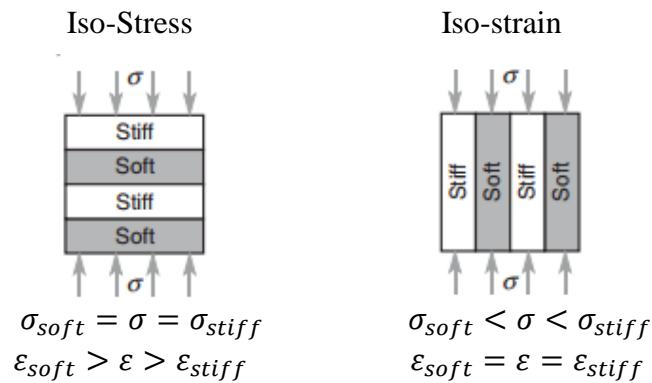


Figure 3: Schematic of layered shale model parallel and perpendicular to the bedding plane (Sone, 2013)

With the increase in hydraulic fracturing as a stimulation method, the industry has emphasized the efforts to understand the interaction between proppant and rock and its relationship with fracture conductivity with the goal of finding a way to predict fracture conductivity behavior. Chen et al. (2015) tried to mimic the interaction between the rock matrix and the proppant during production with a triaxial test and Marcellus cores in different orientations. They observed that the bedding plane direction has significant effect on the development of microscopic fractures on the surface that could

potentially increase fracture conductivity; samples parallel to the bedding plane had a higher chance to develop fractures. Alramahi et al (2012) studied the proppant embedment and its effect on hydraulic fracturing based on laboratory experiments where rock mineralogy and mechanical properties were taken into account. They observed that samples with high clay content usually have a low young modulus which is associated to high proppant embedment and conductivity loss. Based on the experiments, they were able to develop a correlation between Young modulus and proppant embedment (mm) at a specific stress, which could lead to prediction for the fracture conductivity loss. Zhang et al. (2013) studied the fracture conductivity behavior of unpropped and propped fractures for natural and artificially induced fractures in Barnett samples. They explain that the conductivity loss in unpropped fractures consist of plastic mechanical compaction of the matrix layers and plastic deformation of the asperities. They found that unpropped fracture conductivity correlates with shale brittleness index and that with a higher proppant concentration, the rock properties' influence in fracture conductivity decreases. Guzek (2014) and Briggs (2014) did experimental research on fracture conductivity of Eagle ford and Fayetteville shale respectively. They agree with Zhang et al. that with high proppant concentration, the rock properties are less important. Jansen et al. (2015) investigated the relationship between rock properties in unpropped and propped fracture conductivity. They found that for unpropped fractures, the fracture surface roughness controls the magnitude of the conductivity and the Young's modulus controls the ratio of conductivity lost: the higher the Young's modulus the smaller the conductivity lost. They also found that this phenomenon is observed as well in proppant

monolayer concentrations for formations with a Young's moduli smaller than 2 Mpsi. They agreed with the previous studies that at higher proppant concentrations the conductivity will be controlled by the proppant pack characteristics. McGinley (2015) conducted experimental research on fracture conductivity at different proppant loading levels for two different locations in the Marcellus shale (Allenwood and Elimsport). For each location samples parallel and perpendicular to the bedding planes were used. They found that vertical samples display higher conductivity values than the horizontal samples. These differences can be attributed to the anisotropy of the samples. He also states that propped fracture conductivity is not dependent on fracture surface roughness and the anisotropy can be related to the differences in fracture conductivity with different samples orientation. They observed that the increase in proppant concentration increase conductivity values at high closure stress.

1.4 Problem Description

The most popular stimulation technique to produce from the shale plays in North America is known as hydraulic fracturing. This technique makes the production of tight reservoirs economically viable, and it is a crucial part of the development of any well. Many efforts have been put to optimize the fracture propagation and fracture conductivity during the stimulation process. In order to maximize fracture propagation, companies target brittle zones which are characterized by high Young's moduli and low Poisson's ratios which indicate that the formation is prone to fractures. Once the fracture is open, the fracture conductivity become relevant in the stimulation process; many

studies have shown that fracture conductivity has a significant influence in cumulative production. Therefore, understanding the parameters that control this phenomena could help to optimize production from shale plays.

In low permeability formation, fracture conductivity is created by placing sand or ceramic spheres (proppant) along the fracture to keep it open, which increase the reservoir exposure. Proppant concentration can be modified to maximize fracture conductivity. Many studies have shown that parameters such as proppant concentration, proppant strength, surface roughness and formation properties affect the fracture conductivity. However, the results vary greatly from formation to formation, which indicates that formation properties are likely a relevant parameter controlling fracture conductivity. Figure 4 shows how the fracture conductivity varies with proppant type and surface roughness.

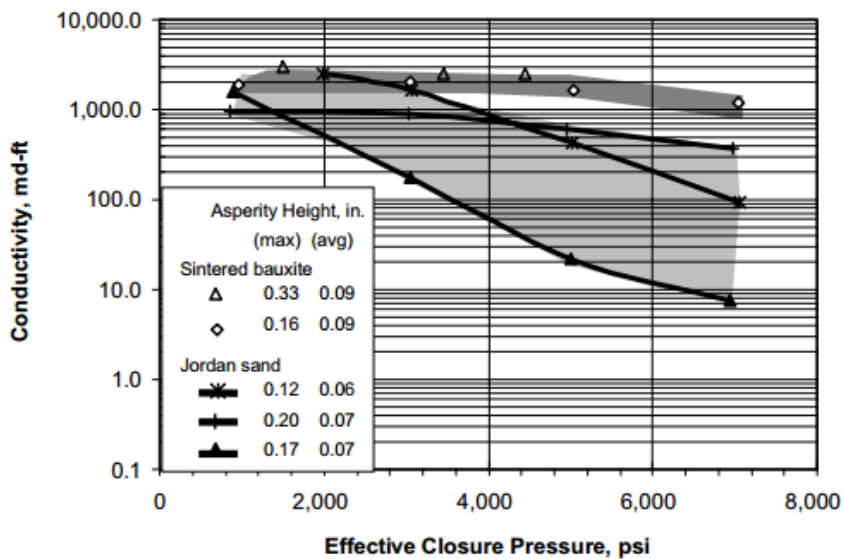


Figure 4: Fracture conductivity at 0.1lb/ft² proppant concentration (Fredd, 2001)

For the figure above, the proppant concentration was kept constant and the type of proppant varied from high-strength ceramic (Sintered bauxite) to low-strength (sand) which is most commonly used. The results from Jordan Sand show a greatly variation in conductivity which was not expected since the conditions were kept constant, this behavior may be related to variation in formation properties and surface roughness, therefore, understanding the role that the formation properties plays in the conductivity could be the key to predict successfully fracture conductivity. This study focuses on the relationship between fracture conductivity of propped fractures, rock mechanical properties and mineralogy for Marcellus shale outcrops; the orientation dependency of the rock properties (anisotropic) is also taken into account in this study.

1.5 Research Objectives

The main purpose of this research is to study the relationship between the fracture conductivity behavior and the corresponding rock mechanical properties of Marcellus shale outcrops, and how the sample orientation (anisotropy) could influence this relationship. In order to investigate the relationship between these two parameters multiple factors were taken into consideration such as Young's modulus, Poisson's ratio, ultimate compressive strength, mineralogy and surface roughness. Each factor is going to be evaluated individually and compared on the fracture conductivity behaviour. Any relationship found during this study will help to better understand and predict fracture

conductivity to optimize production from Marcellus Shale. In order to investigate this relationship, the following objectives were established:

1.5.1 Rock mechanical properties and mineralogy composition of Marcellus Shale outcrop

1. Develop a standard experimental procedure to test rock mechanical properties for outcrop samples using the industry standards ASTM D4543 – 08 (2008) and ASTM D7012 – 14 (2014) for triaxial compression testing as basis.
2. Measure Young's modulus, Poisson's ratio and ultimate compressive strength using the triaxial compression apparatus at different orientations for Marcellus shale outcrops. The cores used for testing should correspond to the fracture conductivity samples.
3. Measure mineralogical composition of the samples using X-ray Diffraction (XRD) and surface roughness for fracture conductivity samples.

1.5.2 Relationship between fracture conductivity and rock mechanics

1. Analyze how the anisotropic affects the rock mechanical properties and the role of inelastic deformation in fracture conductivity.
2. Analyze each parameter measured and its effect on fracture conductivity. Determine if there is a significant relationship with any parameter studied. If there are multiple parameters, determine which one is the controlling parameter for Marcellus shale outcrops.

2. LABORATORY APPARATUS AND EXPERIMENTAL PROCEDURE

This section presents in detail the laboratory apparatus and experimental procedures which include sample preparation and properties measurements used to evaluate the rock samples. Additionally, the considerations made, the parameters that were kept constant through all the experiments and the actions taken to control measurement errors will be discussed.

2.1 Description of Laboratory Apparatus

The American Society for Testing and Materials (ASTM) developed the standards to test the compressive strength and elastic moduli of intact rock cores. This document defines the required laboratory equipment and experimental procedure to test rocks. This study slightly differs from the ASTM D7012-14 standard to characterize the mechanical properties of the Marcellus shale.

The GCTS RTX-1500 Triaxial Rock Testing System was used in this study to measure Young's modulus and Poisson's ratio. This system is specially designed to measure the stress-strain-strength properties of rocks at different confining and pore pressures, which can be controlled through the digital regulators. The system has the flexibility to measure material properties of samples with diameters of 1 inch and 2 inches due to the metal support dimensions restrictions: the length of the sample can vary depending of the user requirements but there is a limit due to the load piston length. The force that can be applied by the piston to the sample has an upper limit of 1500 kN. The hydrostatic pressure that can be applied by the system for confining pressure purposes

has an upper limit of 20,000 psi, which is the same limit for the pore pressure limit that the system can maintain. For the purposes of this research, the samples were not tested to the pressure limits of the system; low confining were used. The pore pressure capabilities were not used at all.

This system meets the requirements and specifications of the International Society of Rock Mechanics for rock triaxial testing. Unlike other apparatus in the industry, the GCTS RTX 1500 has a benefit associated with the deformation instrumentation, which is located internal and directly in contact with the sample, that isolates the deformation of the piston and apparatus from the sample deformation measurements. This deformation system uses two Linear Variable Differential Transformers (LVDTs) to measure axial deformation and one LVDT to measure radial deformation, all with a resolution of 0.001 millimeters.

The GCTS RTX-1500 system consist of the followed components:

- GCTS hydraulic load frame with 1500 kN loading capacity
- GCTS High Pressure Triaxial cell with a 20,000 psi capacity
- Seal piston/platen system to apply axial load
- Two 140 MPa servo-controller pressure intensifier system cabinets
- Internal deformational instrumentation (3 LVDTs)
- Data acquisition system (SCON -2000 Digital System Controller)
- GCTS Hydraulic Power Supply (HPS)
- Data acquisition software GCTS CATS

Figure 5 shows the schematic of the system and its components.

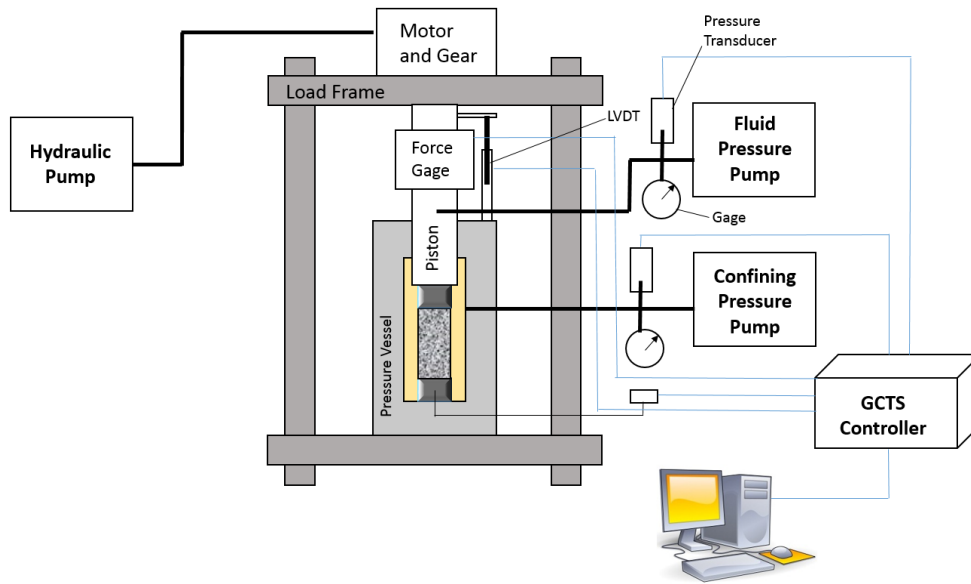


Figure 5: Schematic of the basic components of triaxial test apparatus

The external components of the system can be seen in Figure 6. This figure shows the system positioning in the laboratory.



Figure 6: Experimental set up for the GCTS RTX-1500 system

The triaxial cell is the main component of the system and it is controlled by the hydraulic frame which moves up and down (Figure 7). The base of the triaxial cell has a small cylinder that accommodates the rock sample; around this piece, there are eight connectors for the Linear Variable Differential Transformer (LVDTs). This research uses only three LVDTs. The last part of this cell is the high-pressure seal that is formed between the vessel's wall and the base. This part allows the system to be pressurized up to 20,000 psi. In order to secure the seal, the base and the vessel must be in contact and tightened to each other by the eight steel poles with nuts and washers around the triaxial cell. If the nuts are not tight enough, there can be serious leaks that will appear around the base and will prevent the oil to reach the desired hydrostatic pressure value.



Figure 7: Triaxial cell photography

Figure 8 shows the top part of the triaxial cell, and a circular opening in the center of the vessel with a seal around that allows to pass through the vessel. This hole has a seal to leakages. This pole is in direct contact with the loading piston and the top platen of the sample apparatus. The contact pole has a flat ending at the bottom for a better contact and load transmission with the loading piston and a concave bottom for a better contact with the convex part of the top platen.



Figure 8: Top part of the triaxial cell

Figure 9 shows the cell pressure cabinets that store the external fluids needed to test the rock. This system contains one oil reservoir that holds enough oil to fill up the cell in order to apply confining stress, and one water reservoir to keep enough water to apply pore pressure. For this case, only the oil reservoir will be used. The cabinet uses compressed air at approximately 80 psi to move the oil to the cell and drain it from it. The cabinet has an oil level indicator that shows the oil level in the triaxial cell. It also has two valves that isolate the reservoir from the cell in order to apply cell pressure. This pressure will be provided by the servo-controller intensifier, which is able to maintain the cell pressures up to 20,000 psi. The cell pressure is measured using a pressure

transducer with a resolution of $\pm 0.1\text{MPa}$. It is very important to monitor the closed and opened valves because they will allow the proper performance of the systems and they will avoid accidents due to excess of pressure.



Figure 9: Cell pressure cabinet front (left) and oil reservoir (Right)

The internal components of the system are those in direct contact with the sample, and they are responsible for the deformation measurements. Therefore, the user should be very careful when assembling them. Figure 10 shows all the internal components assembled and ready for testing. The two metal cylindrical supports are the base for the rock sample, which is going to be located in the middle of these supports. The bottom support has a threaded ending so it can be secured to the base of the triaxial cell. It also has a cylindrical stand of 1 inch diameter for rock sample placement. The stand has two channels with different functionalities: the lower channel accommodates

an O-ring for sealing purposes to isolate the rock from the oil, and the upper channel acts as a support for internal instrumentation. The upper support has a convex ending which fits perfectly with the loading bar, and it gives to the system the flexibility to adjust for rock imperfections or shifting. This support has a stand with two channels for the same purpose of the bottom support. Both supports have a circular hole in the center that connects to the water reservoir to apply pore pressure; however, these holes were sealed during the experimental testing done in this study. The Upper support, rock sample and bottom support are sealed by a thin polyolefin heat-shrink wrap to isolate the rock from the pressurized confining oil, to avoid an undesired increase in pore pressure.

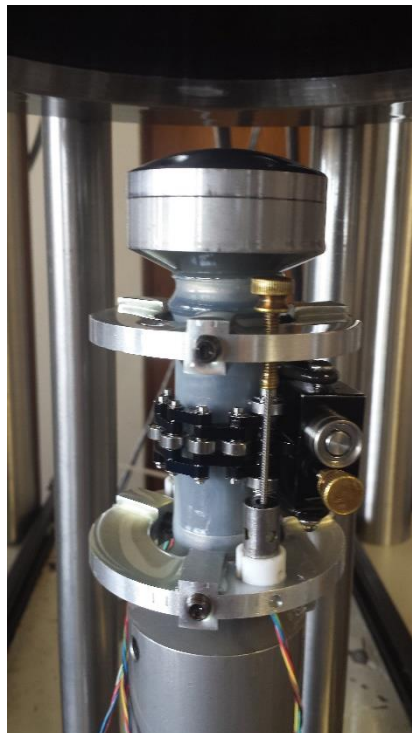


Figure 10: Sample ready to be tested (LVDT position can be seen)

Figure 11 shows the aluminum platens that are the support for the axial LVDTs and its ferromagnetic cores. The upper platen is fixed to the sample through three lateral spring plungers. This platen holds the core and rod that are going to transmit the deformation of the sample. It will also keep the core fixed to the same position, avoiding lateral movements that could affect the reading of the LVDT. The lower platen holds the two LVDTs and keep it in the same position to avoid lateral movements. The positioning of these two platens is important and it needs to be done carefully, making sure that the platens are completely parallel to each other in order to reduce the error associate to the axial deformation measurement. Additionally, each LVDT is located on opposite sides of the rock so that two measurement points can be taken to verify the displacement value.

Each LVDT is able to detect small changes in position related to the magnetic field caused by the movement of the ferromagnetic cores. The resolution of these sensors is 0.001 mm.



Figure 11: Metal supports for LVDT's

Figure 12 shows the third LVDT which is used to measure radial deformations. This sensor is attached to a chain that contain a series of rollers connected between them, and they give the flexibility to wrap the diameter of the sample to capture the radial deformation. One of the chain ending has a mounting block that secures the LVDT and the opposite ending has a mounting block that holds the core and a metal bar that gives stability to the system. The two endings can be held in tension with elastic bands that are flexible enough to not restrict the free movement of the LVDT during deformation. This three LVDT configuration will allow measuring the whole deformation of the sample. The LVDT signal is processed by the data acquisition system GCTS CATS through connectors located in the triaxial cell.

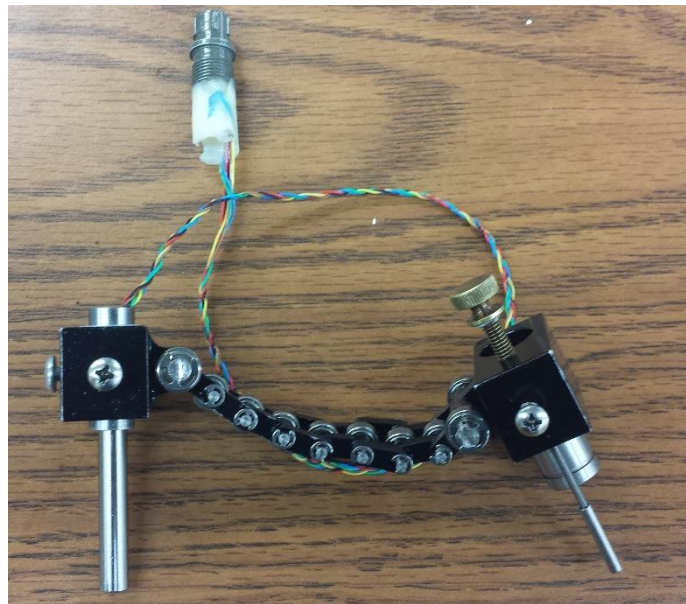


Figure 12: LVDT circumferential device

While running the experiment, it is very important to supervise the sample all times. While the apparatus' control system can abort the test when there is a large cumulative deformation, taking the sample to failure without notice can damage the apparatus, especially those items in contact with the sample. It is also important to keep in mind the maximum pressure values at which the system can operate.

2.2 Experimental Procedure

The experimental procedure used in this work consists of three steps: sample collection, sample preparation, and rock mechanical property measurement. Each step was design to be repeatable for each core in order to get a set of measurements that can be compared in a consistent way across samples from different locations.

2.2.1 Sample collection

The samples used in this research were collected from two different locations in Pennsylvania. The two locations can be seen in Figure 13.

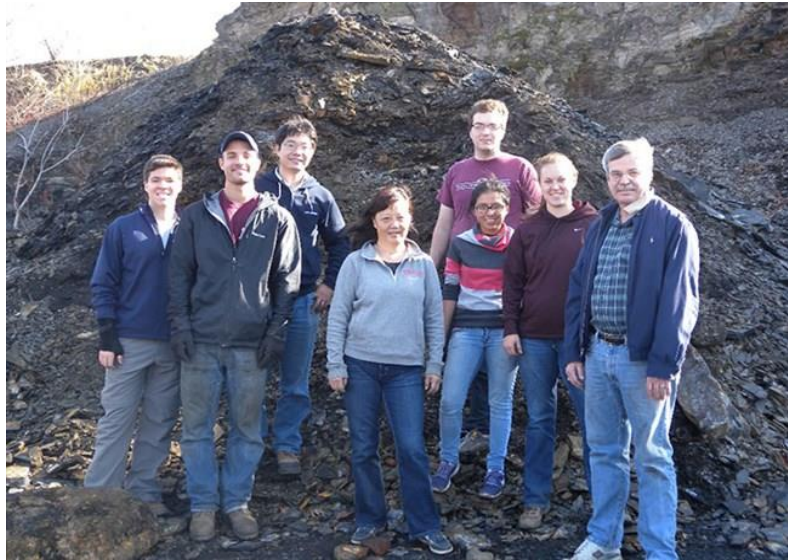


Figure 14: Research group at ElimSPORT Quarry (McGinley, 2015)

The second set of samples was collected from a site in Allenwood, Pennsylvania. These samples were taken from approximately 40 feet depth to obtain “fresh” samples that had not been exposed to atmospheric effect that could cause damage. In this case, the samples were cut from a single large and intact block, instead of multiple blocks like the first set of samples.

2.2.2 Sample preparation

Eighteen cylindrical cores were cut from the two Marcellus shale locations with dimensions of 1 inch diameter and 2 inches length. The core sample size was chosen based on the rock block dimensions and the triaxial compression test apparatus limitation that has only two metal support sets: One for 1 inch diameter core and another one for 2 inches diameter core. Shale mechanical properties are not isotropic. In order to account for this, core samples were cut in two different orientations: Parallel and

perpendicular to the bedding planes. The core samples parallel to the bedding plane were difficult to cut without damaging the sample, some of them were destroyed due to the opening between the layers that form the core. For this reason, less parallel samples were tested. For the conductivity test, the fracture was induced perpendicular and parallel to the bedding plane as well, in order to compare with the cylindrical cores. Additionally, each core sample was cut with a corresponding fracture conductivity sample from the same rock block, in order to best measure the mechanical properties of the fracture conductivity samples. It is impossible to measure the mechanical properties of the fracture conductivity samples directly due to their geometry and the induced fractures. The Elmsport samples were cut from the best rock block available, each pair of samples was obtain from a different block. On the other hand, Allenwood samples were all cut from the same rock block. Keeping the same rock for the conductivity and rock mechanics samples will allow comparing them better, minimizing the error associated with the properties of each set of rocks.

Once the apparatus limitations were identified, the standard procedure for preparing rock core for mechanical testing, defined by ASTM were followed. The ASTM D4543-08 (Standard Practices for Preparing Rock Core as Cylindrical Test Specimens and Verifying Conformance to Dimensional and Shape Tolerances) was used to make sure that every core was within the tolerances required to reduce error associated to the core sample dimension. The ASTM D4543-08 standard delimits the tolerances for the core samples as follows (2008):

- A length-to-diameter ratio (L/D) of 2.0 to 2.5 and a diameter of not less than 1- $\frac{7}{8}$ inches or 47 mm.
- A cylindrical surface generally smooth and free of brusque irregularities, with all the elements straight to within 0.020 inches or 0.508 mm over the full length of the specimen of the core.
- The ends to be cut parallel to each other and at right angles to the longitudinal axis. The end surfaces shall be surface ground or lapped flat to a tolerance not to exceed 0.001 inches.
- The ends should not depart from perpendicularity to the axis of the specimen by more than 0.25°.

The core samples were cut to meet the ASTM standards. However, due to the fragile and limited nature of these samples, meeting those standards was not always possible. This meant that several samples that were close to meeting the tolerances had to be used for testing. Once the core samples were obtained, the straightness of the element on the Cylindrical surface was checked using the assembly in Figure 15. A flat surface, a V-block and a displacement gage assembly were used to make sure that the cylinder surface was free of irregularities.

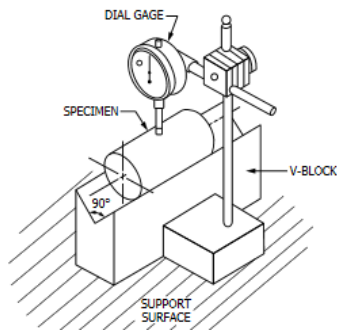


Figure 15: Experimental set up to check cylindrical surface (ASTM, 2008)

Once the core sample has the required dimensions, it is ready to test. However, before putting the core inside the triaxial test apparatus, the sample needs to go through a preparation process. This process is explained below:

1. Measure the cylinder dimensions (Diameter and length). Take three readings of the diameter in the middle of the cylinder while rotating in order to ensure an accurate diameter value.
2. Make sure that the bottom and top metal support have their corresponding O-ring, and are located in the external channel of the support.
3. Place the core sample on the bottom metal support. Make sure that the sample is in the center of the support.
4. Measure and cut a piece of polyolefin heat-shrink tubing, and put it around the core sample. Make sure that the tubing is covering the top and bottom O-rings.
5. Start heating up the heat-shrink tubing from bottom to top using a heat gun. Make sure that the core stays in the center of the metal support and the tubing shrinking is even without creases. Keep heating until the tubing has the same dimension of the sample and stop when it is close to the core sample top.

6. Place the bottom and top LVDT holder ring around the core sample. Make sure that the instrumentation holes are aligned between the top and the bottom holder.
7. Place the top metal support onto the rock sample and continue heat shrinking until the tubing is constricted to the rock and over the top O-ring.
8. Wait for several minutes until the sample cools down and the heat shrink cools down.
9. Place the LVDT top brass components in the top LVDT holder ring.
10. Mount the top LVDT holder ring to the top metal support using the empty channel to position the LVDT holder ring. Tighten the three screws very carefully using the same number of turns to keep the holder ring as centered as possible.
11. Place the circumferential chain gauge on the center of the rock sample and use two springs to keep the two ends together. Make sure that the chain is snug.
12. Place the LVDT detector into the bottom holder ring, and make sure they are snug.
13. Mount the bottom LVDT holder ring to the bottom metal support using the empty channel to position the LVDT holder ring. Tighten the three screws very carefully using the same number of turns to keep the holder ring as centered as possible. Ensure that the bottom and top LVDT components are aligned.
14. Thread the LVDT ferromagnetic core into the brass component.
15. Make final adjustments to the assembly:

- Make sure that the ferromagnetic core is all the way inside the LVDT detector; otherwise the reading will be wrong.
- Make sure that the ferromagnetic core is in the center of the LVDT detector and it can move freely.
- Make sure that the LVDT holder ring are secure and not moving to prevent shifting during the experiment.

16. Screw the core sample assembly into the triaxial testing machine until it is fixed to the base.

17. Connect the LVDT wires to the corresponding ports.

18. Adjust the initial position of the LVDT core, using the top brass screws. Make sure that the axial cores are at the same starting point. The starting value will depend of the type of rock. In this research, the starting value for axial deformation was -1.8 mm and the radial deformation +0.5 mm.

Once all the steps are completed, the core sample is ready to be tested.

2.2.3 Rock mechanical properties measurement

The American Society for Testing and Materials (ASTM) developed a standard to test compressive strength and elastic moduli of intact rock cores (ASTM D7012-14), where a compression apparatus is used in order to measure the mechanical properties of the rock.

Due to the quality of the rock, this ASTM standard was modified in such a way that those variations were kept constant for all the samples in order to have comparable

data. Since the rocks tested in this research were very brittle and fragile, a small confining pressure was used in order to keep the sample together and avoid any instrumentation damage due to rock failure at high stresses.

The core samples were tested at 2 MPa confining stress; this stress is low enough to make an insignificant change in the value of the measurements, but high enough to keep the core together in case of failure. It is important to highlight that any confining stress used will alternate the Young's modulus and Poisson's ratio values; therefore, this study will be measuring the Young's modulus at 2 MPa confining stress. Usually, an increase in confining stress will increase the Young's modulus and decrease Poisson's ratio; however, since the confining stress in this research is so low, the difference in values is going to be small.

Other than the confining stress, the rate at which the pressure is applied can affect the Young's modulus value (Paterson, 2005). For this reason, the pressure increase rate will be constant for all the cores through the whole experiment at 1MPa/minute. This slow loading rate will prevent a sudden uncontrolled rock failure that could damage the apparatus. The unloading rate was 2Mpa/minute until a 1MPa contact pressure was reached.

Each core sample was taken to failure after a cyclical loading where Young's modulus was identified. The samples were tested in the elastic region until they reached a constant slope. It usually took three full loading-unloading cycles for each core to get a repeatable and robust value. The samples were tested in the elastic region until 70% of the peak stress value, which range between 6000 psi-12000 psi.

After the core samples are prepared, the rock properties can be measured. The detailed procedure to obtain the properties of the cores is described below:

1. Turn on the hydraulic pump to drive the servos
2. Using the cell lift controller, lower the triaxial vessel. Make sure that no LVDT wires are going to be caught under the seal.
3. Release the vessel from the cell lift and raise the cell lift to the original position.
4. Tighten the eight cell rod nuts in a star pattern. Make sure that each one of them is tight enough to avoid any dangerous situation or leakage.
5. Using the roller lift, raise the close vessel and push it until it is under the axial load piston.
6. Deactivate the lift assembly from the user interface to prevent accidental movements.
7. Using the software, lower the axial load piston slowly until it makes contact with the cell piston.
8. Apply a 1 Mpa contact differential stress (called deviator stress in GCTS software) with the axial load piston to make fully contact with the same. From this point, the sample is under load.
9. Fill the triaxial vessel with hydraulic oil, using the triaxial pressure intensifier cabinet.
10. Isolate the triaxial vessel from the reservoir closing the cell isolation valves.
11. Using the cell pressure controller through the software, apply a constant confining stress of 2 MPa. Wait for the system reach equilibrium.

12. Create a new project in the GCTS software and from there input the characteristics of your core sample (diameter and length) for proper strain calculations.
13. Set the LVDT deformation to zero.
14. Execute the triaxial test program:
 - Increase the differential stress at 1 MPa/min until the stress desired is reached or until failure (Loading process).
 - Decrease the differential stress at 2 MPa/min until 1Mpa is reached (Unloading process)
 - Pause the experiment for a minute and repeat the cycle until equilibrium is reached or the sample fails.
15. Stop the triaxial test program.
16. Lower the differential pressure to 3 MPa to prepare the sample for drainage. This applied pressure will prevent the piston from moving due to hydraulic pressure.
17. Lower the cell confining pressure to 0.2 MPa
18. Open valves B and C and start draining the triaxial vessel.
19. Turn on the air pressure to allow the oil migration from the vessel to the reservoir. It takes approximately 20 minutes. The oil indicator will indicate when the vessel has been drained.
20. Once the vessel is drained, turn off the air pressure and wait for couple minutes to allow the vessel to reach the atmospheric pressure.
21. Lower the differential stress to 0.5 MPa

22. Displace the load piston axially very slowly, making sure that there is not residual air pressure. Keep raising the piston until it is not in contact with the triaxial vessel.
23. Turn on the lift assembly from the software and use the roller lift to displace the triaxial cell out of the loading frame.
24. Turn on the roller lift to set the triaxial set in a fixed position.
25. Unscrew the eight cell rod nuts.
26. Lower the cell lift, attached the triaxial cell to the lift, and raise the triaxial cell with the lift.
27. Unscrew the lower part of the metal support and take the sample out of the triaxial testing apparatus.
28. Examine the sample to make sure that no oil was infiltrated to the sample and that the LVDT holder ring is still tight; if it does, the results might be altered by the presence of oil, the sample needs to be get dry or discarded.
29. Remove all the instrumentation very carefully
 - Start from the ferromagnetic cores
 - Remove the circumferential chain gauge and its springs
 - Cut the sample jacket and remove the upper metal support
 - Remove the LVDT holder rings
30. Export the experimental data to an excel file, using the GCTS software and analyze the data.

2.2.4 Elasticity

The theory of elasticity is based on two concepts: Strain and Stress. These two concepts are related and strain can be considered as an effect of using force on an object. Elasticity behavior occurs when a specimen keeps its original dimensions after a force is applied to and retired from the object. If the force is no longer applied and the specimen dimensions are different, non-elastic behavior is present.

Stress is defined by the force acting through a cross-section or surface. The specimen's reaction to this force will depend mainly on the composition of the material. The stress can be express as:

$$\sigma = \frac{F}{A} \quad (2.1)$$

Once the force is applied to the specimen, a deformation will take place as a response to the force; this deformation is quantified using the strain concept, which is defined as the change in relative position of the particles relative to the original position. Strain can be expressed as:

$$\varepsilon = \frac{l-l'}{l} = \frac{\Delta l}{l} \quad (2.2)$$

The theory of linear elasticity is based on linear relationships between applied stresses and subsequent strains. Robert Hooke described the linear behavior of a sample in 3 dimensions as:

$$\varepsilon_{11} = \frac{1}{E}(\sigma_{11} - \nu(\sigma_{22} + \sigma_{33})) \quad (2.3)$$

Where E is the elastic moduli that describes the stiffness of the sample, or the resistance to compression; ν is the Poisson's ratio and σ_{ij} is the stress component for a 3D solution.

The axial elongation is not the only reaction to the applied force; a lateral elongation will take place as a reaction and it can be described with the Poisson's ratio. This is another elastic parameter that measures the lateral deformation relative to the axial deformation. This parameter is expressed as:

$$\nu = -\frac{\varepsilon_l}{\varepsilon_a} \quad (2.4)$$

Where ε_l is the lateral deformation and ε_a is the axial deformation. Usually, the sample cores are cylindrical, therefore the lateral deformation will be associated to the change in diameter due to force, and then radial deformation can be expressed as:

$$\varepsilon_l = \varepsilon_r = \frac{\Delta r}{r} \quad (2.5)$$

In order to test the rock mechanical properties such as Young's modulus and Poisson's ratio, the stress conditions should be recreated in the laboratory. The most common way to achieve the triaxial state of stress is applying a confining pressure and a uniaxial stress. Figure 16 shows the stress conditions for a cylindrical core, similar to the ones used on this study.

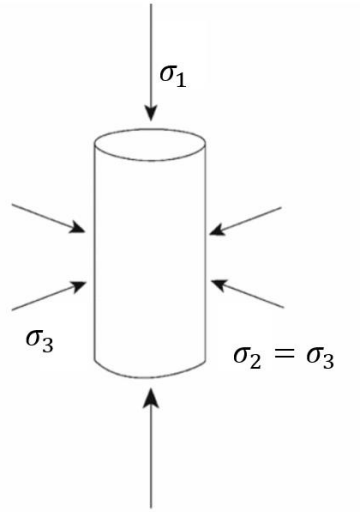


Figure 16: System of stresses in a conventional triaxial test (Paterson and Wong, 2005)

In this scenario, there are three principal stresses applied to the sample. σ_1 is the greatest stress and it is parallel to the to the compression axis, σ_2 is the intermediate stress and σ_3 is the least principal stress. For a triaxial test, σ_2 is equal to σ_3 , which is applied by the confining pressure radially and at the top and bottom of the sample. This concept is important to analyze the Young's modulus values, it has been proved that an increase in confining stress has an effect on Young's modulus, and it will have a more relevant effect on Poisson's ratio since it is obstructing the sample expansion. The amount by which the confining stress diverges from the axial stress is called differential stress, which is simply the difference between the greatest and the least principal stress:

$$\sigma_d = \sigma_1 - \sigma_3 \quad (2.6)$$

This differential stress will be the value plotted in the graphs presented in this study.

The plot generated from the differential stress and the axial strain will be used to calculate the Young's modulus; the linear part of the data will be fit using a linear least-square fit. For Poisson's ratio, a similar approach is used where the plot of radial strain against axial strain will be fit using a linear curve over the same range used for determining Young's modulus. In order to get reliable values, the data interpretation has to be done very carefully to make sure that each point can be comparable between them. For this study, we will define a Young's modulus and based on this definition we will calculate the values for different samples. Then, Young's modulus will be consider as the value for the best linear fit between 30% and 70% of the peak stress, where it could be consider as a tangent modulus. Figure 17 shows the different definitions of Young's modulus.

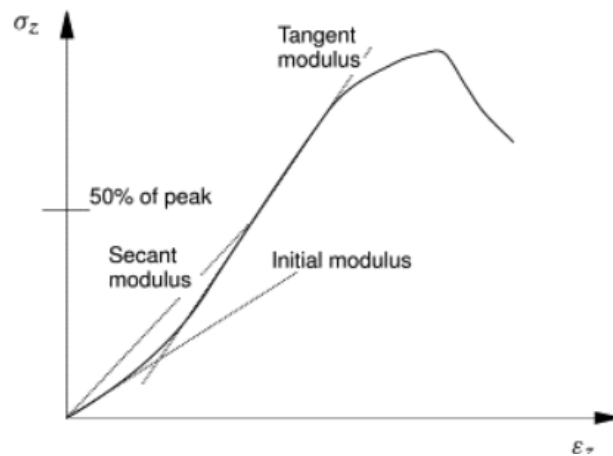


Figure 17: Different definitions of Young's modulus based on the stress-strain curve (Fjaer et. al, 2008)

From the figure, it can be seen that the Young's modulus can be defined in different ways, and this definition should be constant true all the samples; each slope used to find the Young's modulus is different and it will take into account different behaviors within the elastic zone, therefore a consistent Young's modulus is necessary for comparison purposes.

In a similar way, Poisson's ratio will be consider as the best linear fit for the axial strain values between 30% and 70% of the peak stress. These two definitions will be used for every sample. In this study, the samples will also be taken to failure in order to analyze the plastic behavior of each sample.

2.2.5 Permanent deformation

When a rock has been exposed to high stresses, the sample can experience permanent deformation followed by failure. This study will take into consideration the permanent performance of the rock, since it plays an important role in fracture conductivity lost in shale formations.

The creation of a conductive path in a shale play requires pumping proppants into the fracture. The contact area of each proppant with the rock is very small which generates a high localized stress that might exceed the yield stress causing permanent deformation in the rock and sometimes proppant failure. The permanent deformation caused by the proppant is known as embedment and it can be seen after a fracture conductivity test, where permanent marks are left in the rock, which proves that permanent deformation is occurring as the fracture closes. The stress at which the

permanent changes start occurring is known as the yield point. This point will dictate the beginning of permanent deformation which is going to be followed by the compressive strength or uniaxial compressive strength if the sample has not confining stress. Figure 18 locates the end of the elastic deformation zone and the peak strength in the strain-stress curve. For brittle rocks the ductile region is very small or almost none existing. In this study the yield point will not be considered due to the difficulty in locating it. Instead the compressive strength will be used to account for the plastic phenomenon. D'Andrea (1965) and Sone (2003) have shown a relationship between Young's modulus and compressive stress in their studies, which could help us understand the role of the elastic deformation in fracture conductivity loss.

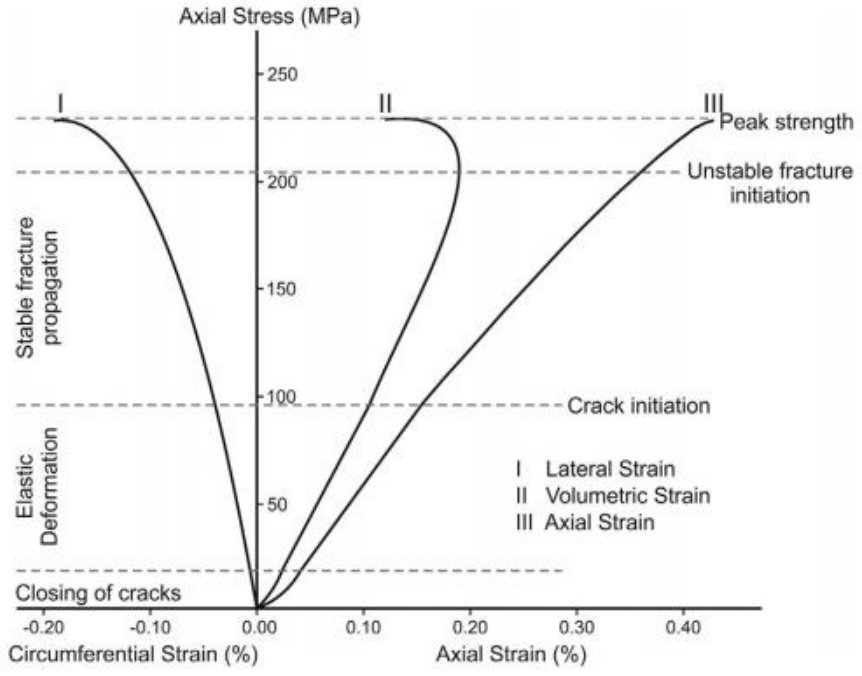


Figure 18: Stress-Strain diagram showing mechanics of brittle fracture (Undul et. al, 2015) Modified from Bieniawski (1997)

2.2.6 Anisotropy

In most of the problems of elasticity in petroleum engineering, the elastic regime is usually analyzed assuming isotropic behavior for simplification. However, previous studies have found that most of rocks, especially shale are anisotropic (Hornby et al., 1994). Furthermore, if a formation rock is composed of a layered sequence of different material it can be considered to exhibit transverse isotropy, which is one of the most common types of anisotropy for sedimentary rocks. Transverse isotropy assumes the layers composing the rock to have identical properties for any direction but different properties through the layered sequence which shows a directional dependency based on the layer's position. Elastic anisotropy of shales is caused by two main phenomena: Anisotropic fabric which is the result of the clay minerals orientation and the anisotropy of the clay minerals itself. (Sone, 2013).

2.3 X-Ray Diffraction Analysis

XRD analysis was performed on seven samples in order to obtain the mineralogy at the different sample collection locations. Since the samples from the ElimSPORT location were collected from different rock blocks, four randomly selected samples were chosen for XRD analysis, in order to show that they had the same mineral composition. Three samples from Allenwood were analyzed as well. The process was done at the Harold Vance Department of Petroleum Engineering and it consisted of sample preparation, XRD experiment and analysis.

2.3.1 Sample preparation

In order to determine the mineral composition of the samples. A homogeneous powder of 200 micrometers from the sample is needed; 10 grams of sample was ground in agate mortar and then passed through a sieve to produce a homogeneous powder (Figure 19).



Figure 19: Agate mortar and sieved used to get Marcellus powder

2.3.2 XRD analysis

X-ray powder diffraction (XRD) is a quick analytical technique primarily used for phase identification of a crystalline material and for structural properties identification. This technique was used to identify the mineral present in the samples, once the sample was ready to be tested (homogenized powder). The sample passed through a powder diffractometer where a detector collect the diffracted X-ray beams that produce a two dimensional pattern with the angular positions (2θ) and the intensities of

the diffracted peaks; the pattern generated is compared with a pattern of a known material that has been standardized by the Joint Committee on Powder Diffraction Standard (JCPDS).

There are many software programs that offer “pattern-matching” services, this software compare experimental diffractograms with patterns of known compounds; the software used in this study is called: Diffract Eva V.3. In order to qualify the phases present in the sample, intensity lines from the mixture were compared to a line from a pure phase. With a normal care, the type of technique used for this study has an accuracy about $\pm 3\text{wt } \%$ (Brime, 1985), this value is related to the experimental technique, it is highly possible that during the pattern marching process, this value could increase due to human errors, however, the decrease in accuracy is hard to quantify.

3. EXPERIMENTAL RESULTS AND DISCUSSION

Marcellus Shale outcrop samples from two different locations were used to run a series of triaxial compression test and X-ray diffraction analysis. The first set of samples were collected from Elmsport in Pennsylvania, the second set of samples were collected from Allenwood, approximately 10 miles away from the first site. These samples were from forty feet below the surface to avoid damage due to weathering. In the Elmsport location, eight samples from different rock blocks were used to get cores parallel and perpendicular to the bedding plane. In the Allenwood location, ten samples from the same rock block were used to get horizontal and vertical cores. The cutting directions were modified in order to study the effect of anisotropic behavior of these rocks on fracture conductivity.

In the following sections, the experimental results from the triaxial compression test for Elmsport and Allenwood samples will be presented in the elastic and inelastic range, along with the analysis of the results. Then, X-ray diffraction analysis will be presented, and surface roughness will be summarized. Finally, the measured fracture conductivity will be summarized in order to analyze any relationship between the rock characteristics and the fracture conductivity behavior.

3.1 Marcellus Shale (Elmsport) Results

This section will give a detailed explanation of the different tests ran on these samples and the experimental results. Samples were cut in different directions. For the following sections, a bed-perpendicular sample will be defined as a core cut

perpendicular to the bedding plane and bed-parallel sample will be cut parallel to the bedding plane. Figure 20 illustrates the core samples.

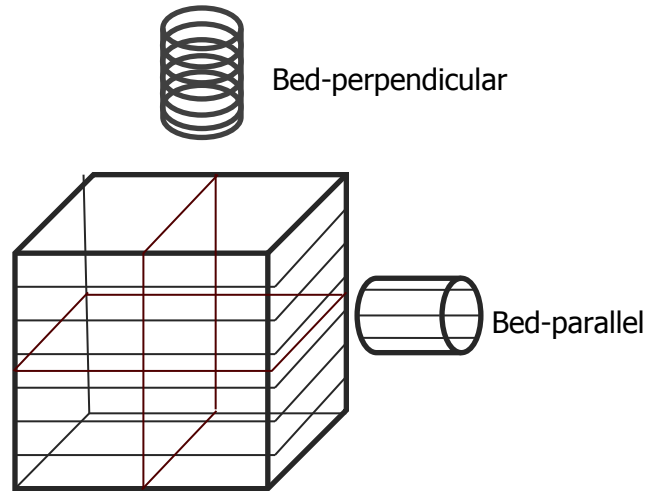


Figure 20: Core sample orientation

3.1.1 Marcellus shale (Elimsport) rock mechanics

The quality of the samples collected was such that cores of the desired dimensions were obtainable. Samples of one inch diameter and two inch length were used. Each sample was tested at least three times in the elastic regime, and once a constant measure was reached, the sample was taken to failure. Five bed-perpendicular samples and three bed-parallel samples were tested in order to confirm repeatability of the measurements.

Figure 21 shows a stress-strain curve for the bed-perpendicular samples to determine Young's modulus, and Figure 22 is the stress-strain curve for the bed-parallel samples. The related radial-axial strain curve is shown in Figure 23. For the bed-parallel

samples, Figure 24 display an example of these curves. The complete triaxial test results for this rock can be found in Appendix A. For both sample orientations, the loading process was the same. First the sample was loaded to 4000 psi, and then the loading was increased to 6000 psi on the subsequent loading cycles. 6000 psi is also the maximum closure stress used in the fracture conductivity testing. Then, the sample was taken to failure. As mentioned, the Young's modulus is defined as the slope of the best linear fit between 30% and 70% of the peak stress. This value will be used for subsequent analysis. For most samples, the cores had to be loaded three times, with some needing four cycles. The samples consistently showed a low Young's modulus in the first load cycle and non-linear behavior at low pressures that can be attributed to the presence of inelasticities such as micro-fractures and pore closure.

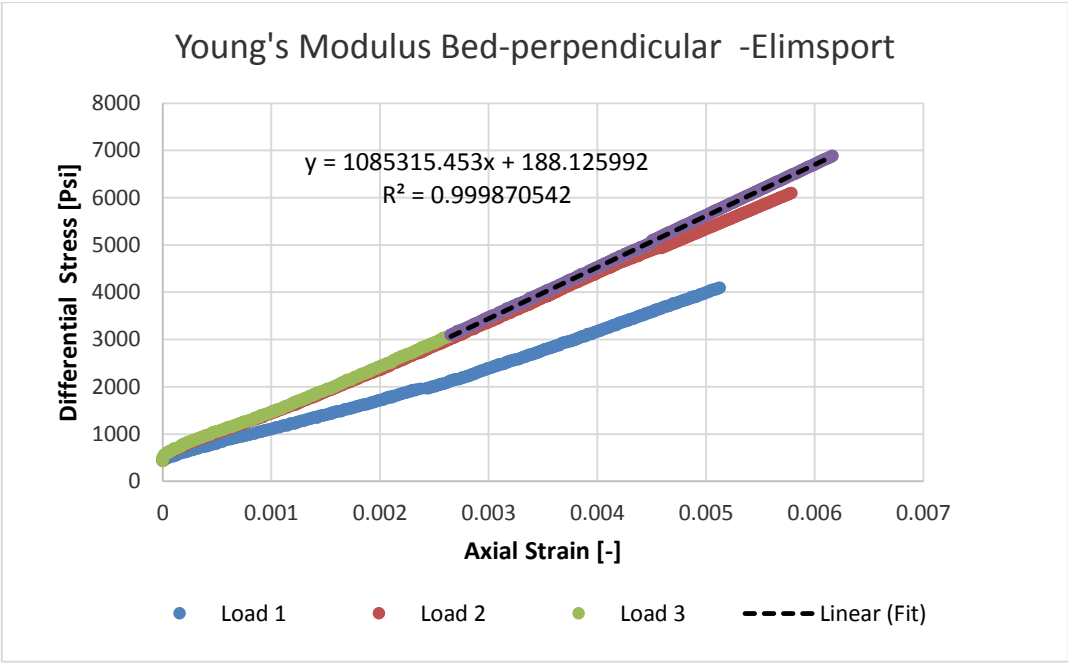


Figure 21: Stress-strain curve for a bed-perpendicular sample from Elimsport location

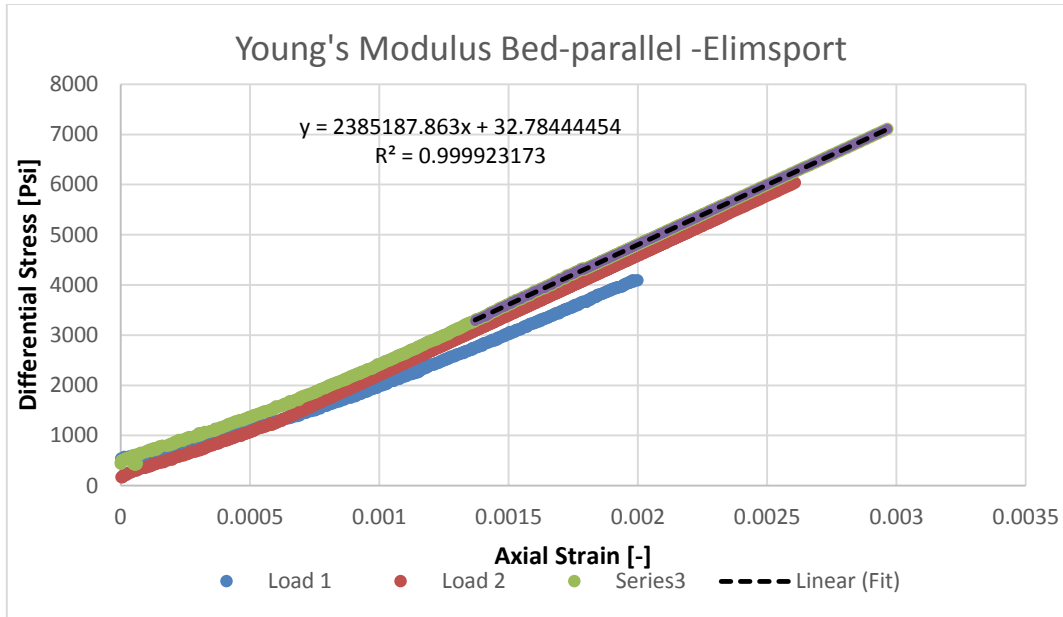


Figure 22: Stress-strain curve for a bed-parallel sample from Elimsport location

Young's modulus is obtained using the data for the best linear fit between 30% and 70%, which is nothing but the ratio between the change in differential stress to the change in axial strain.

$$E = \frac{\sigma_{70\%} - \sigma_{30\%}}{\varepsilon_{70\%} - \varepsilon_{30\%}} \quad (3.1)$$

3.1.1.1 Young's modulus evolution

The young's modulus evolution is clear for both samples. During the first loading cycle the Young's modulus is affected by the closure of microcracks and pores. This requires additional loads in order to assure linear elastic behavior.

The first loading increases the stiffness of the rock in both samples. However the effect on the bed-perpendicular sample is higher due to the layer position and layer

compaction. The bed-parallel sample shows an increase of 11% on Young's modulus, while the bed-perpendicular sample has an increase of 25%. After the first load (2nd and 3rd cycles), the increase in Young's modulus is almost negligible.

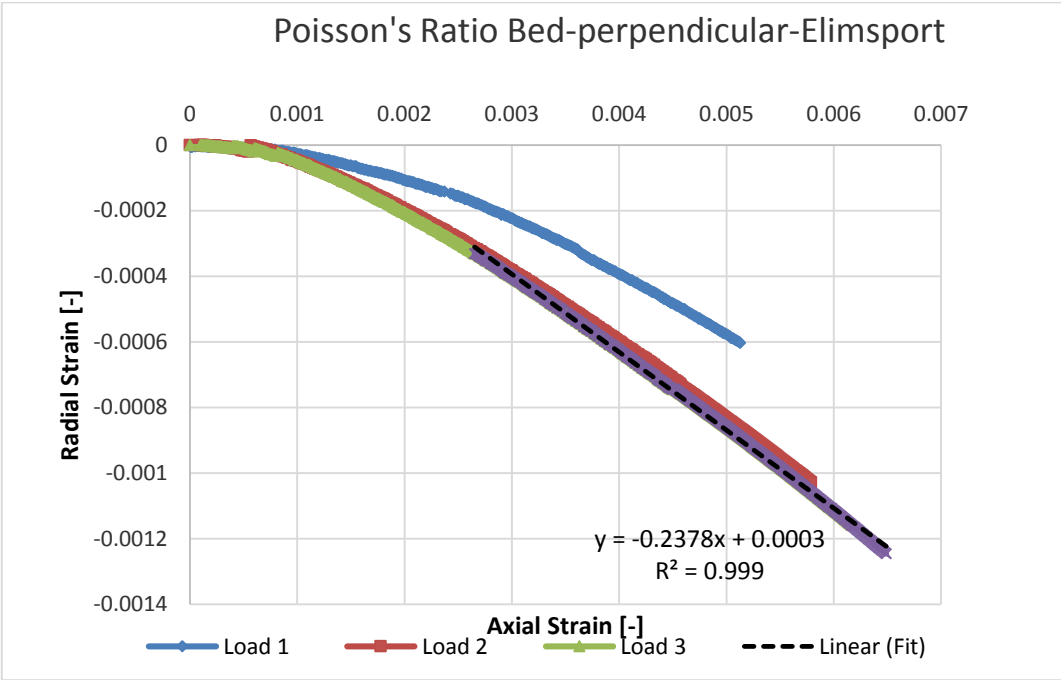


Figure 23: Radial-axial strain curve for a bed-perpendicular sample from Elimsport location

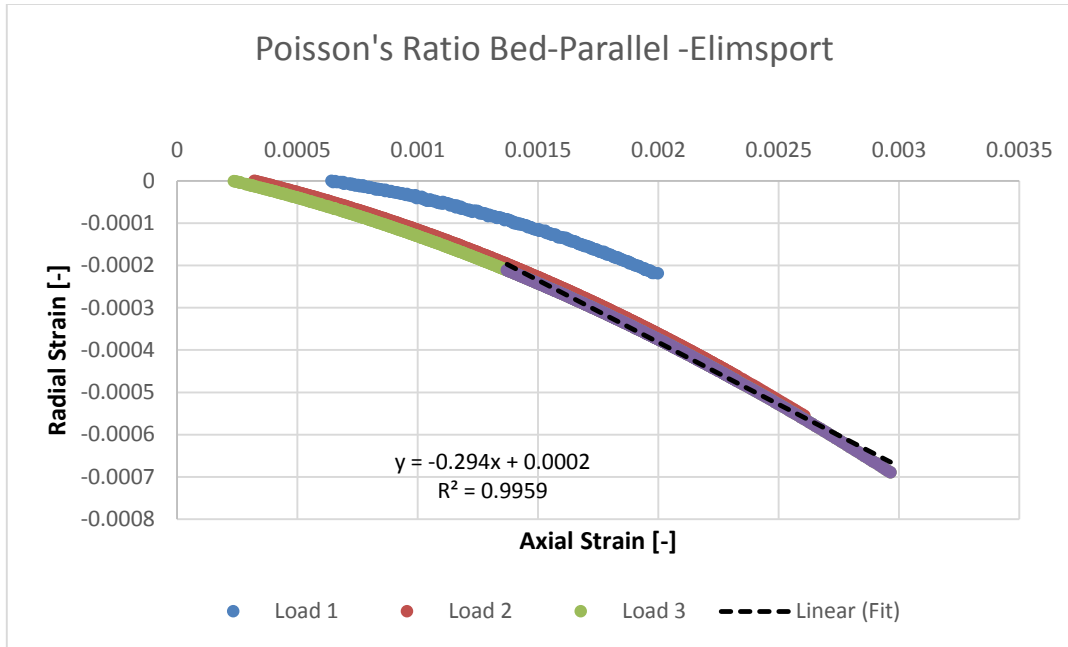


Figure 24: Radial-axial strain curve for a bed-parallel sample from Elimsport location

The radial-axial strain curve for determining Poisson’s ratio in bed-perpendicular and bed-parallel samples can be seen in Figure 23 and 24 respectively. The evolution of Poisson’s ration from the first loading cycle to the second it is noticeable as well; it seems that this phenomenon occurs consistently in all the samples. Since the graphs show a high curvature, the linear fit becomes more subjective. For this reason, the Poisson’s ratio was selected using a curve fit in the same range as the Young’s modulus curve fit. In this way, the values obtained were consistent through every sample.

Poisson’s ratio is obtained using the data for the best linear fit between 30% and 70%, which is the ratio between the change in lateral strain to the change in axial strain.

$$\nu = \frac{\epsilon_l@70\% - \epsilon_l@30\%}{\epsilon_a@70\% - \epsilon_a@30\%} \quad (3.1)$$

For the third loading cycle the sample is taken to failure as can be seen in Figure 25. The different phases of triaxial deformation can be seen in this curve: Elastic deformation and its transition into the permanent deformation. Since these samples present a brittle behavior, the permanent deformation zone is minimal before failure occurs. The yield point is very difficult to locate, which can lead to errors in the analysis. Therefore the ultimate compressive strength will be used to characterize the plastic behavior of each sample. The severe decrease of differential stress present in the figures indicate the failure of the rock.

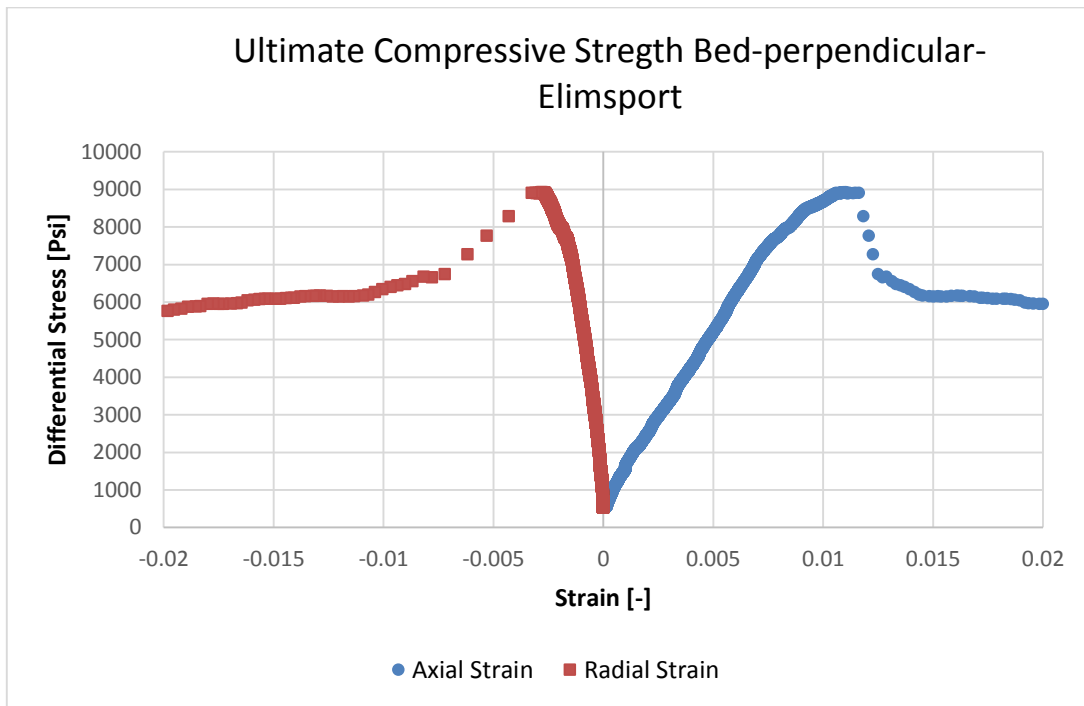


Figure 25: Stress-strain curve for a bed-perpendicular sample from Elimsport location

The results obtained from the eight triaxial tests performed for Elimsport samples (5 bed-perpendicular and 3 bed-parallel) can be seen in Table 1:

Table 1: Summary of Elimsport mechanical properties

Samples	Bed-perpendicular			Bed-parallel		
	Young's Modulus [psi]	Poisson's Ratio [-]	Ultimate Compressive Strength [psi]	Young's Modulus [psi]	Poisson's Ratio [-]	Ultimate Compressive Strength [psi]
EL (1)	9.3E+05	0.239	8.13E+03	2.39E+06	0.293	1.02E+04
EL (2)	1.3E+06	0.223	9.57E+03	2.41E+06	0.307	1.14E+04
EL (3)	1.1E+06	0.237	9.83E+03	2.39E+06	0.326	1.04E+04
EL (4)	9.9E+05	0.231	8.92E+03	-	-	
EL (5)	1.0E+06	0.233	8.90E+03	-	-	
Average	1.1E+06	2.3E-01	9.1E+03	2.4E+06	3.1E-01	1.1E+04
Standard Deviation	1.49E+05	6.23E-03	6.63E+02	9.62E+03	1.66E-02	6.32E+02
Percentage Standard Deviation	14%	3%	7%	0.4%	5%	6%

The difference in the rock properties between the bed-parallel samples and bed-perpendicular samples is evident. The bed-parallel samples present an average Young's modulus of 2.4 Mpsi which is more than twice the value of the bed-perpendicular samples. This means that the bed-parallel samples are stiffer than the bed-perpendicular samples. These results show that Elimsport samples have a strong orientation dependency or anisotropic. This significant difference in Young's modulus could have an impact on fracture conductivity values. Additionally, it seems that Poisson's ratio values follow the same trend as the Young's modulus values where bed-parallel samples present higher values than bed-perpendicular samples. This might be caused by the differences in local mineralogy for each layer. Since the difference in elastic properties is significant, some conductivity effects might be attributable to these properties. The

inelastic parameter (ultimate compressive strength) follows the previous trend as well. Overall, the values obtained for rock mechanical properties present low variation, which leaves us with a small possible range of rock properties values.

3.1.2 Marcellus shale (Elmsport) mineralogical composition

The mineralogical composition of the Elmsport samples was determined using X-ray Diffraction (XRD) analysis. The analysis of the test was done using the software Diffrac.Eva V3.1. Since the samples were collected from different rock blocks for each sample orientation, four tests were ran with different samples chosen randomly to compare mineralogy. The results are presented in Figure 26:

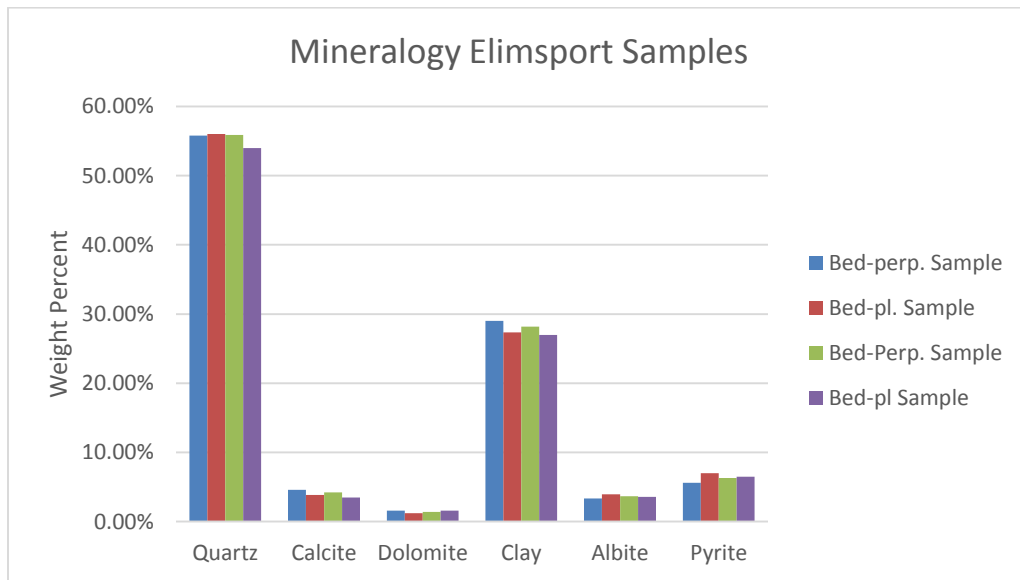


Figure 26: Mineralogy composition Elmsport samples

In general, all samples have similar mineralogy composition which means that the differences in rock properties are not likely related to mineralogy. These samples have an average composition of 56% Quartz, 4% calcite, 1.4% dolomite, 28% clay and 6% pyrite. These values are very close to those presented by Lash and Engender (2011) for Marcellus Shale. Since the values from both samples are very similar, their effect on conductivity might be hard to observe.

3.1.3 Surface roughness

A visual inspection of the surface roughness for each sample was made. From the samples a clear difference between bed-perpendicular and bed-parallel samples could be seen. Figures 27 and 28 show how the bed-parallel samples have a rougher surface than the bed-perpendicular sample. Rough fracture surface at low proppant concentration can have a significant impact on conductivity reduction (Fredd et. al, 2001). Since the proppant experiences different stress conditions due to the rough surface, this might increase the crushing effect and therefore the reduction in fracture width. This parameter will be considered in this study since all the conductivity test were ran at low proppant concentration.



Figure 27: Fracture surface of Elmsport bed-perpendicular sample

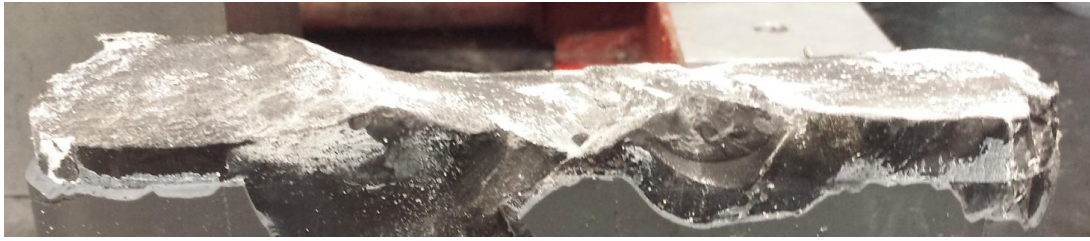


Figure 28: Fracture surface of ElimSPORT bed-parallel sample

The surface roughness was quantified using a laser profilometer to scan the surface. The distance measurements between the object surface and the sensor represent the surface topography. In order to quantify the surface roughness, the deviation of the measurement from the best fit plane was calculated using Root Mean Square (RMS) error. The complete results from ElimSPORT can be found in Table 2 (McGinley, 2015).

Table 2: Summary surface roughness ElimSPORT samples

Z-Measurements	
Bed-perpendicular - RMS Error [in]	Bed-parallel - RMS Error [in]
0.0832	0.12609
0.0802	0.0603
0.0764	0.1744
Average [in]	
0.080	0.120

3.1.4 Marcellus shale (ElimSPORT) fracture conductivity

Fracture conductivity tests were performed on bed-parallel and bed-perpendicular ElimSPORT samples. The details regarding proppant concentration and sample repetitions can be seen in Table 3 (McGinley, 2015).

Table 3: Fracture conductivity experiments design

Proppant Mass	Areal Proppant Concentration	Sample Sets	Number of test
1.6 g	0.051 lb/ft ²	Elimsport - Bed-perpendicular	5
		Elimsport - Bed-parallel	5
3.2 g	0.10 lb/ft ²	Elimsport - Bed-perpendicular	5
		Elimsport - Bed-parallel	5

The samples were tested at 0.051 lb/ft² and 0.10 lb/ft² areal concentration of 40/70 white mesh sand for both orientations. A summary of the average conductivity behavior for Elimsport samples is shown in Figure 29. The focus of this study will be in the conductivity values at 0.051 lb/ft² concentration since they seem to be more affected by the rock properties and they are comparable with the Allenwood samples at the same concentration. Unpropped conductivity tests would be ideal for a direct comparison with rock properties. However the tests were difficult to perform and the results obtained were not meaningful.

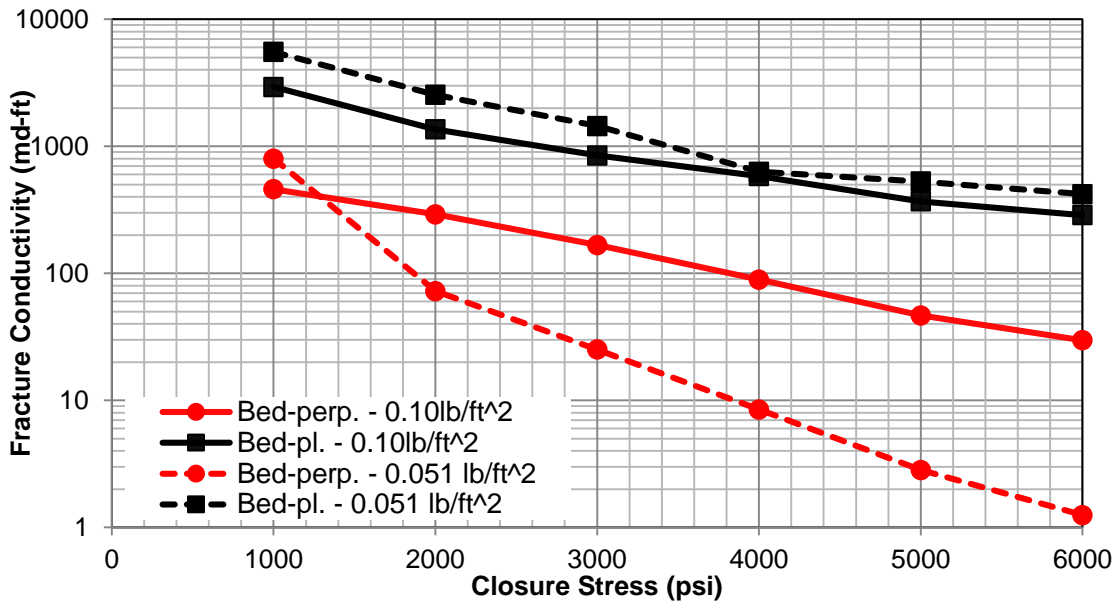


Figure 29: Summary of the average conductivity behavior for Elimsport samples

3.2 Marcellus Shale (Allenwood) Results

This section will give a detailed explanation of the different test ran in Allenwood samples and the experimental results. These samples were cut in different directions as well, and all the samples were cut from the same rock block.

3.2.1 Marcellus shale (Allenwood) rock mechanics

Triaxial compression test were performed on 10 different cores of one inch diameter and two inches length, 5 of them were cut perpendicular to the bedding plane and 5 parallel to the bedding plane. Since the samples came from the same rock block, it was assumed that each conductivity samples was directly related to a core sample. Each sample was tested at least three times in the elastic regime, and once a constant measure was reached, the sample was taken to failure. The test procedure and data analysis

methodology was unchanged from that used on the Elimsport samples. Figure 31 shows a stress-strain curve for a bed-perpendicular sample to determine Young's modulus, and Figure 32 shows a stress-strain curve for the bed-parallel samples. The related radial-axial strain curve for bed-perpendicular samples is shown in Figure 33. For the bed-parallel samples, Figure 34 displays an example of curves obtained to calculate Poisson's ratio. The first load consistently shows a lower Young's modulus which can be related to the large amount of deformation present in the first cycle due to microfractures closing and pore compression. However, it seems from the figures that the stiffer the sample the smaller the gap between the first and last cycle. Bed-perpendicular samples show an irregular behavior at low differential stress that could be related to the presence of micro fractures that are opening and closing at low stresses or by the fact that these samples had a calcite vein that could affect the behavior of the sample at low stresses. Figure 30 shows an example of this behavior.



Figure 30: Elimsport core with a calcite vein

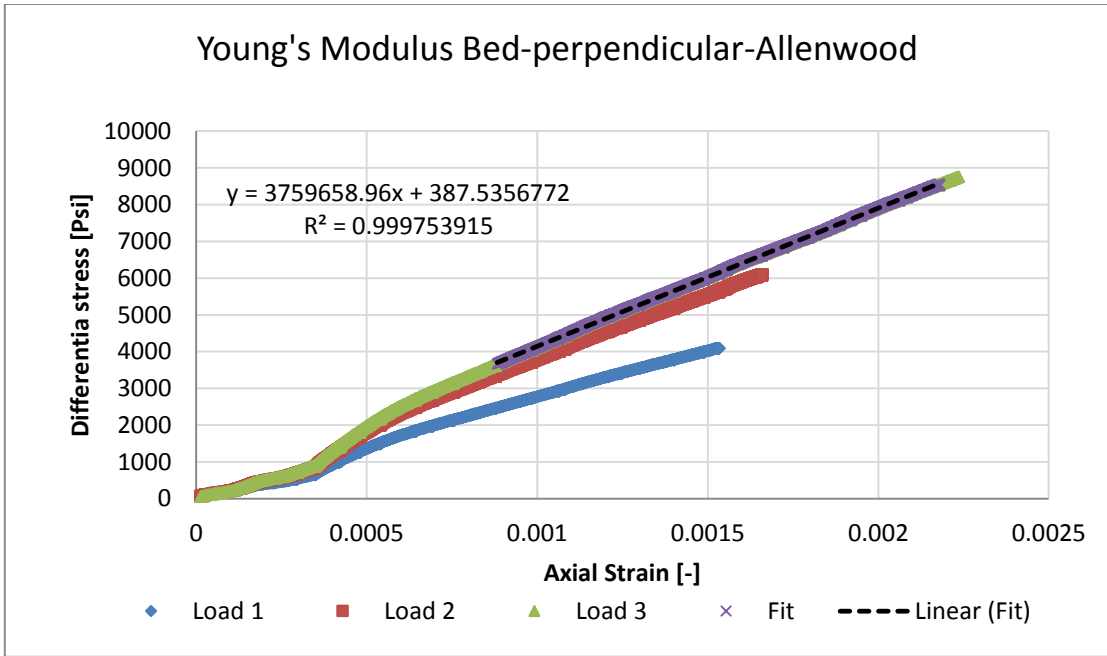


Figure 31: Stress-strain curve for a bed-perpendicular sample from Allenwood location

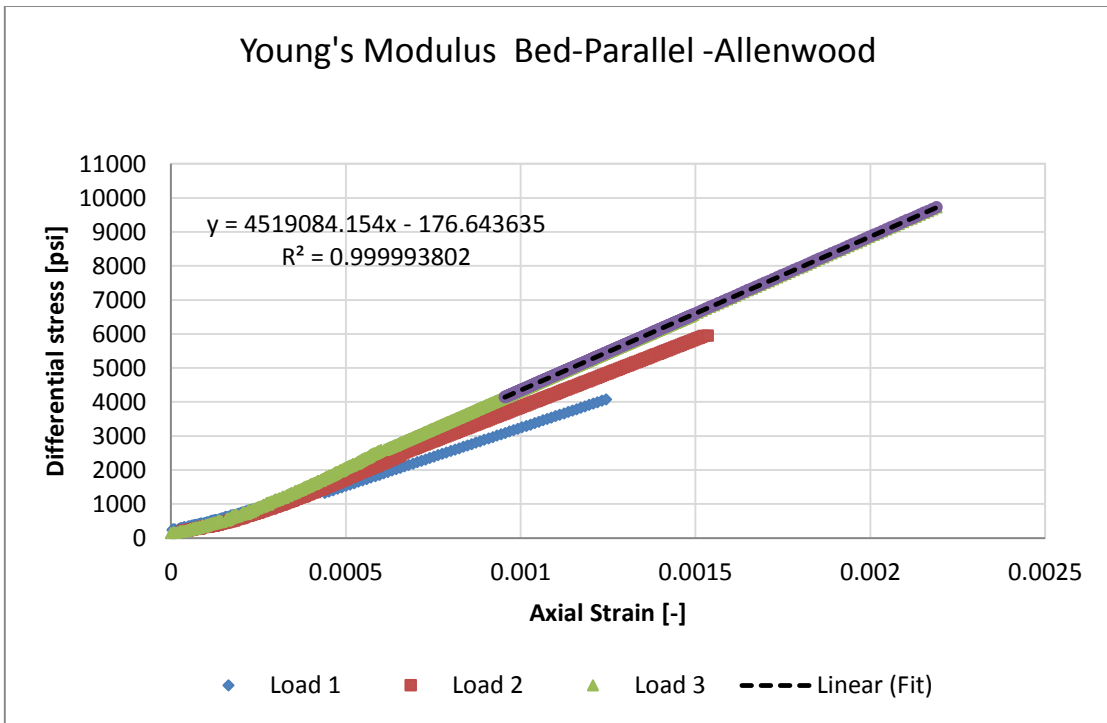


Figure 32: Stress-strain curve for a bed-parallel sample from Allenwood location

3.2.1.1 Young's modulus evolution

The Allenwood samples show a clear Young's modulus evolution for bed-perpendicular and bed-parallel samples as well. During the first loading cycle the Young's modulus is affected by closure of microcracks, and then additional loading cycles are required in order to ensure linear elastic behavior.

The increase of Young's modulus from first cycle to second cycle varies with orientation, for bed-perpendicular samples the Young's modulus increases 19%, and for bed-parallel samples 15%. The difference between the first and second cycle for bed-perpendicular samples in Allenwood is lower, and it might be related to the fact that the samples were collected at 40 feet under the ground, since there is less sample relaxation. However there is no evidence to support this idea.

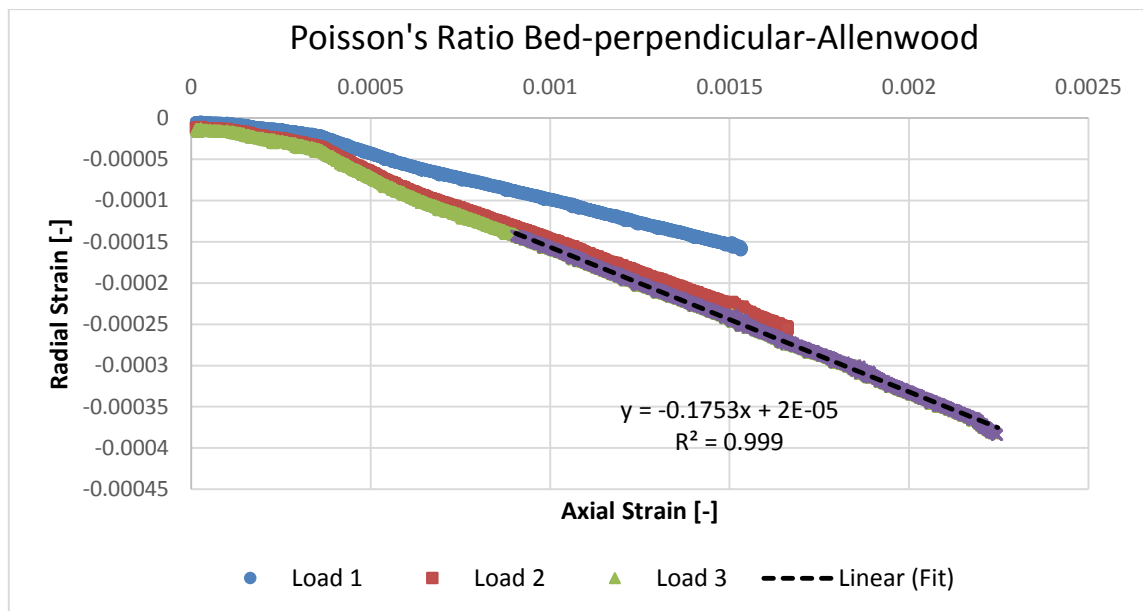


Figure 33: Radial-axial strain curve for a bed-perpendicular sample from Allenwood location

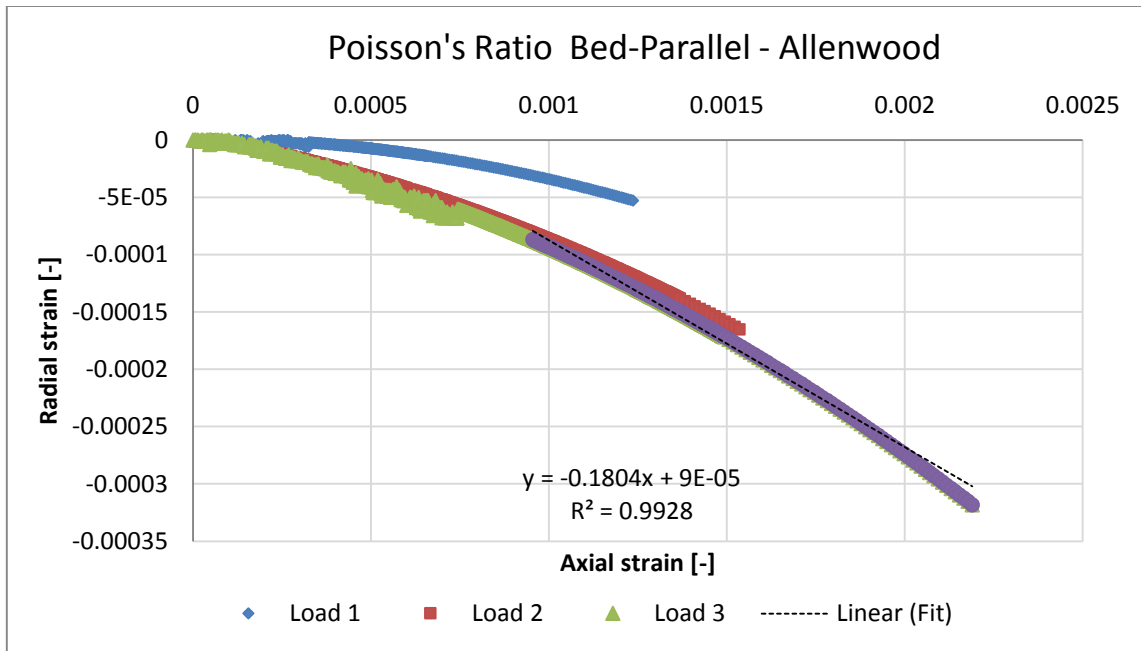


Figure 34: Radial-axial strain curve for a bed-parallel sample from Allenwood location

The radial-axial strain curve to determine Poisson's ratio in bed-perpendicular and bed-parallel samples can be seen in Figures 33 and 34 respectively. For this set of samples the evolution of Poisson's ratio from the first loading cycle to the second it is noticeable as well; it seems that this phenomenon occurs consistently in all the samples. The method to find Poisson's ratio was the same used for the Elimsport samples. The results for all the samples run can be seen in Appendix B.

Figure 35 shows a typical curve for the samples taken to failure. For Allenwood samples was also difficult to locate the yield point since the plastic range is minimum, therefore the ultimate compressive strength was used to characterize the permanent deformation behavior and make it comparable with Elimsport results.

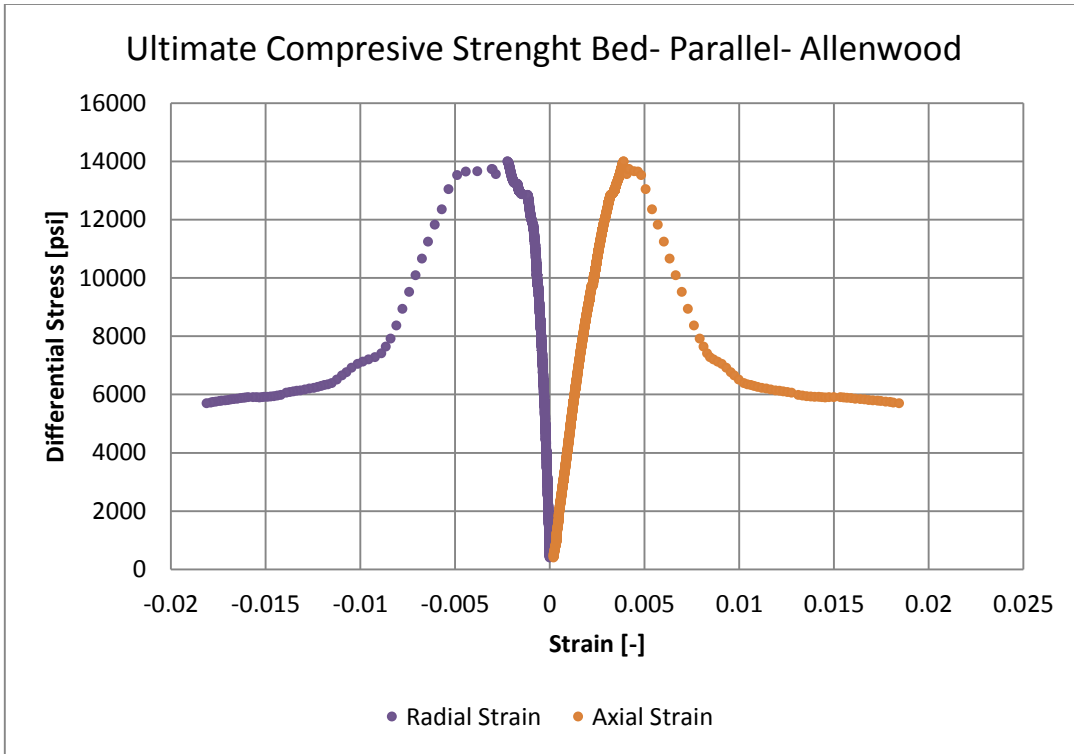


Figure 35: Stress-strain curve for a bed-perpendicular sample from Allenwood location

The results obtained from the 10 triaxial tests performed for Allenwood samples (5 bed-perpendicular and 5 bed-parallel) can be seen in Table 4:

Table 4: Summary of Allenwood mechanical properties

Samples	Bed-perpendicular			Bed-parallel		
	Young's Modulus [psi]	Poisson's Ratio [-]	Ultimate Compressive Strength [psi]	Young's Modulus [psi]	Poisson's Ratio [-]	Ultimate Compressive Strength [psi]
AL (1)	3.9E+06	0.196	1.28E+04	4.52E+06	0.180	1.38E+04
AL (2)	3.8E+06	0.175	1.21E+04	4.42E+06	0.198	1.60E+04
AL (3)	3.9E+06	0.227	1.25E+04	4.38E+06	0.24	1.40E+04
AL (4)	4.1E+06	0.246	1.01E+04	4.50E+06	0.187	1.61E+04
AL (5)	4.1E+06	0.219	1.41E+04	4.59E+06	0.174	1.48E+04
Average	3.9E+06	2.1E-01	1.2E+04	4.4E+06	2.1E-01	1.46E+04
Standard Deviation	1.45E+05	2.76E-02	1.46E+03	6.92E+04	3.08E-02	1.19E+03
Percentage Standard Deviation	4%	13%	12%	1.6%	15%	8%

From the table, it can be observed that the anisotropic effect exists for the Allenwood samples as well. The bed-perpendicular orientation shows a lower Young's modulus than the bed-parallel orientation. However, the ratio of bed-parallel to bed-perpendicular values is significantly smaller than the one presented by Elimsport samples, which is somewhat surprising since they are coming from the same geological zone, it would be expected similar properties. The ultimate compressive strength values showed the same behavior for the different sample orientation where bed-parallel samples keep showing higher values. Conversely, the average Poisson's ratio does not present any significant variation with orientation which make it hard to assign any conductivity effect to this parameter.

3.2.2 Marcellus shale (Allenwood) mineralogical composition

The mineralogical composition of the Allenwood samples was determined using X-ray Diffraction (XRD) analysis. The testing method was the same as the one used for the Elmsport samples. Since the samples were cut from the same rock block, only three tests were performed to obtain mineralogy. The results obtained for Allenwood can be seen in Figure 36:

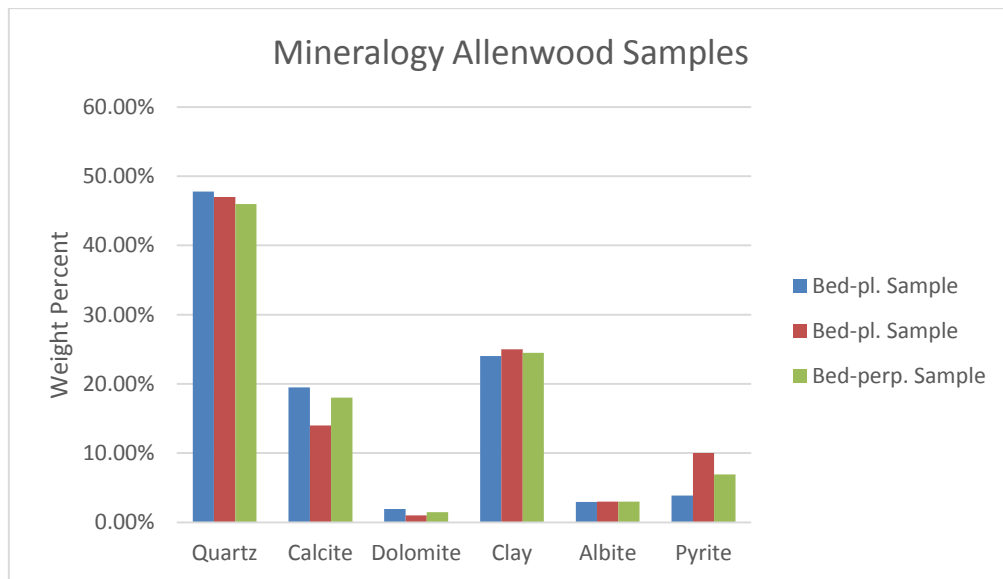


Figure 36: Mineralogy composition Allenwood samples

This sample presents in average 46% Quartz, 17% calcite, 1% dolomite, 25% clay and 7% pyrite, these values are within the typical range composition for Marcellus Shale. There is not a clear difference in mineralogy for the bed-perpendicular and bed-parallel samples therefore we could assume that the difference in Young's modulus of this samples is not related with mineralogy composition.

3.2.3 Surface roughness

Figures 37 and 38 show the surface of bed-perpendicular and bed-parallel samples from Allenwood respectively. From a visual inspection, it is hard to find any difference between the samples, they both seem to have a rough surface.



Figure 37: Fracture surface of Allenwood bed-perpendicular sample



Figure 38: Fracture surface of Allenwood bed-parallel sample

Table 5 shows the complete results for surface roughness quantification (McGinley, 2015).

Table 5: Summary surface roughness Allenwood samples

Z-Measurements	
Bed-perpendicular - RMS Error [in]	Bed-parallel - RMS Error [in]
0.11071	0.1249
0.0954	0.1318
0.1076	0.1474
0.1051	0.1634
0.0664	0.2615
Average	
0.097042	0.1658

3.2.4 Marcellus shale (Elmsport) fracture conductivity

Fracture conductivity tests were performed on bed-parallel and bed-perpendicular Allenwood samples. The experimental details for proppant concentration and test repetition can be seen in Table 6.

Table 6: Allenwood fracture conductivity experiments design

Proppant Mass	Areal Proppant Concentration	Sample Sets	Number of test
0.4 g	0.013lb/ft ²	Allenwood - Bed-perpendicular	5
		Allenwood - Bed-parallel	5
0.8 g	0.025lb/ft ²	Allenwood - Bed-perpendicular	5
		Allenwood - Bed-parallel	5
1.6 g	0.051lb/ ft ²	Allenwood - Bed-perpendicular	2
		Allenwood - Bed-parallel	3

The Allenwood samples were tested at 0.051 lb/ft², 0.025 lb/ft² and 0.013 lb/ft² areal concentration of 40/70 white mesh sand for both orientations. Figure 39 shows a summary of the average conductivity behavior.

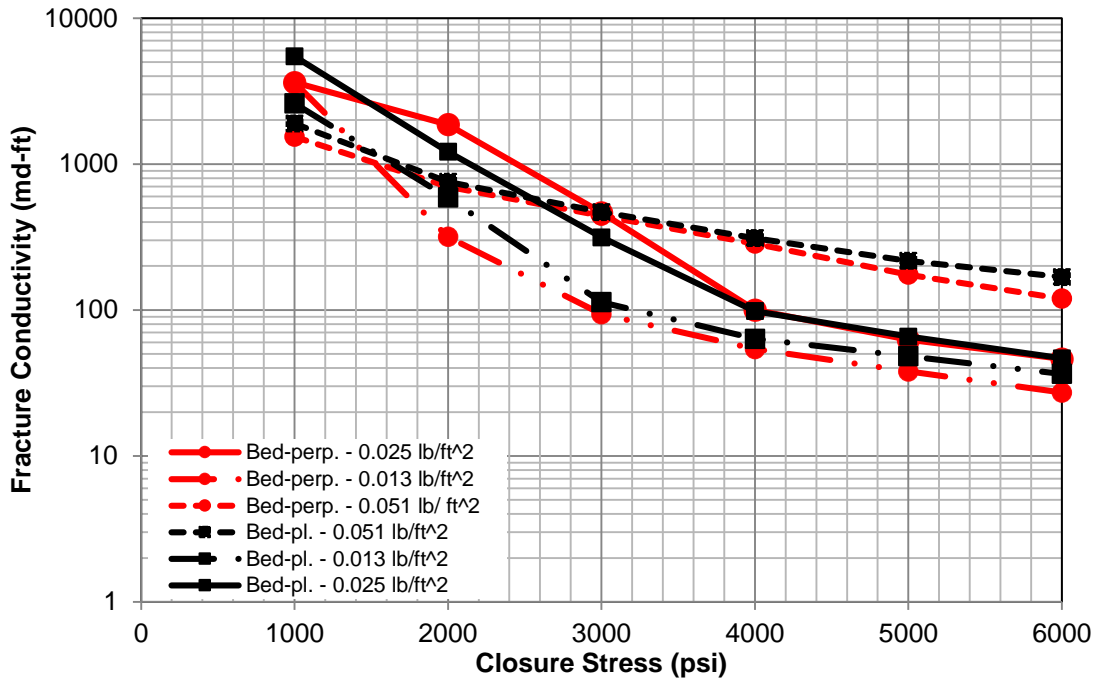


Figure 39: Summary of the average conductivity behavior for Allenwood samples

3.3 Effect of Rock Properties on Fracture Conductivity

In order to analyze the impact of the rock properties measured previously on fracture conductivity, it is necessary to quantify the differences between the samples from the two different location and how the change in sample orientation differs for each location. Table 7 recapitulates the mechanical properties for each location at orientation.

Table 7: Summary of mechanical properties

		Bed-perpendicular			Bed-parallel		
		Young's Modulus [psi]	Poisson's Ratio [-]	Ultimate Compressive Strength [psi]	Young's Modulus [psi]	Poisson's Ratio [-]	Ultimate Compressive Strength [psi]
Elimsport	Average	1.07E+06	2.33E-01	9.07E+03	2.40E+06	3.09E-01	1.06E+04
	Standard Deviation	1.49E+05	6.23E-03	6.63E+02	9.62E+03	1.66E-02	6.32E+02
	Percentage Standard Deviation	14%	3%	7%	0.4%	5%	6%
Allenwood	Average	3.94E+06	2.13E-01	1.23E+04	4.44E+06	2.06E-01	1.46E+04
	Standard Deviation	1.45E+05	2.76E-02	1.46E+03	6.92E+04	3.08E-02	1.19E+03
	Percentage Standard Deviation	4%	13%	12%	2%	15%	8%

The Young's modulus values associated with Allenwood samples are almost double the values obtained from Elimsport for the bed-parallel samples and more than double for bed-perpendicular samples, which is surprising since both samples are coming from the same geological stratigraphic zone (lower Marcellus). One possible reason for this difference it could be related with mineralogy composition. The anisotropic effect is notorious for both locations. For the Elimsport samples the ratio between Bed-parallel to Bed-perpendicular for Young's Modulus is 2.2 which is a significant difference in properties just for a change in orientation and it may have an

impact in conductivity. For Allenwood samples the ratio between Bed-parallel to Bed-perpendicular Young's Modulus is 1.1 which is smaller than the ratio presented by Elimsport. Since the values for bed-parallel and bed-perpendicular samples are close to each other, it would be expected that they have a small impact in conductivity. The differences in anisotropic ratio for each location might be related to the fact that Allenwood samples were collected from 40 feet underground, avoiding environmental exposure; it can also be related with differences in mineralogy composition. Figure 40 summarizes the mineralogy for each location.

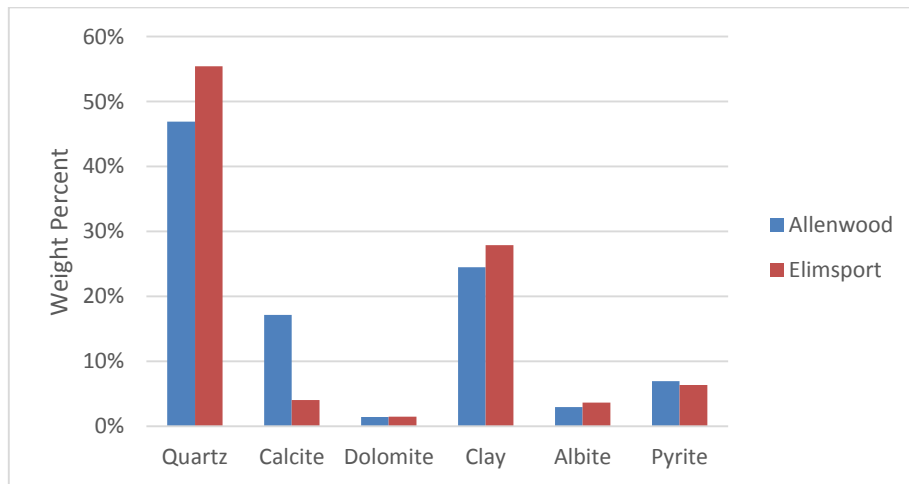


Figure 40: Average mineralogy composition

The main difference between Elimsport and Allenwood composition is the increase of calcite by 13% for the Allenwood Location, the reduction of clay minerals by 3% and the reduction of quartz by 10%; this change in composition might be the cause for the increase in stiffness for Allenwood, although the quartz content is lower for Allenwood, the overall content of “Stiff” components (Quartz and Calcite) is higher for

Allenwood. The increase in mechanical anisotropy observed in Table 7 for Elimsport samples can be related to the higher clay content and lower calcite content presented in contrast to Allenwood values. Previous studies have shown that mechanical anisotropy increases with soft component volume (clay and organic content) (Sone et.al, 2013, Vernil et.al, 1997). However, if the accuracy of the technique used is taken into account, the difference in mineralogy between the two set of samples in not big enough to draw a conclusion.

The comparison between the rock properties and fracture conductivity, takes into account the orientation of the samples for all the experimental procedure; in order to be consistent, cylindrical samples cut perpendicular to the bedding plane are going to be compare with fracture conductivity samples cut in the same way, therefore the pressure will be apply in the same direction for both set of samples. Figure 41 illustrates the sample group.

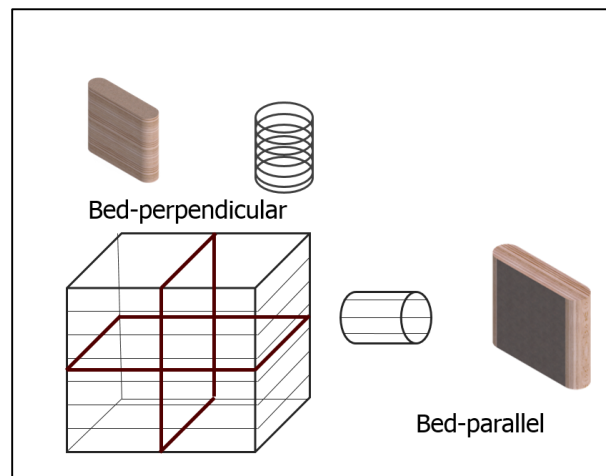


Figure 41: Sample orientation comparison

In order to quantify the relationship between rock properties and fracture conductivity using the samples collected from the two different locations, it is necessary to make sure to keep constant parameters that can affect fracture conductivity for both locations. Previous studies have shown that factors such as proppant concentration, proppant size and proppant strength can have an effect on fracture conductivity. For this reason, this section will only discuss conductivity results at 0.051 lb/ft² areal concentration of 40/70 white mesh sand. This proppant concentration simulates a partial monolayer in the fracture surface. Because there is a single layer of proppant on the fracture surface, the majority of conductivity loss will be related to proppant – rock interaction or rock-rock interaction in the absence of proppant. The effect of proppant pack compression will not be considered in this study.

During the fracture conductivity test, the proppant layer exerts force on the fracture surface causing the rock to deform. The ratio by which a material deforms under stress is known as Young's Modulus and it can be related to the proppant-rock embedment. It would be expected that a higher Young's Modulus would maintain wider flow channels than a low Young's Modulus, which could be represented in a higher fracture conductivity if the surface characteristics are the same (Jansen, 2014). In order to investigate how the Young's modulus affects fracture conductivity, the conductivity results were compared for Elimsport and Allenwood samples. Figure 42 shows the average fracture conductivity for the Elimsport location.

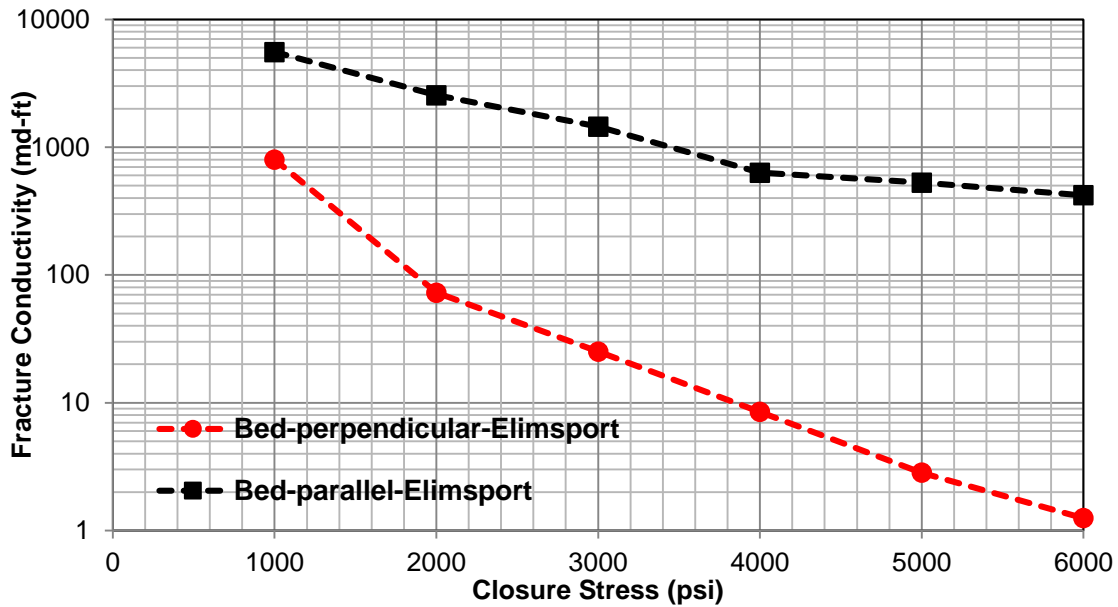


Figure 42: Average conductivity behavior for Elimsport samples at 0.051 lb/ft² proppant concentration

In the graph, there is a significant difference between the conductivity of bed-parallel and bed-perpendicular samples. Bed-parallel orientation conductivity is one order of magnitude higher than bed-perpendicular conductivity; this behavior could be explained by the rock characteristics. The Young's modulus values for bed-parallel samples are twice as high as the bed-perpendicular samples' value. The Poisson's ratio and ultimate compressive strength follow the same trend, where the bed-parallel samples had higher values for all the three parameters. A higher Young's modulus will maintain the flow channels and high Poisson's ratio might create micro flow channels as stress increases as part of the deformation process. The high values of each parameter could be represented in a higher conductivity overall, as we observed in Figure 42. Although it appears that the rock mechanical properties are directly related to conductivity, it is hard

to attribute the difference in conductivity to the Young's modulus and Poisson's ratio only since there are other parameters that might cause this phenomena, one of them being surface roughness. Fredd (2001) mentioned the relevance of surface roughness in conductivity, for Elimsport samples the bed-parallel orientation present a rougher surface than the bed-perpendicular, any small shear displacement or removal of small shale pieces generated in the fracturing process could create flow paths that might be contributing to the large conductivity values observed in Figure 42. Therefore, it is not possible to identify the main driver in the fracture conductivity values observed.

In order to understand better the behavior observed in Elimsport samples, the results from Allenwood samples at the same proppant concentration were incorporated to the existing analysis. Figure 43 shows the results.

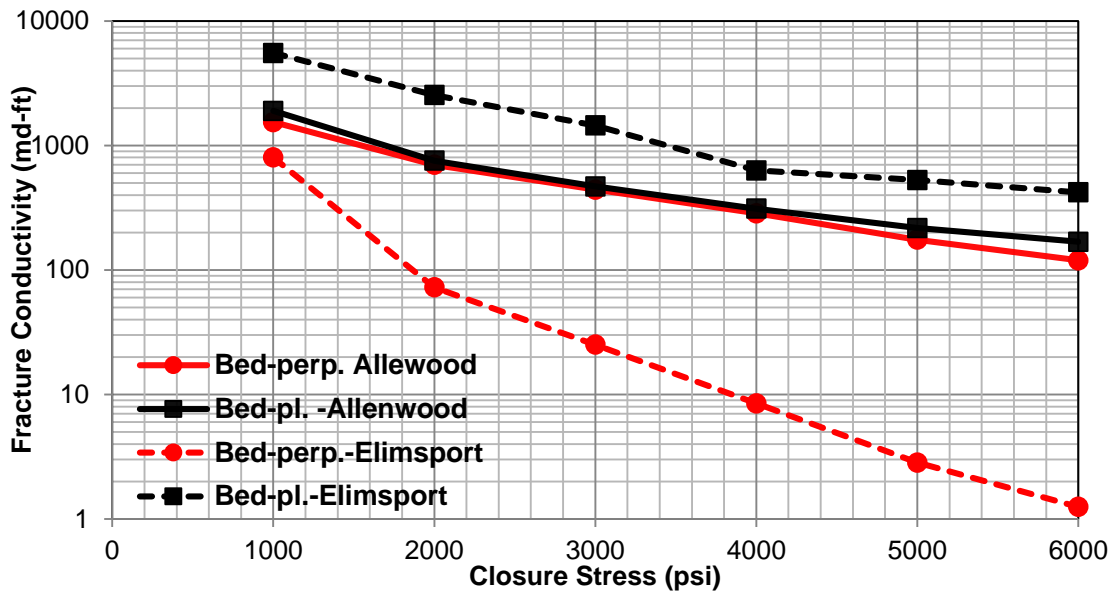


Figure 43: Summary of the average conductivity behavior at 0.051 lb/ft² proppant concentration

From the graph two interesting behaviors can be observed: Allenwood bed-parallel and bed-perpendicular conductivity have very close values and Allenwood conductivity values are smaller than Elimsport bed-parallel conductivity samples. This is somewhat surprising, since Allenwood has a higher Young's modulus and a rougher surface, and from the observations in Elimsport, it would be expected that these parameters would show higher conductivity; therefore, it seems that Young's modulus or surface roughness are not the only parameters affecting the conductivity magnitude. The anisotropic effect is not as pronounced for Allenwood samples as for Elimsport, but still it can be seen that there is a slightly higher conductivity for bed-parallel samples, this behavior is present in both sample locations.

From the results, it seems that fracture conductivity values could not be related to Young's modulus, unless the surface roughness is helping to increase the conductivity value presented by Elimsport bed-parallel samples. However, for both Allenwood samples, the surface roughness quantification showed a rougher surface, which means that this parameter might not be increasing the conductivity value of bed-parallel samples from Elimsport; therefore, there should be another parameter affecting the conductivity magnitude and it might be related to proppant placement. If the bed-perpendicular and bed-parallel samples are analyzed separately, it appears that the bed-perpendicular samples have higher conductivity with higher Young's Modulus and rougher surface. However, there is not enough data to confirm the possible relation with rock mechanical properties for the bed-perpendicular samples, see Figure 44.

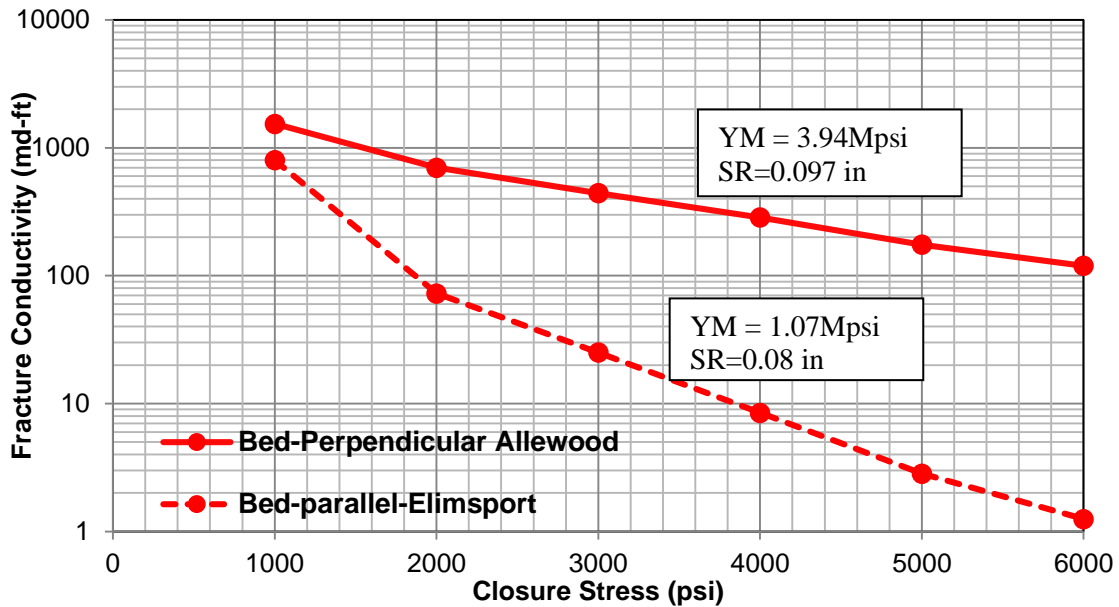


Figure 44: Comparison between bed-perpendicular samples

For bed-perpendicular samples, it can be seen a clear relationship between the surface roughness and the initial flow aperture, the rougher the surface the higher the conductivity. It also can be observed how the higher Young’s modulus maintain the conductivity through the different closure stress better than the low Young’s modulus. This was also observed by Jansen (2015) for bed-perpendicular samples. However, bed-parallel samples behave completely different, showing no correlation with roughness surface.

The effect of Poisson’s ratio on conductivity is not clear; the values presented by each sample appear to have no correlation with conductivity. Since the individual analysis of Young’s modulus and Poisson’s ratio did not show any correlation with conductivity, an analysis including both could bring different results. In order to include both parameters in a single term, the brittleness index definition will be used. Brittleness

Index is known as an indicator of how easy the rock can be fractured, there are many definitions of this index, the index proposed by Rickman et al. (2008) will be used in this study to analyze its relation with conductivity, this index combines Young's modulus and Poisson's ratio.

$$BI = \frac{E_B + \nu_B}{2} \quad (3.1)$$

Where

$$E_B = \frac{E - E_{min}}{E_{max} - E_{min}} \quad (3.2)$$

$$\nu_B = \frac{\nu - \nu_{max}}{\nu_{min} - \nu_{max}} \quad (3.3)$$

The maximum and minimum values were defined by Rickman et al. (2008).

Table 8: Brittleness index for Elimsport and Allenwood samples.

Elimsport		Allenwood	
BI (Average)- Bed-perpendicular	BI (Average)- Bed-parallel	BI (Average)- Bed-perpendicular	BI (Average)- Bed-parallel
0.34	0.28	0.58	0.63

From the Table 8, it can be concluded that brittleness index (BI) has not relationship with conductivity values, it is somewhat surprising that the sample with higher conductivity (Bed-parallel Elimsport) shows the lower BI meaning that it is the

worse prospect to fracture among the samples studied. The differences in Young's Modulus and Poisson's ratio do not have any correlation with conductivity values.

Previous studies have shown that the conductivity loss presents an exponential decline curve at increasing closure stress (Guzek, 2014. Briggs, 2014). However, for the Marcellus shale samples, at low closure stress (between 1000-2000 psi) it seems that the ratio of conductivity loss deviates from the exponential trend observed when closure stress present values smaller than 2000 psi. This behavior might be attribute to a change in the rate at which the proppant embeds, at low closure stress it could be reasonable to expect that the proppant embeds in the elastic zone of the rock, therefore, the change in slope of the conductivity loss at 2000 psi observed in Figure 44 could be caused by the transition from the elastic zone to the zone of permanent deformation. In order to verify if that was the reason for the sharp behavior at low closure stress, microscopic images were taken after a sample of flat surface was tested at 1000 psi and 0.051 lb/ft² areal concentration. Figure 45 and 46 shows the photos after the test.

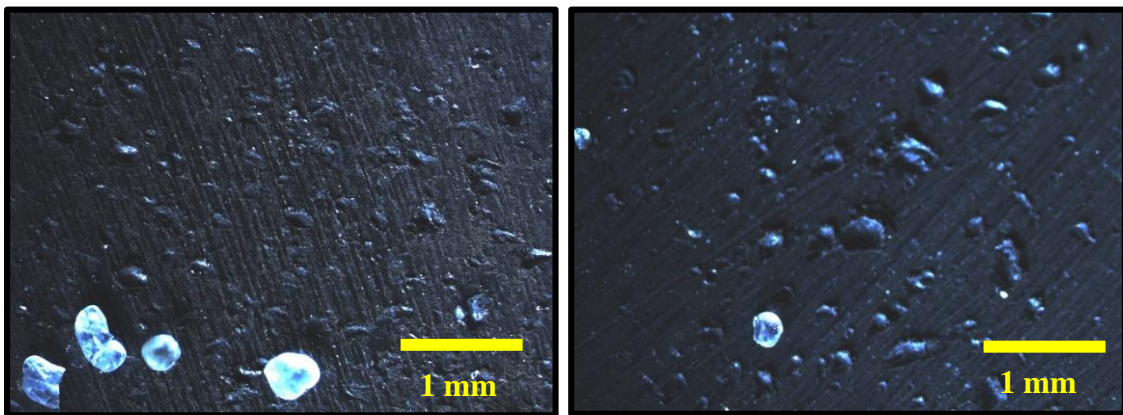


Figure 45: Embedment for Elimспорт samples at 1000 psi. (Left bed-perpendicular sample, right bed-parallel sample)

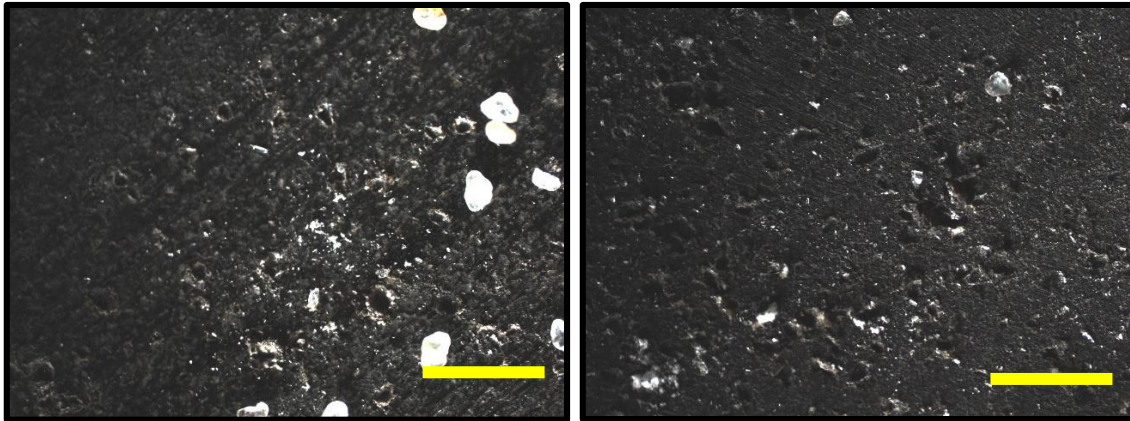


Figure 46: Embedment for Allenwood samples at 1000 psi. (Left bed-perpendicular sample, right bed-parallel sample)

From the images it can be observed that Elimsport and Allenwood samples at 1000 psi are already in the permanent deformation zone. The contact area of a sand proppant with the rock is very small which generates a high localized stress that it is going to cause a permanent deformation and the proppant to embed in the formation. It is important to highlight that for this study case the embedment is not expected to be as drastic as it would be in the presence of water. The images have the purpose to better understand the role of elastic behavior in conductivity loss. It seems that due to the high localized stress, the rock-proppant interaction goes directly to the plastic zone of the rock. Therefore, the conductivity loss will be related to the plastic behavior other than the elastic behavior. For this study, the plastic behavior will be quantified using the ultimate compressive strength, it would be expected that this parameter correlates better with conductivity than Young's modulus. Previous studies have shown that the Young's modulus of a rock is related to the compressive strength (D'Andrea, 1965, Chang et al.,

2006). Figure 47 shows the results of young's modulus and ultimate compressive strength for Marcellus samples.

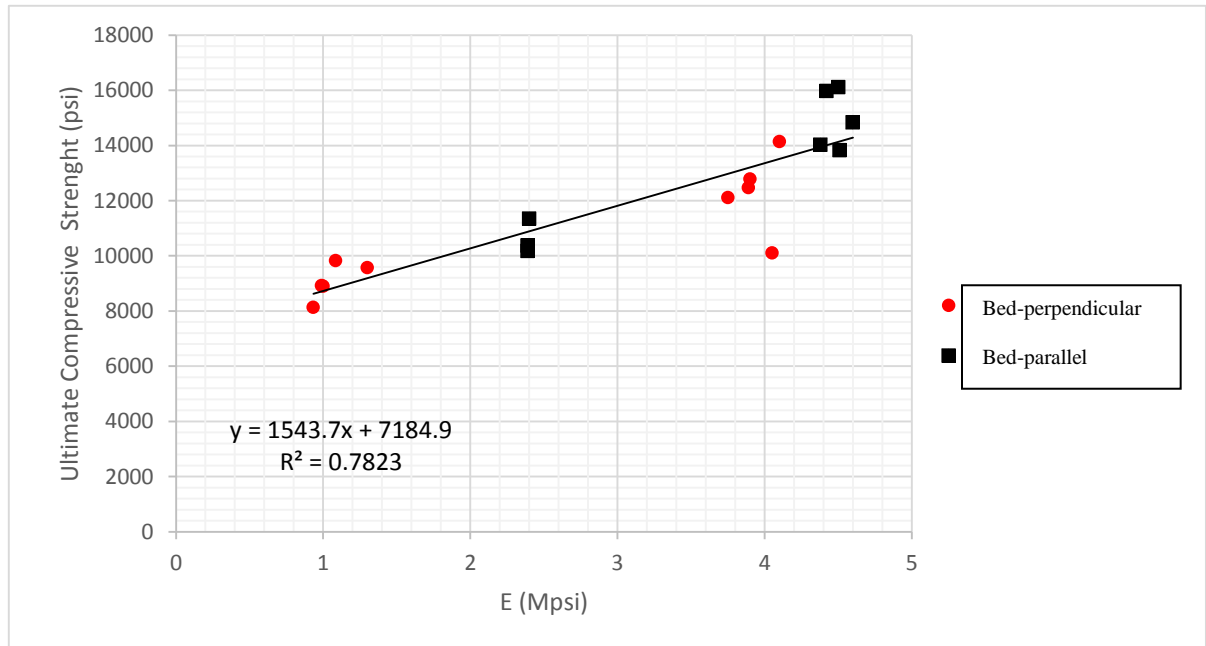


Figure 47: Relationship between Young's modulus and ultimate compressive strength

The results from Allenwood and Elimsport confirms that there is a relationship between Young's modulus and ultimate compressive strength. A larger Young's modulus seems to have a larger compressive strength, which brings back the relevance of Young's modulus in the conductivity behavior. The intention with the trend line is to make the relationship between the two variables clearer, but there is not enough data to support the linear trend observed between Young's modulus and ultimate compressive strength. There is not a straight-forward explanation for this apparent correlation between Young's modulus and rock strength since the failure depends mainly on the

microscale failure distribution because these ones will control where the rock starts to fail (Lockner et al., 1992).

3.4 Effect of Rock Properties on Fracture Conductivity Loss

The fracture conductivity loss is related to the increase in closure stress. For this analysis, the decline rate of each sample will be compared against the rock mechanical properties. The conductivity values at 1000 psi will be not taken into account since they deviate from the trend at the higher closure stress, additionally, such a low closure stresses might not happen in a real stimulation process due to the depth at which Marcellus Shale is typically drilled. Jansen (2014) proposed the following relation to describe how the conductivity behaves at different closure stresses.

$$k_f w_f \cong (k_f w_f)_0 e^{-\lambda \sigma_c} \quad (3.4)$$

Where $(k_f w_f)_0$ is the conductivity value at 0 psi closure stress, λ is the conductivity decline rate constant, and σ_c is the closure stress. Figure 48 and 49 shows the average propped conductivity with the exponential fit.

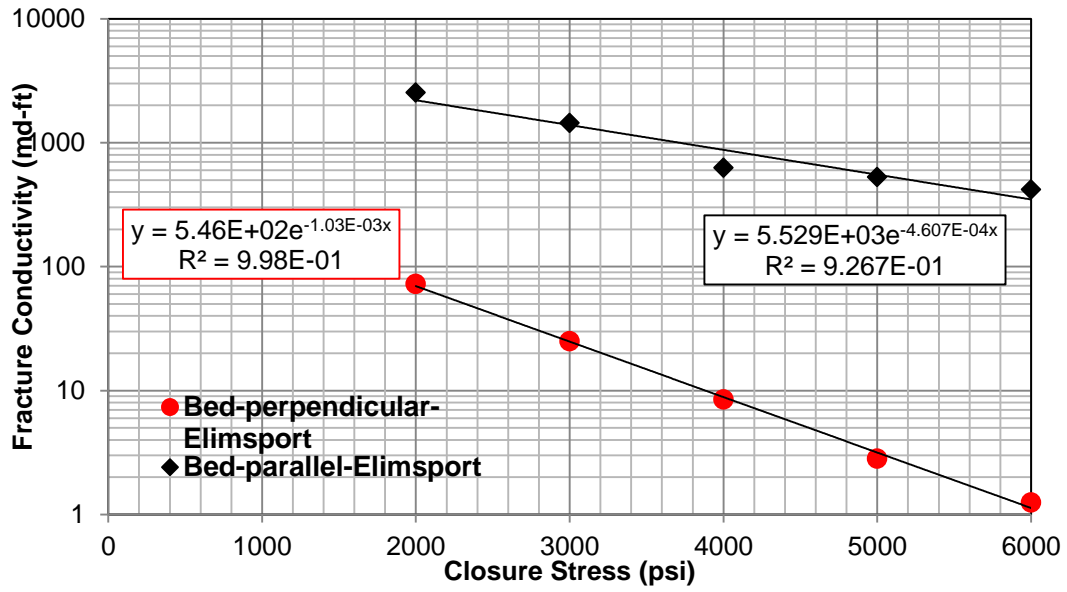


Figure 48: Elimsport average propped conductivity with the exponential fit.

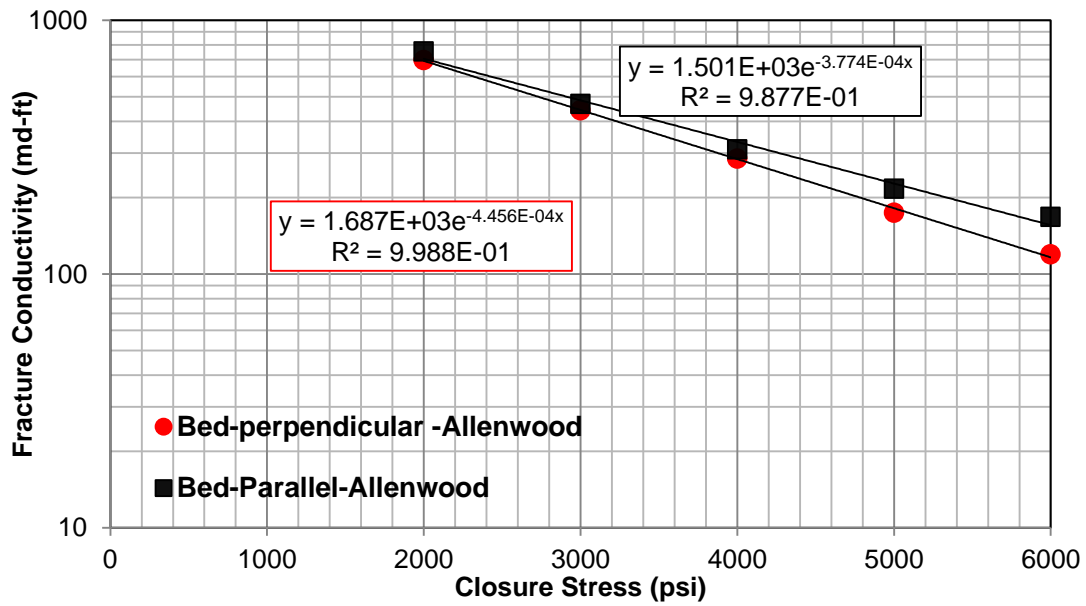


Figure 49: Allenwood average propped conductivity with the exponential fit.

The exponential fit shows a good relation with all the samples, which agrees with the behavior represented by equation 3.4. The Allenwood samples show smaller decline rates than The Elimspport samples. For the bed-parallel samples, Allenwood has a decline constant of $3.77 \times 10^{-4} \text{ psi}^{-1}$ which is smaller than the Elimspport sample of $4.60 \times 10^{-4} \text{ psi}^{-1}$. The same behavior can be observed for the bed-perpendicular samples where Allenwood has a decline rate of $4.45 \times 10^{-4} \text{ psi}^{-1}$ and Elimspport $1.03 \times 10^{-3} \text{ psi}^{-1}$. The results support the idea that a higher Young's modulus is related to a lower decline rate of conductivity. A correlation with ultimate compressive strength can also be observed. It appears that when Young's modulus is higher than 2 Mpsi, the differences in the decline rate among the samples becomes smaller. However it is hard to quantify if this behavior is related to only Young's modulus since the surface roughness could be affecting the rate at which conductivity decreases. For rough surfaces the proppant placement and contact area could help to keep the fracture open, which could result in a lower decline rate. Therefore, we could expect that the difference in decline rate is smaller than what it is shown in the previous graphs. Additionally, the quantification of surface roughness shows a correlation with conductivity decline rate as well, where the rougher surface is associated with the samples with the lowest decline rate and the smoother surface with the highest decline rate. This makes it difficult to quantify the real effect of young's modulus in conductivity loss. It is important to mention that the observations made from this results only took into account four different sets of samples. Although each set was tested multiple times, an irregular set of samples could lead into a wrong conclusion. For this reason, the behavior observed should be verify with multiple set of

samples with a variety of rock mechanical properties to corroborate the behavior observed in this study.

Due to the relative closeness of the values in the decline rate for samples with Young's modulus greater than 2Mpsi, it could be said that the relationship between the rock mechanical properties and the conductivity decline rate is non-linear. Figure 50 shows the trend found between these two variables. Each conductivity sample was plotted with its corresponding Young's Modulus result.

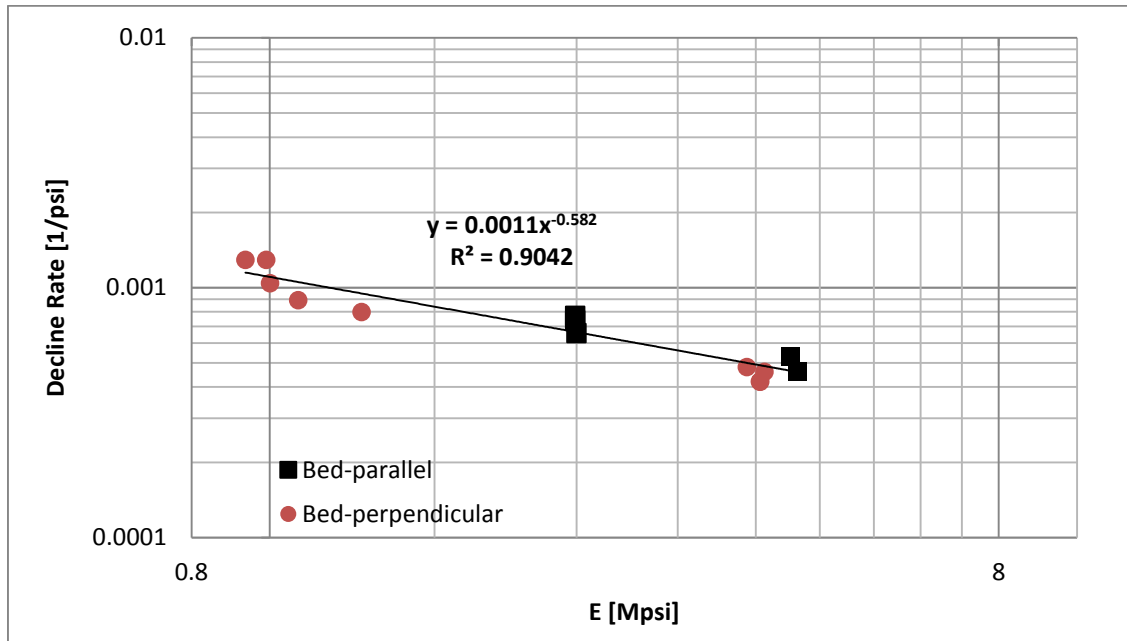


Figure 50: Relationship between Young's modulus and conductivity decline curve at 0.051 lb/ft² proppant

As mentioned earlier, the conductivity decline rate does correlate with Young's modulus. The power trend line was selected to describe the behavior over the Young's modulus range tested. The relationship between decline rate and Young's modulus for

Marcellus shale at 0.051 lb/ft² areal concentration of 40/70 white mesh sand follows the function:

$$\lambda (\text{psi}^{-1}) = f(E) = 0.0011E^{-0.582} \quad (3.5)$$

The power trendline indicates that the conductivity decline rate increase with decreasing Young's modulus, and it sharply increases with Young's modulus smaller than 2 Mpsi. Low Young's moduli are considered characteristic of "ductile" shales and it would be challenging to maintain the flow path for economic production.

Alramhi et al. (2012) studied the relationship between proppant embedment and Young's modulus using high strength bauxite proppant of 20/40 mesh and a monolayer of proppant. Their relationship between proppant embedment depth at 5000 psi and Young's modulus is the following:

$$\text{Proppant Embedment (mm)} = 0.3685E^{-0.549} \quad (3.6)$$

This correlation has a similar behavior to the one presented for the Marcellus Shale. It seems that the power trendline explains how the proppant embeds with different Young's modulus, since both correlations show such a similar behavior where the proppant embedment ratio and decline rate ratio are close, we could concluded that the main mechanism for conductivity loss is proppant embedment. The slight difference between both correlations could be caused by the effect of surface roughness in conductivity loss, the differences in experimental set ups or proppant crushing. However, it seems that this behavior scales proppant sizes and types as well as different formations.

Proppant embedment is mainly controlled by plastic deformation, as it was shown previously, therefore we would expect that the correlation between ultimate compressive strength and conductivity decline rate has a similar behavior as the proppant embedment correlation. Figure 51 shows the correlation between conductivity loss and ultimate compressive strength.

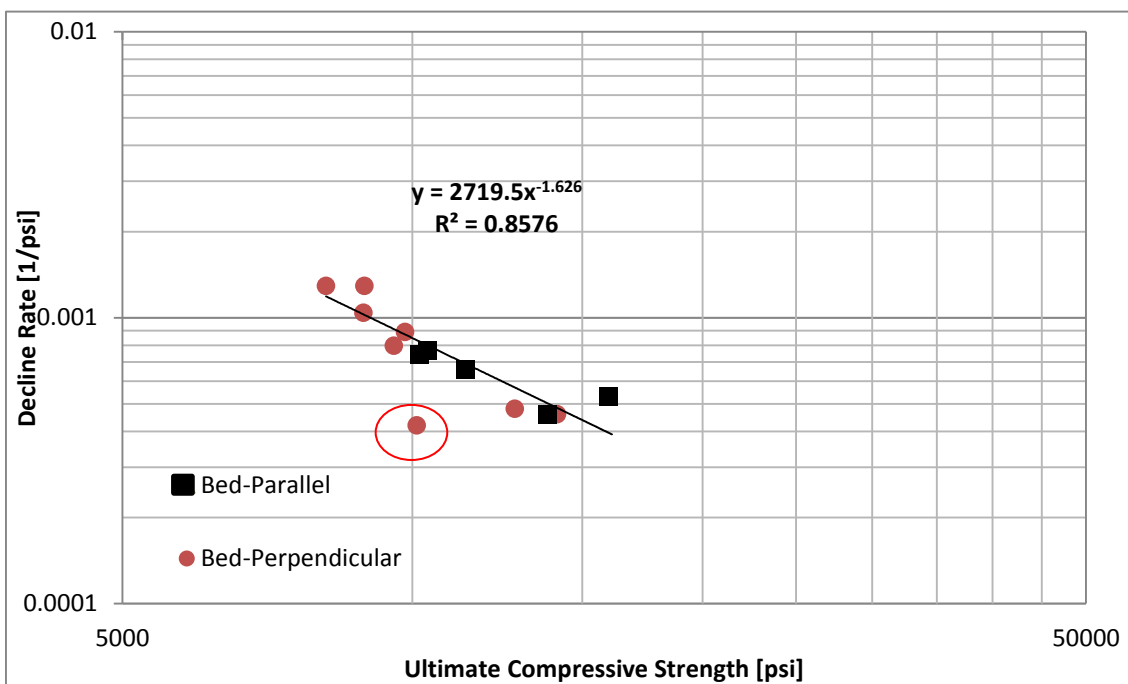


Figure 51: Relationship between ultimate compressive strength and conductivity decline rate

From the graph, it can be seen that the correlation between ultimate compressive strength and conductivity decline rate has the shape of a power trendline as well. This was somewhat expected, but it seems the correlation with strength values is not as good as with Young's modulus. There are some outliers values that might change the correlation between these two variables. The circled value in Figure 51 is an outlier

value since it is below the 1.5 interquartile range of first quartile, and it was thought to be the result of the presence of a small fracture that led to an earlier failure of the sample. Ultimate compressive strength is more susceptible to be affected by irregularities. The correlation between ultimate compressive strength and conductivity decline rate might be highly influenced by other factors such as micro scale failure distribution which can be unique for each specimen and it makes this graph less reliable.

The main lesson that we can take from the results is that higher Young's modulus generally leads to a higher ultimate compressive strength and these parameters accompanied by a rough fracture surface decreases the ratio of conductivity loss. Proppant embedment seems to be the main mechanism for conductivity loss. Proppant embedment was shown to be permanent deformation, not elastic behavior for the Marcellus Shale; the relationship between Young's modulus and ultimate compressive strength is creating a false correlation between Young's modulus and embedment, and also with conductivity loss.

For Young's modulus higher than 2 Mpsi or ultimate compressive strength higher than 9000 psi the differences in decline rate are smaller. This correlation was observed for proppant monolayer concentration. When proppant concentration increases to form multiple layers on the fracture surface, the correlation between conductivity loss and rock mechanical properties might change.

Multiple layers of proppant reduce the effect of rock properties on conductivity behavior. Conductivity loss will be control by the proppant pack compression and the effect of proppant-rock behavior will be minimum.

3.5 Mechanical Anisotropy

Elastic anisotropy of Marcellus shale was observed for Elimsport and Allenwood locations. For the Elimsport samples the anisotropy effect is far more pronounced between bed-parallel and bed-perpendicular samples than in the Allenwood samples. This might be the reason why the conductivity values and decline rate present such a different values between the different orientations. In order to investigate if the anisotropy of these samples has any effect to the conductivity results observed, the anisotropy ratio of the elastic properties will be compared with the ratio of the conductivity decline curve for both locations. Table 9 shows the results for this comparison.

Table 9: Summary of anisotropy and conductivity decline rate values

Sample	Anisotropy – Core samples $c' = 0.5 \left(\frac{E_{max}}{E_{min}} + \frac{\nu_{max}}{\nu_{min}} \right)$	Error (%)	Anisotropy – Conductivity samples $c = \frac{\lambda_{max}}{\lambda_{min}}$	Error (%)
Elimsport	1.78	52	2.23	55.3
Allenwood	1.08	10.6	1.18	15.2
Sample	Anisotropy – Core samples $c' = \left(\frac{E_{max}}{E_{min}} \right)$	Error (%)	Anisotropy – Conductivity samples $c = \frac{\lambda_{max}}{\lambda_{min}}$	Error (%)
Elimsport	2.24	55.4	2.23	55.3
Allenwood	1.12	11.2	1.18	15.2

The table presents two different definitions for elastic anisotropic in core samples. The first includes Young’s Modulus and Poisson’s ratio, and the second only

includes Young's modulus. Both anisotropy definitions are compared with the ratio of bed-perpendicular conductivity decline rate to bed-parallel. The results show that the difference in average Young's modulus due to orientation is directly related to the difference in average conductivity decline rate. This comparison shows that higher the anisotropy ratio, the higher the gap between the conductivity decline rate for bed-perpendicular and bed-parallel samples, therefore anisotropy does have an effect in conductivity loss. The inclusion of Poisson's ratio seems to change the anisotropy ratio that does not compare as well with the conductivity decline rate, thus, the effect of Poisson's ratio is still undetermined.

4. CONCLUSIONS AND RECOMMENDATIONS

4.1 Conclusions

This thesis presents the results of the comparison between the rock mechanical properties and the fracture conductivity for the Marcellus Shale. A series of different experiments were performed in order to gather data to understand the relationship between these properties. The rock mechanical properties were obtained through triaxial compressive tests on cylindrical samples, the mineral composition was acquired using XRD analysis, and the conductivity data was summarized from previous work. The findings present in this study were obtained using four different sets of samples. Although each set was tested multiple times, an irregular set of samples could lead into a wrong conclusion, therefore the rock mechanical properties observed should be confirmed with multiple set of samples. The conclusions obtained from the laboratory experiments are presented below:

- 1) The laboratory results showed that the Marcellus Shale has a wide variation in the elastic properties. Both set of samples presented anisotropic behavior where bed-parallel samples (cut parallel to the bedding plane) showed higher Young's modulus and ultimate compressive strength consistently.
- 2) The elastic mechanical properties presented persistent differences in the values measure during the first loading cycle, which were lower than the values measure during second and third loading cycle.

- 3) Conductivity behavior is controlled by a combination of proppant properties and rock mechanical properties.
- 4) The magnitude of the conductivity for a monolayer concentration does not only depend on Young's Modulus or surface roughness.
- 5) In proppant monolayer concentration for Marcellus shale, the main parameter controlling conductivity loss is proppant embedment. It seems that due to the high localized stress, the rock-proppant interaction leads to the permanent deformation zone of the rock. However, it was shown that higher Young's Modulus leads to a higher ultimate compressive strength, which explains why the elastic mechanical properties shown a relationship with conductivity.
- 6) For proppant monolayer concentration, the results support the idea that a higher Young's modulus decreases the decline rate of conductivity. This can also be observed with ultimate compressive strength. A Young's modulus higher than 2 Mpsi and ultimate compressive strength higher than 9000 psi decreases the differences in the decline rate among the samples, where a power function describes the relationship between Young's Modulus and conductivity decline curve.

4.2 Recommendations

The scope of this work can be extended in different directions, the following are the recommendation to continue this study:

- 1) Most of the observations came from Marcellus shale propped conductivity, in order to prove the behavior observed in this study, more samples should be used from additional shale formations maintaining the same proppant characteristics to make the results comparable.
- 2) Unpropped conductivity should be measure for the Marcellus shale in order to understand better the role of the rock mechanical properties and surface roughness in this formation.
- 3) Additional measurements should be performed in order to better understand the fracture conductivity behavior and its relationship with rock mechanical properties. Brinell hardness testing should be incorporated to understand the mechanical behavior in the fracture surface, also the total organic content (TOC) should be measure in order to understand how it could affect the rock mechanical properties.
- 4) Fracture conductivity measurements and rock mechanical measurement should be exposed to fracture fluids in order to understand better how the mineralogy could affect the mechanical behavior of the rock.

REFERENCES

Akrad,O., Miskimins, J., Prasad, M. (2011). The effects of Fracturing Fluids on Shale Rock Mechanical Properties and Proppant Embedment. SPE 146658. SPE Annual Technical Conference and Exhibition. Denver, CO. 2011. Copyright 2011, Society of Petroleum Engineers

Alramahi, B., Sundberg, M.I. (2012). Proppant Embedment and Conductivity or Hydraulic Fractures in Shales. US Rock Mechanics / Geomechanics Symposium. Chicago,Illinois. 2012. Copyright 2012 ARMA, American Rock Mechanics Association.

ASTM Standard D4543-08. (2008). Standard Practices for Preparing Rock Core as Cylindrical Test Specimens and Verifying Conformance to Dimensional and Shape Tolerances. ASTM International. West Conshohocken, PA, 2008. DOI:10.1520/D4543-08. www.astm.org

ASTM Standard D7012-14. (2014). Standard Test Methods for Compressive Strength and Elastic Moduli of Intact Rock Core Specimens under Varying States of Stress and Temperatures. ASTM International. West Conshohocken, PA, 2014. DOI: 10.1520/D7012-14. www.astm.org

Borstmayer, R., Stegent, N., Wagner A., Mullen J. (2011). Approach Optimizes Completion Design. The American Oil & Gas Reporter. www.aogr.com.

Barton, N., Bandis, S., Bakhtar, K. (1985). Strength, Deformation and Conductivity Coupling of Rock Joints. *Int. J. Rock Mech. Min. Sci. & Geomech.*, vol. 30, No 3, 1985.

Briggs, K. (2014). The Influence of Vertical Location on Hydraulic Fracture Conductivity in the Fayetteville Shale. Master's Thesis: Texas A&M University Petroleum Engineering. Copyright 2014, Kathryn Elizabeth Briggs.

Brime, C. (1985). The Accuracy of X-ray Diffraction Methods for Determining Mineral Mixtures. *Mineralogical Magazine*, Vol. 49. Pp. 531-538

Che, C., Martysevich, V., O'Connell, P., Hu, D., Matzar, L. (2014). Temporal Evolution of the Geometrical and Transport Properties of a Fracture-Proppant System under Increasing Mechanical Loading. Paper SPE 171572-MS presented at the SPE Annual Technical Conference and Exhibition, Calgary, Alberta, Canada, 30 September-2 October. Copyright 2014, Society of Petroleum Engineers.

Cui, A., Glover, K., Wust, R.A.J. (2014). Elastic and Plastic Mechanical Properties of Liquids-Rich Unconventional Shales and their Implications for Hydraulic

Fracturing and Proppant Embedment: A case study of the Nordegg Member in Alberta, Canada. Paper ARMA 14-7556 presented at the 48th US Rock Mechanics/ Geomechanics Symposium, Minneapolis, MN,USA, 1-4 June.

D'Andrea, D. V., Fischer, R. L., Fogelson, D. E. (1965). Prediction of Compressive Strength from Other Rock Properties. United States Department of the Interior, Bureau of Mines. Report of investigations 6702, Washington D.C.

Economides, M.J. and Nolte, K.G. (2000). Reservoir simulation, 3rd Edition, Wiley and Sons Ltd., United Kingdom.

Economides, M.J., Hill, D.A., Ehlig-Economides, C., Zhu, D. (2012). Petroleum Production Systems, Second Edition. Englewood Cliff, N.J. PTR Prentice Hall.

Engelder, T., and Lash, G.G., (2008). Marcellus Shale play's vast resource potential creating stir in Appalachia: The American Oil and Gas Reporter. May 2008, 7 p.

Engelder, T., (2008a). Structural geology of the Marcellus and other Devonian gas shales: geological conundrums involving joints, layer-parallel shortening strain, and the contemporary tectonic stress field. Pittsburgh Association of Petroleum Geologists Field Trip (Sept. 12–13, 2008), 96 p

Engelder, T., and Lash, G.G., (2011). Thickness trends and sequence stratigraphy of the Middle Devonian Marcellus Formation, Appalachian Basin: Implications for Acadian foreland basin evolution. The American Association of Petroleum Geologist. Bulletin, V. 95, NO.1. January 2011.

Fjaer, E., Holt, R.M., Horsrud, P., Raaen, A.M., and Risnes, R. (2008). Petroleum Related Rock Mechanics, Second Edition. Elsevier, Hungary, 2008. ISBN: 978-0-444-50260-5.

Fredd, C. N., McConnell, S. B., Boney, C. L., England, K. W. (2000). Experimental Study of Fracture Conductivity Demonstrates the Benefits of Using Proppants SPE 60326. SPE Rocky Mountain Regional/Low Permeability Reservoirs Symposium. Denver, CO,2000. Copyright 2000, Society of Petroleum Engineers.

Gao, Y., Lv, Y., Wang, M., and Li, K. (2012). New Mathematical Models for Calculating the Proppant Embedment and Fracture Conductivity. Paper SPE 155954 presented at the SPE Annual Technical Conference and Exhibition, San Antonio, Texas, U.S.A., 8-10 October.

Gottschling, J., (2007). Appalachian Basin black shale exploitation: past, present, and future: Presentation IOGA of PA annual meeting. May 2007, 49 p., http://www.wvsoro.org/resources/marcellus/John_Gott_Marcellus%20Shale.pdf.

Guo, J., Liu, Y. (2012). Modeling of Proppant Embedment: Elastic Deformation and Creep Deformation. Paper SPE 157449 presented at the SPE Annual Technical Conference and Exhibition, Doha, Qatar, 14-16 May.

Guzek, J. (2014). Fracture Conductivity of the Eagle Ford Shale. Master's Thesis. Texas A&M University Petroleum Engineering. Copyright 2014, James J. Guzek.

Holt, R.M., Fjaer, E., Nes, O.M. et al. (2011). A shaly look at Brittleness. Paper ARMA 11-366 presented at the 45th US Rock Mechanics/ Geomechanics Symposium, San Francisco, California, USA 26-29 June.

Jansen, T. (2014). The effect of rock properties on hydraulic fracture conductivity in the Eagle Ford and Fayetteville Shales. Master's Thesis. Texas A&M University Petroleum Engineering. Copyright 2014, Timothy A. Jansen.

Karato, S and Wenk, H (Eds). (2002). Plastic Deformation of minerals and rocks. The mineralogical society of America. Washington DC. 2003. ISBN: 0-93995063-3.

Lacy, L.L., Rickards, A.R., Ali, S.A., (1997). Embedment and fracture conductivity in soft formations associated with HEC, borate and water-based fracture designs. SPE Annual Technical Conference and Exhibition. San Antonio, Texas.

National Energy Technology Laboratory DOE/NETL2011/1478, (2011). A Comparative Study of the Mississippian Barnett Shale, Fort Worth Basin, and Devonian Marcellus Shale, Appalachian Basin. U.S. Department of Energy.

Matthews, H. L., Schein, G. W., Malone, M. (2007). Stimulation of Gas Shales: They're All the Same Right?. Paper SPE 106070. SPE Hydraulic Fracturing Technology Conference. College Station, TX, USA. 29-31 January. Copyright 2007, Society of Petroleum Engineers.

Mayerhofer, M.J. and Meehan, D.N. (1998). Waterfracs—Results from 50 Cotton Valley Wells. Paper SPE 49104 presented at the SPE Annual Technical Conference and Exhibition, New Orleans, Louisiana, USA, 27–30 September.

McGinley, M. (2015). The effects of fracture orientation and anisotropy on hydraulic fracture conductivity in the Marcellus Shale. Master's Thesis. Texas A&M University Petroleum Engineering. Copyright 2015, Mark J. McGinley.

Mullen, J. (2010). Petrophysical Characterization of the Eagle Ford Shale in South Texas. Canadian Unconventional Resources and International Petroleum Conference. Calgary, Alberta, 2010. Copyright 2010, Society of Petroleum Engineers.

Paterson, M. S. and Wong, T. (2005). *Experimental Rock Deformation – The Brittle Field*, Second Edition. Springer-Verlag Berlin Heidelberg, The Netherlands, 2005. ISBN: 3-540-24023-3.

Penny, G. S. (1987). *An Evaluation of the Effects of Environmental Conditions and Fracturing Fluids Upon the Long-Term Conductivity of Proppants*. SPE Annual Technical Conference and Exhibition. Dallas, Texas, 1987 Copyright 1987, Society of Petroleum Engineers.

Prasanta, D., Achalpukar, M. (2013). *Impact of Rock Mechanics and Formation Softening Analysis in Shale Fracturing Fluid Design*. SPE Annual Technical Conference and Exhibition, Mishref, Kuwait. Copyright 2013, Society of Petroleum Engineers.

Rickman, R., Mullen, M., Petre, E. Grieser, B., Kundert, D. (2008). *A Practical Use of Shale Petrophysics for Stimulation Design Optimization: All Shale Plays Are Not Clones of the Barnett Shale*. SPE Annual Technical Conference and Exhibition, Denver, Colorado, 2008. Copyright 2008, Society of Petroleum Engineers.

Sone, H., and M. D. Zoback, (2013). Mechanical properties of shale gas reservoir rocks — Part 1: Static and dynamic elastic properties and anisotropy. *Geophysics*, 78, DOI: 10.1190/geo2013-0050.1.

Sumi, L., (2008). Shale Gas: Focus on the Marcellus Shale, for the Oil and Gas Accountability Project/ Earthworks.
<http://www.earthworksaction.org/marcellusshale08.cfm>, accessed July 2009

Undul, O., Amann, F., Aysal, N., Plotze, M. (2015). Micro-Textual Effects on Crack Propagation of Andesitic Rock. Elsevier.

US Geological Survey. (2011). Assessment of Undiscovered Oil and Gas Resources of the Devonian Marcellus Shale of the Appalachian Basin Province. Retrieved from <http://pubs.usgs.gov/fs/2011/3092/pdf/fs2011-3092.pdf>

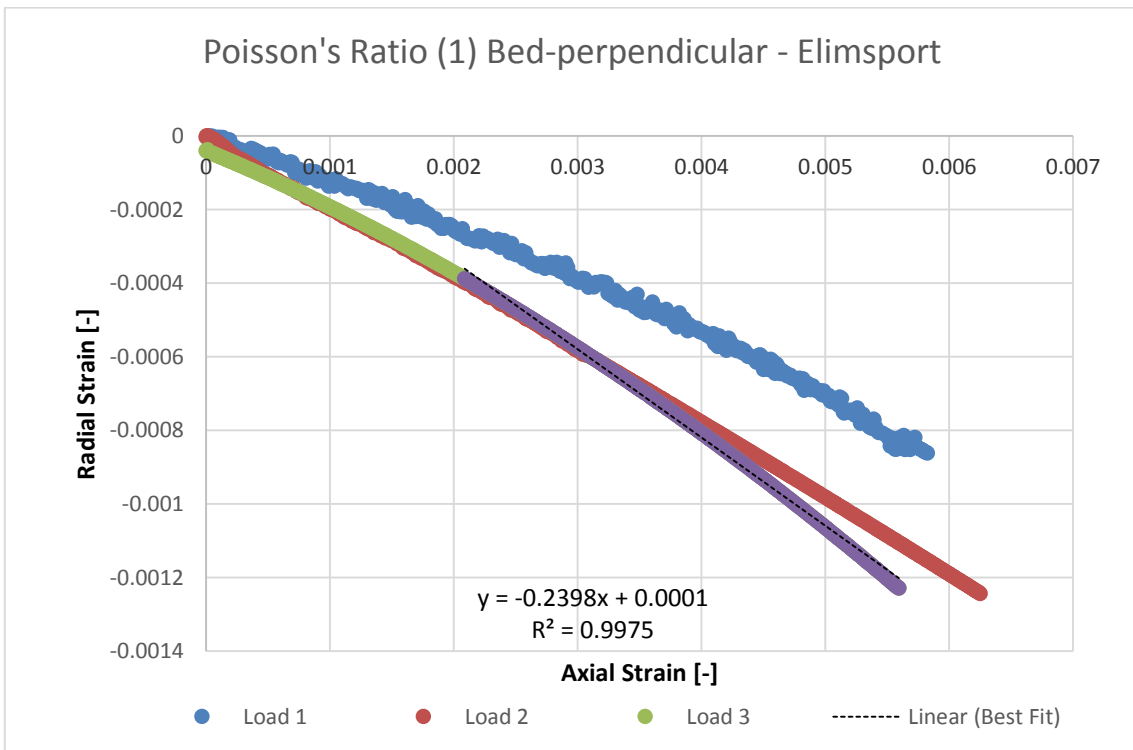
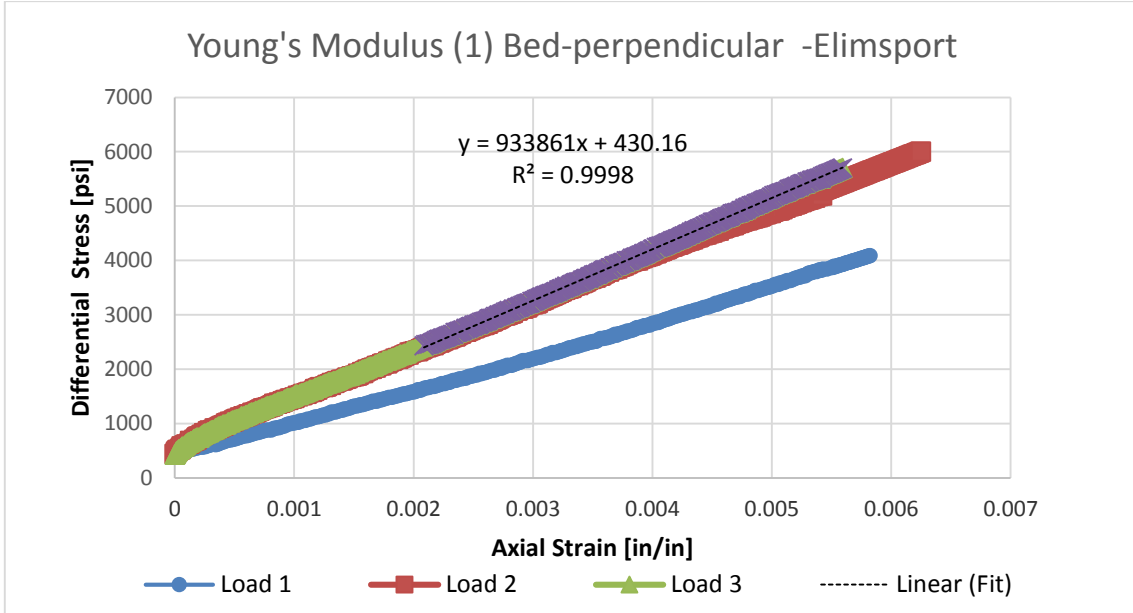
Warpinski, N.R., (2009). Stress Amplification and Arch Dimensions in Proppant Beds Deposited by Waterfracs. SPE Annual Technical Conference and Exhibition. The Woodlands, Texas, USA, 19-21 January. Copyright 2009, Society of Petroleum Engineers

Zhang, Junjing, Kamenov, A., Zhu, D., Hill, A.D. (2013). Laboratory Measurement of Hydraulic Fracture Conductivities in the Barnett Shale. SPE Hydraulic

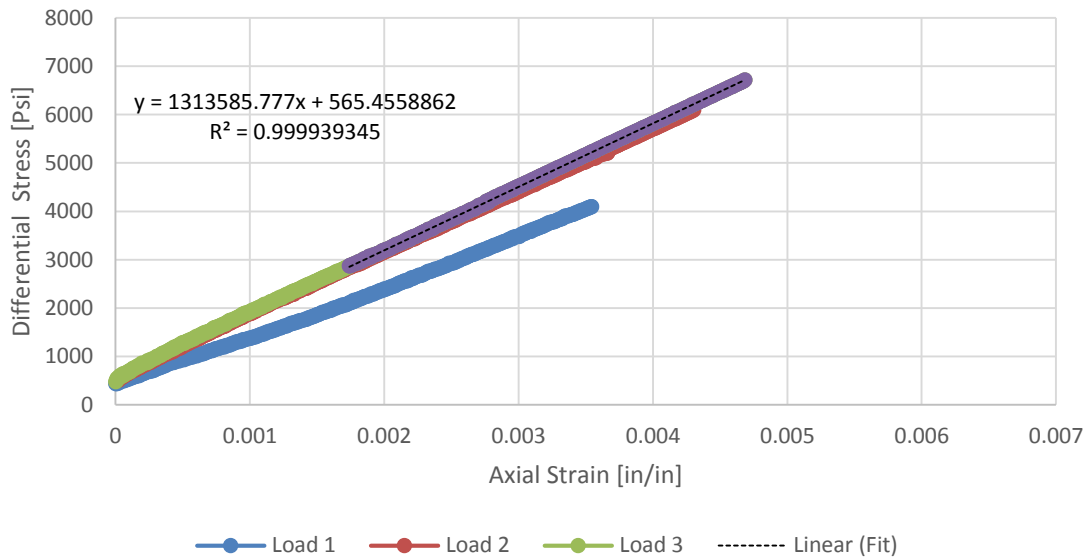
Fracturing Technology Conference, The Woodlands, Texas, 2013. Copyright
2013, Society of Petroleum Engineers.

APPENDIX A

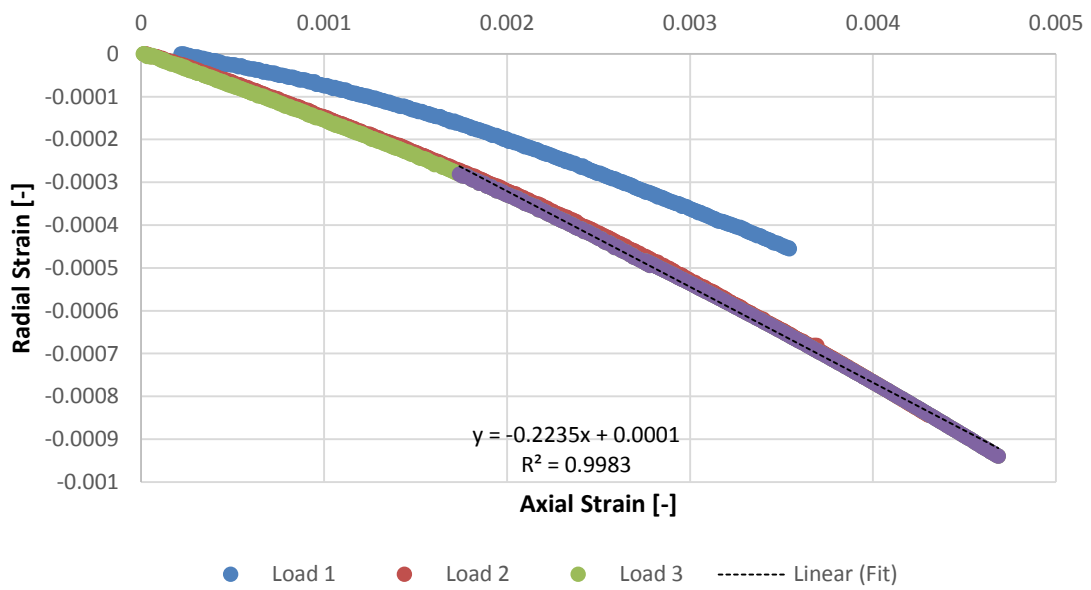
Elimsport Results

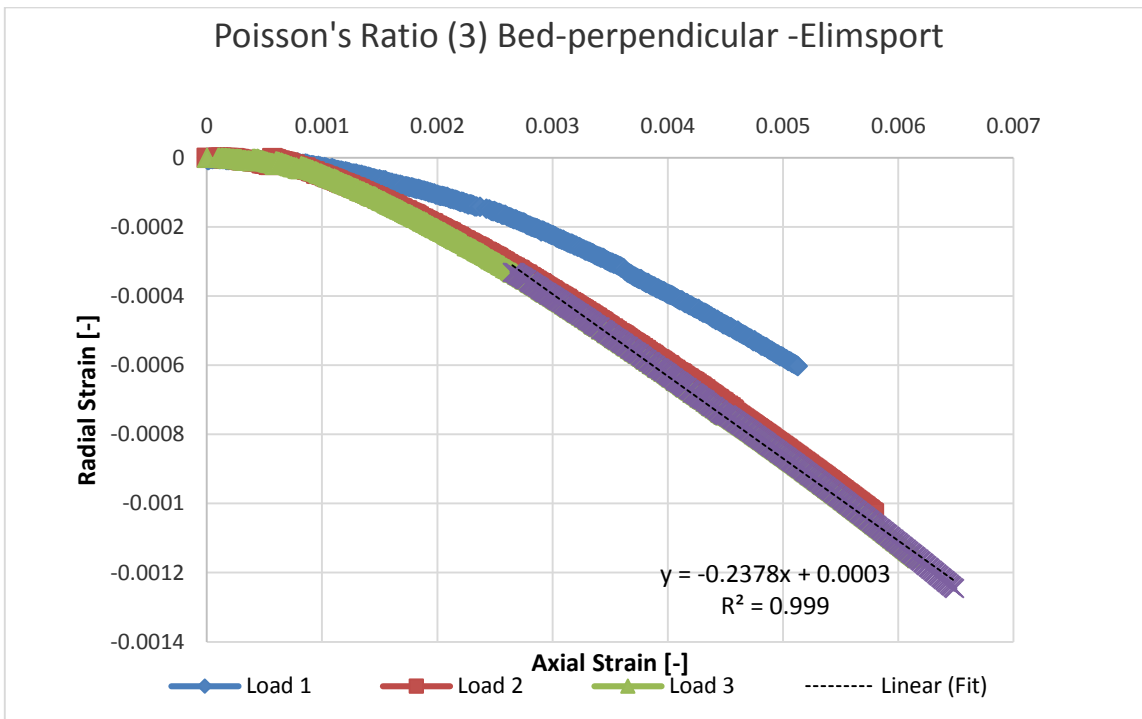
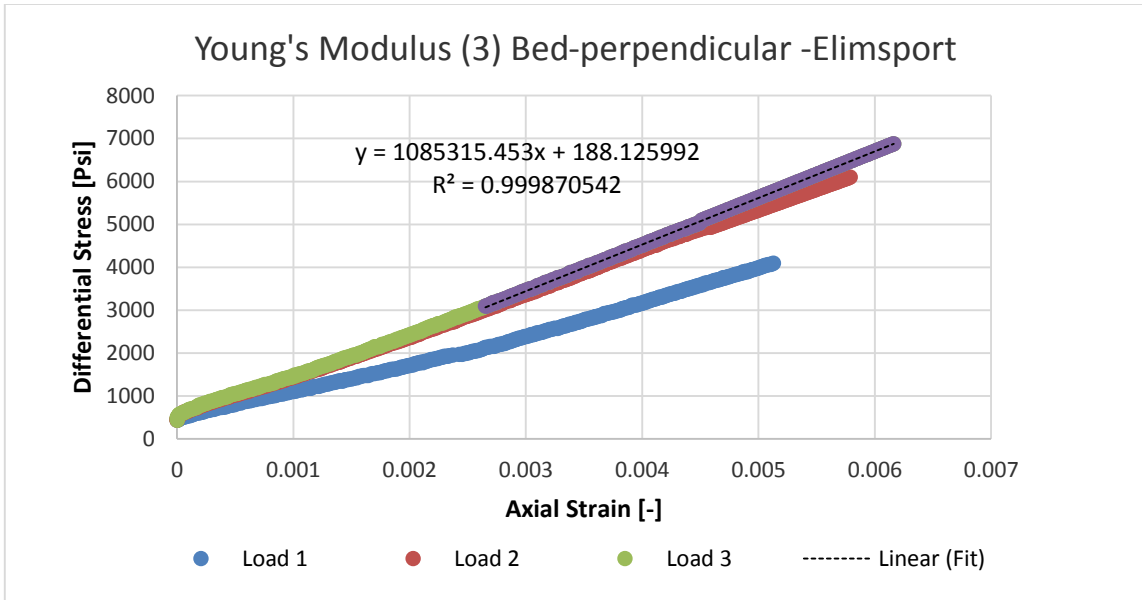


Young's Modulus (2) Bed-perpendicular -Elimsport

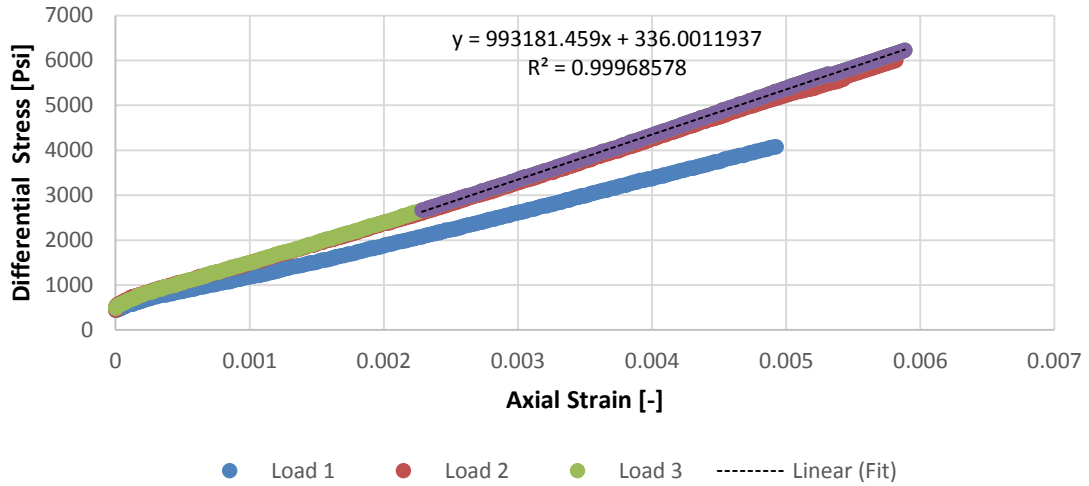


Poisson's Ratio (2) bed-perpendicular - Elimsport

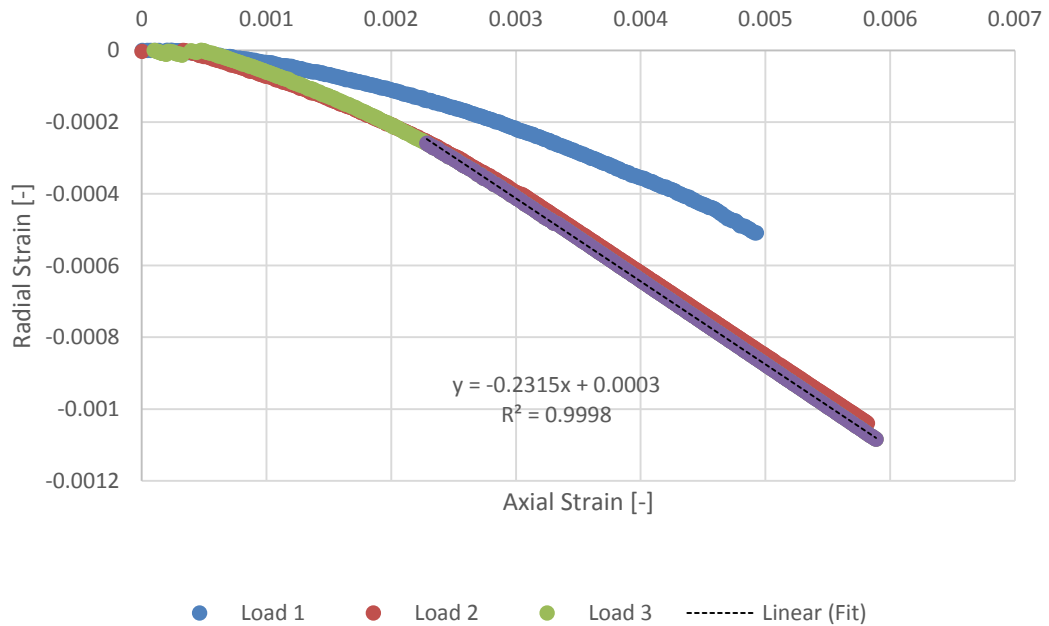




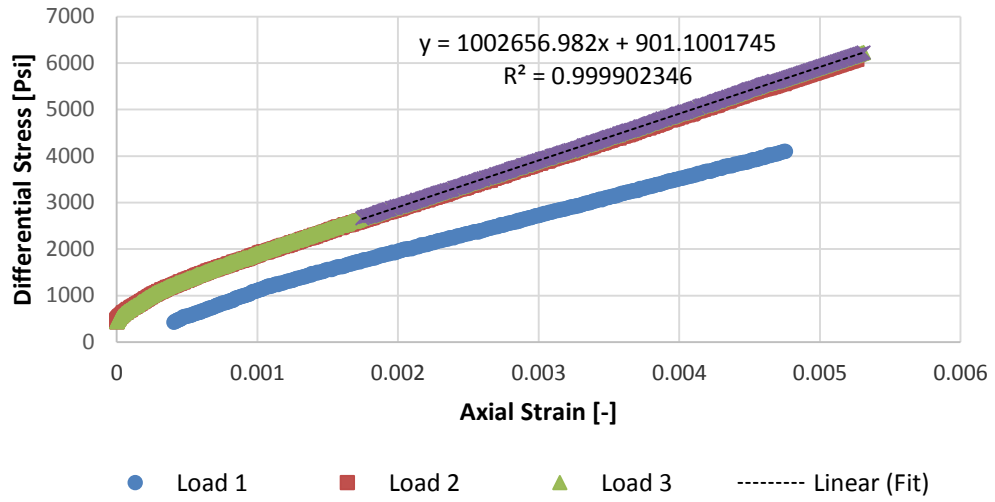
Young's Modulus (4) Bed-perpendicular -Elimsport



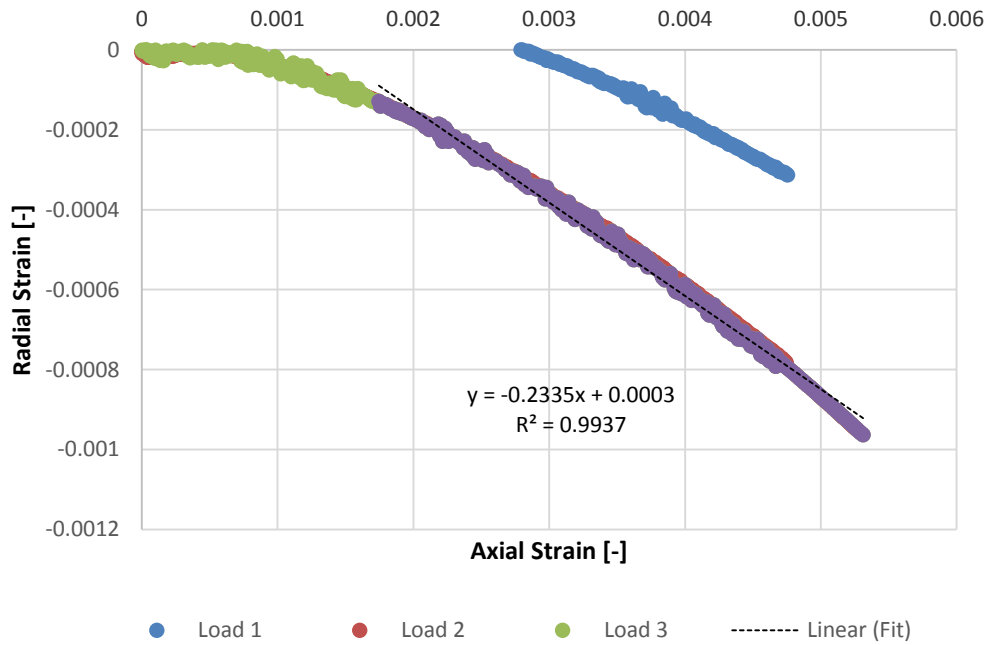
Poisson's Ratio (4) Bed-perpendicular -Elimsport

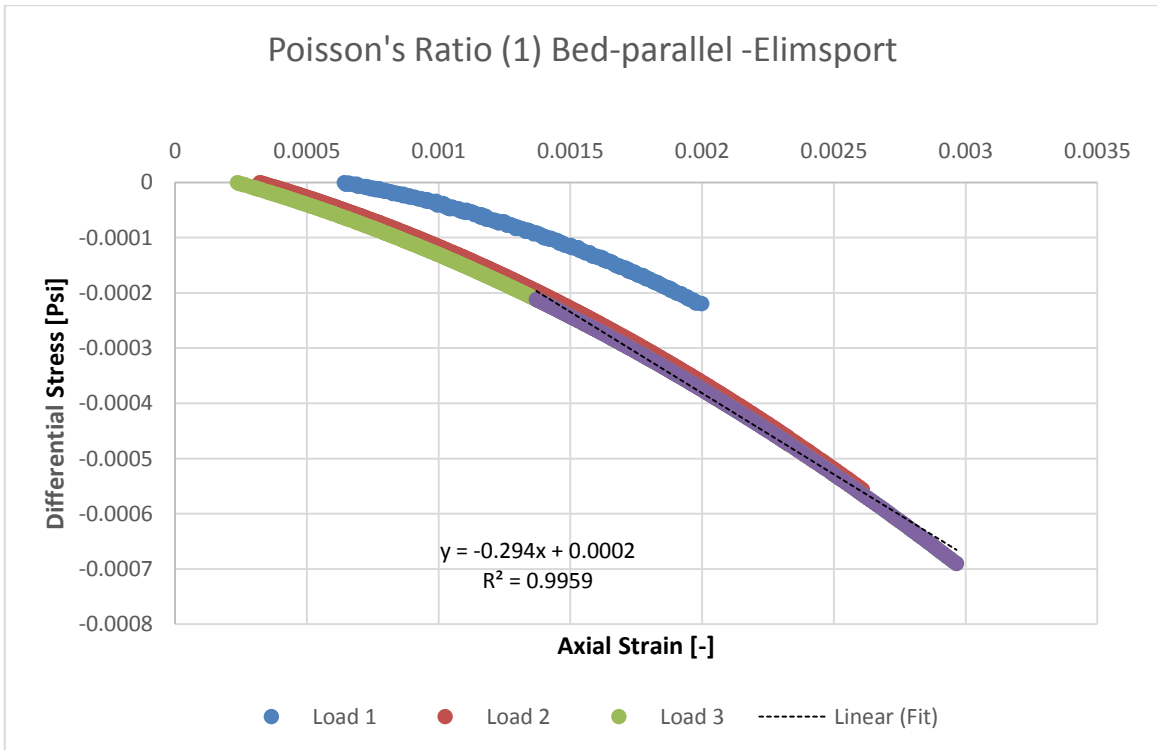
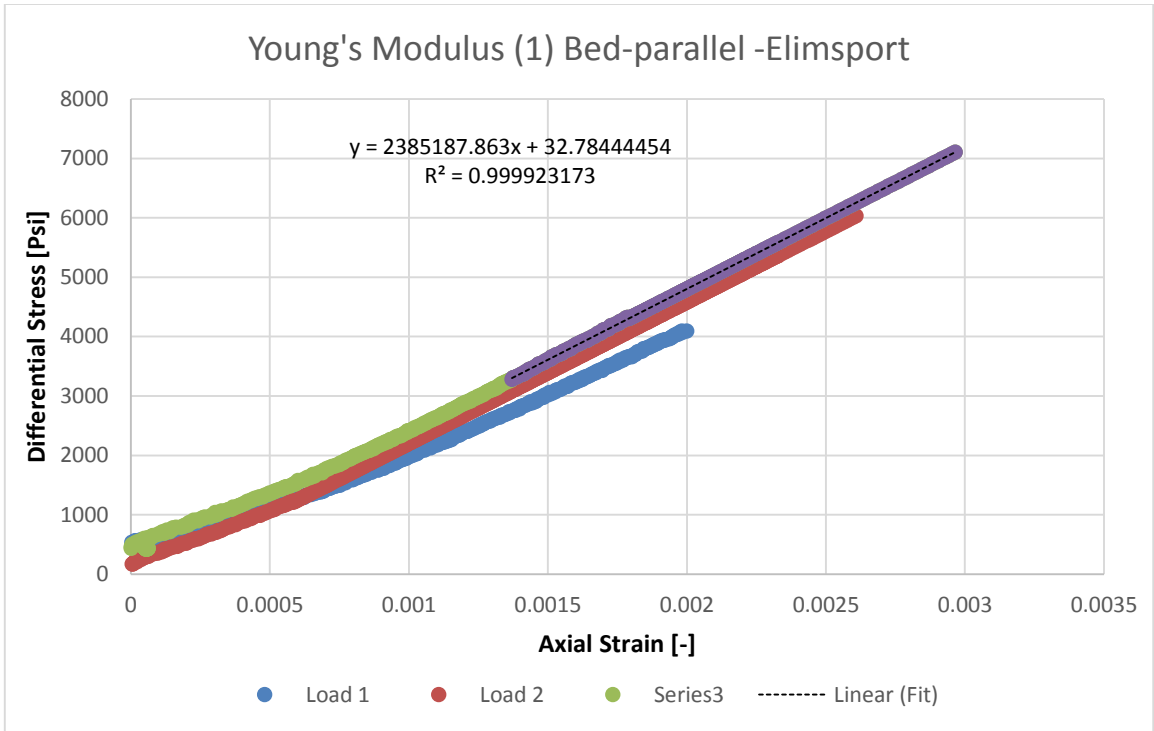


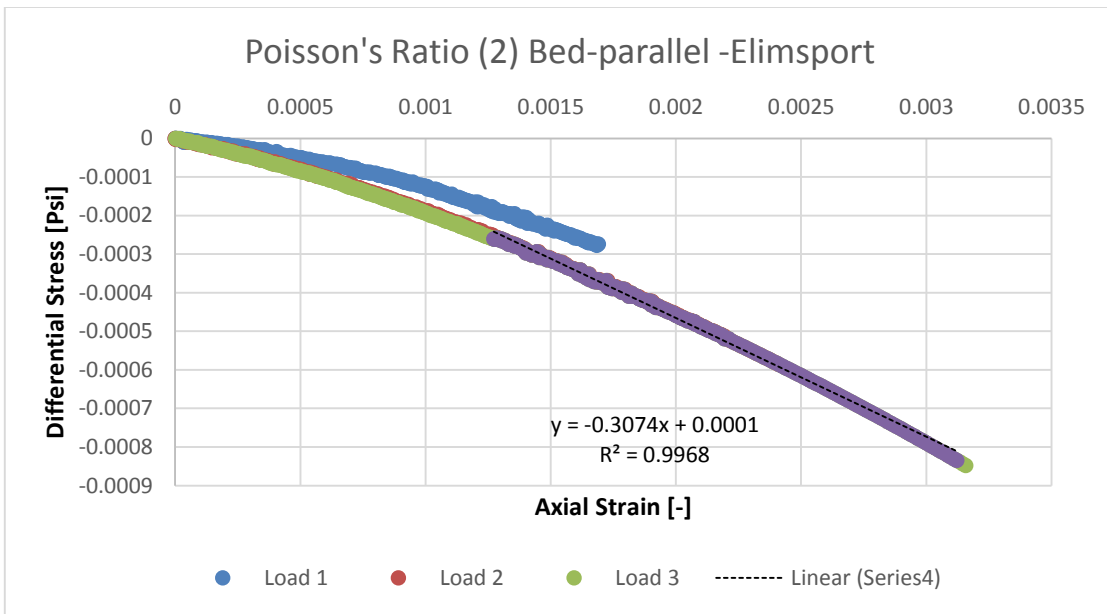
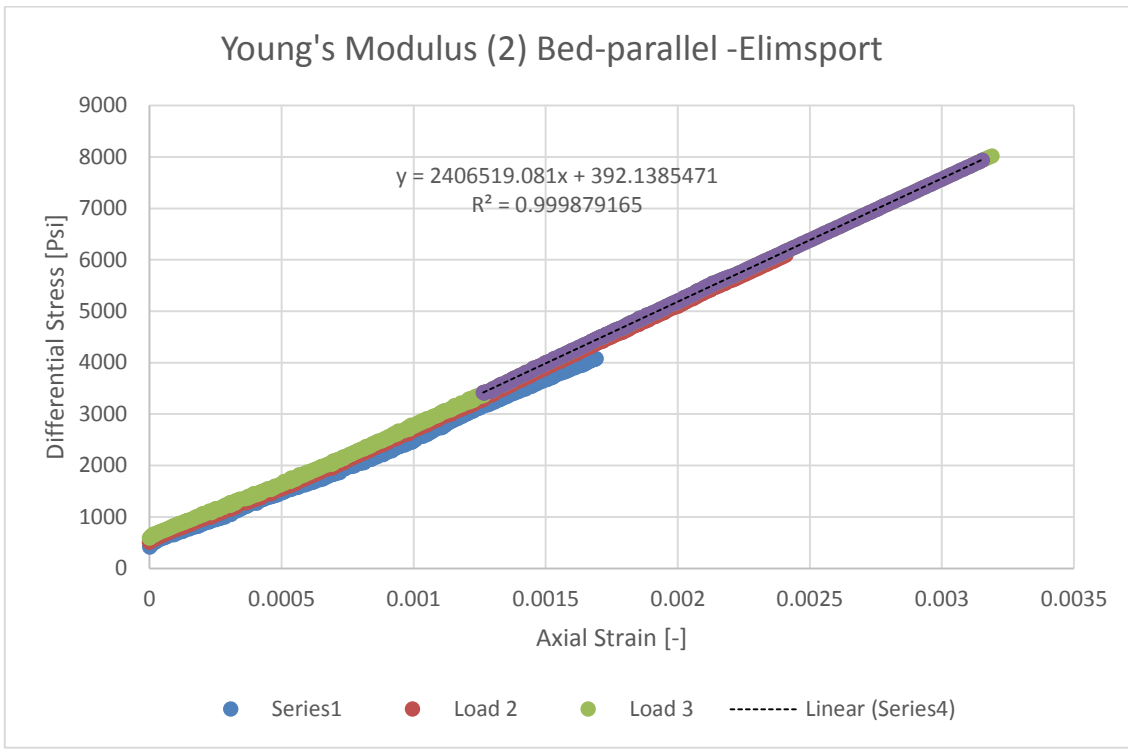
Young's Modulus (5) Bed-perpendicular -Elimsport

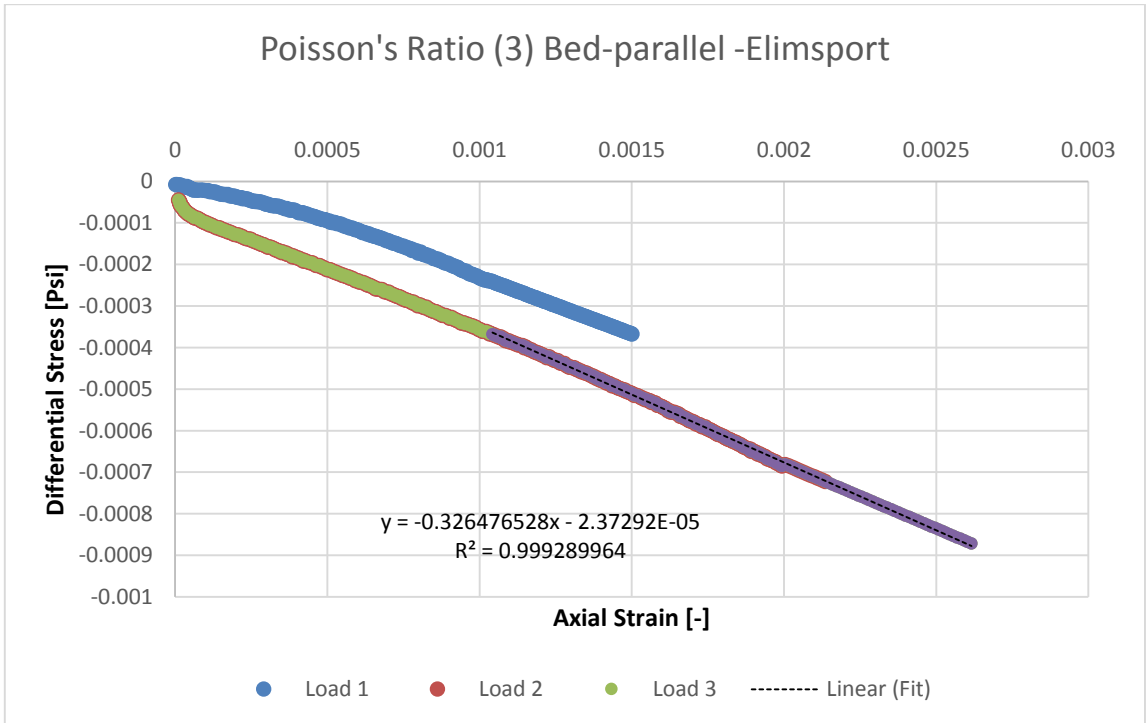
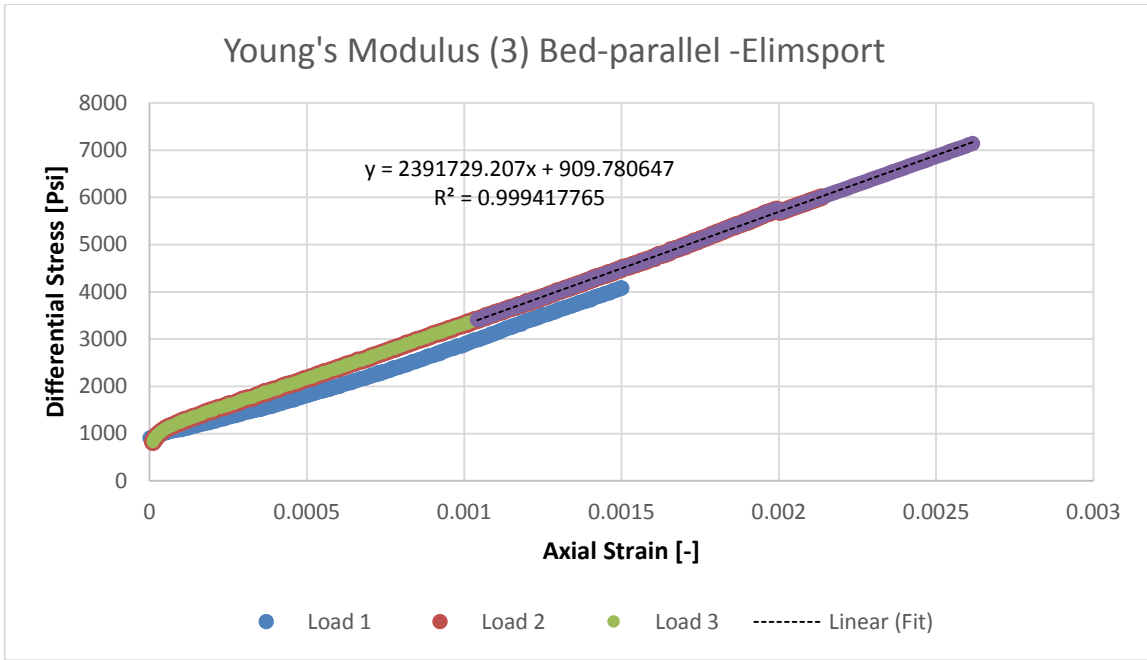


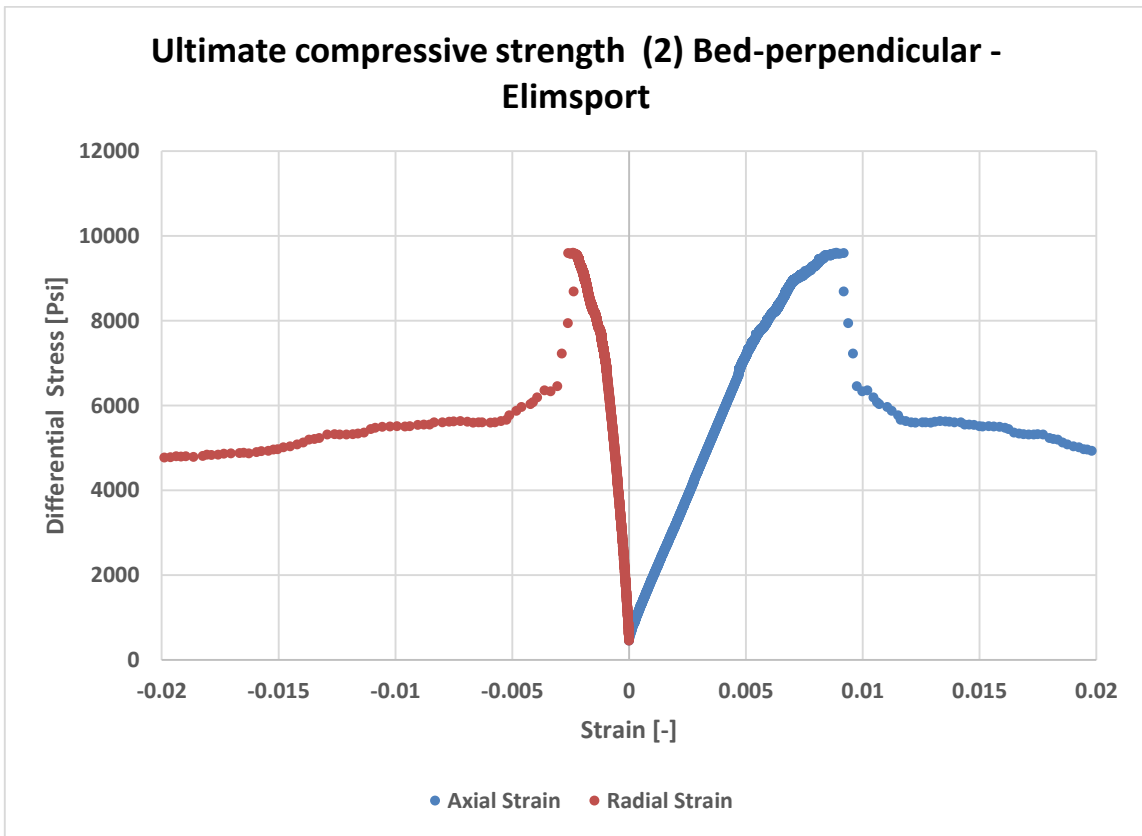
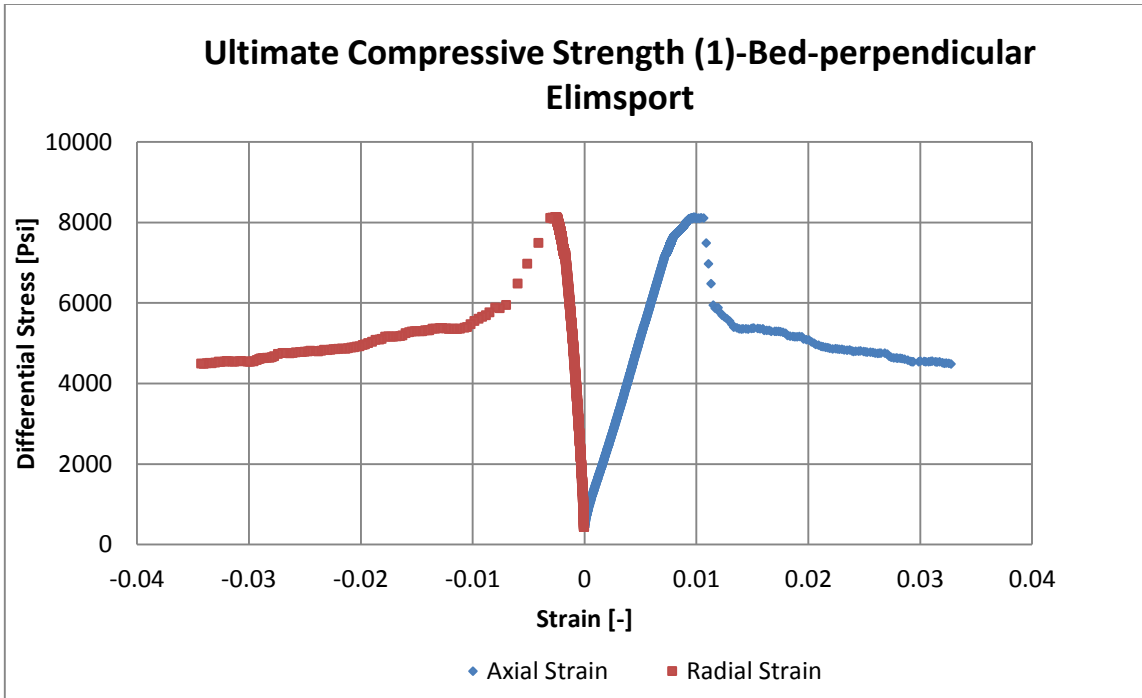
Poisson's Ratio (5) Bed-perpendicular -Elimsport

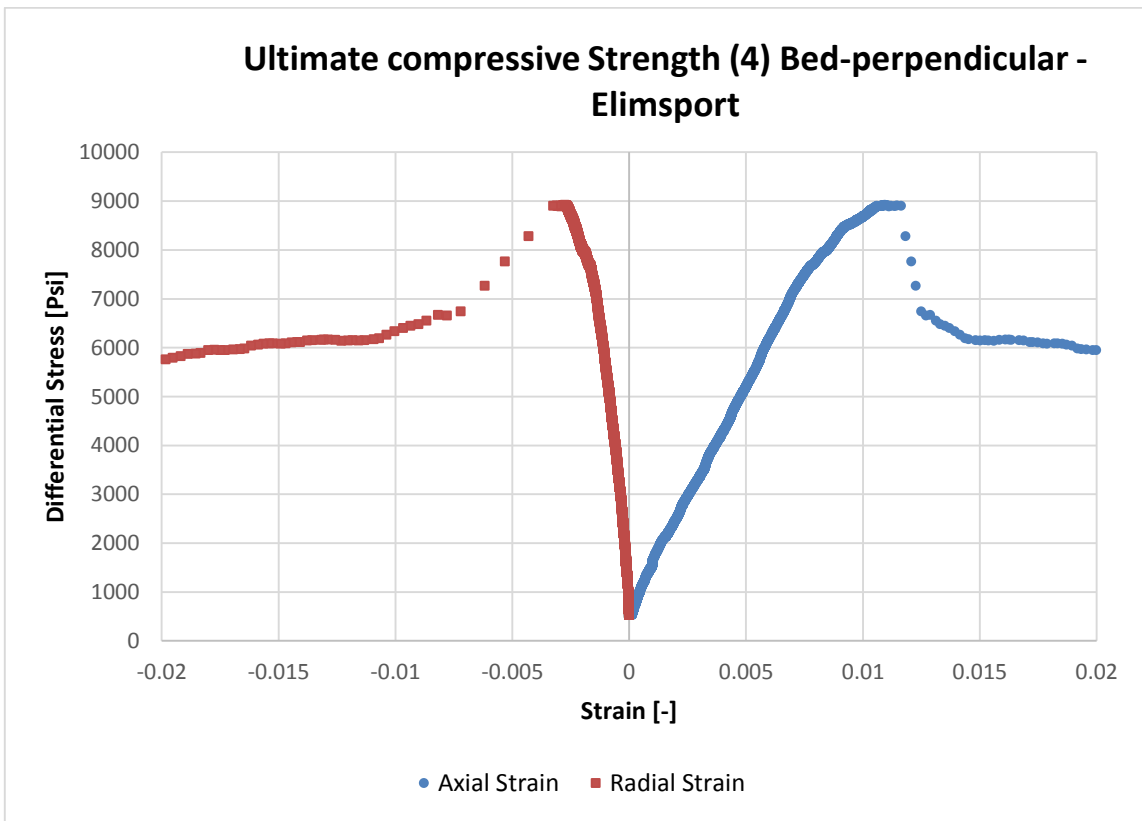
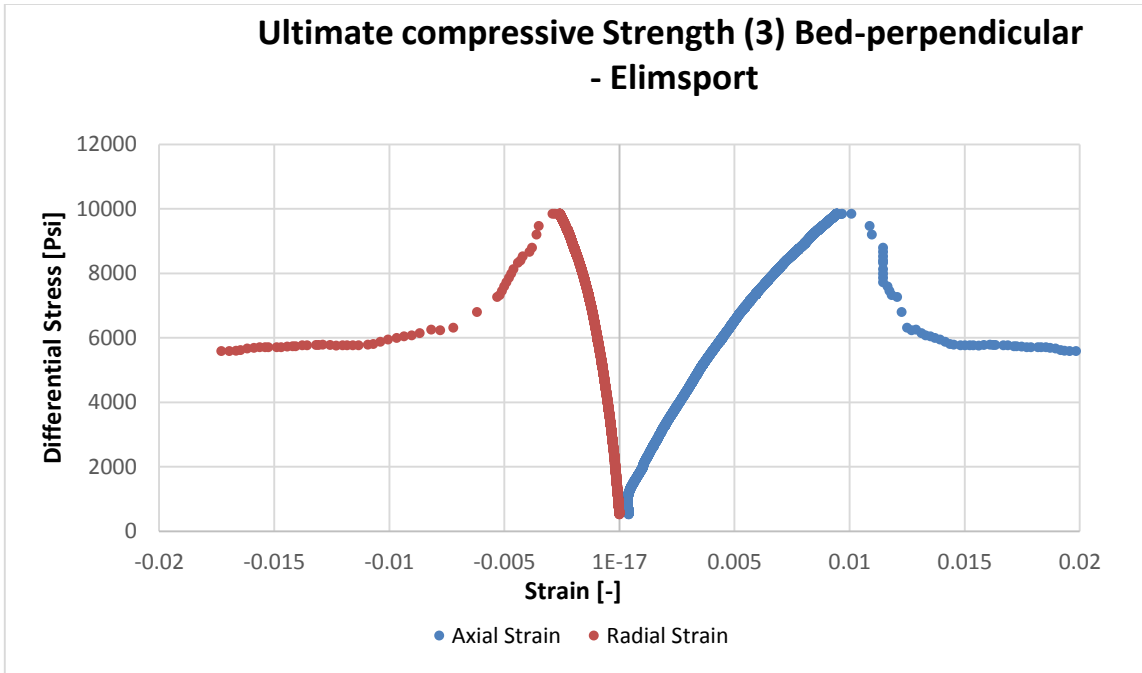




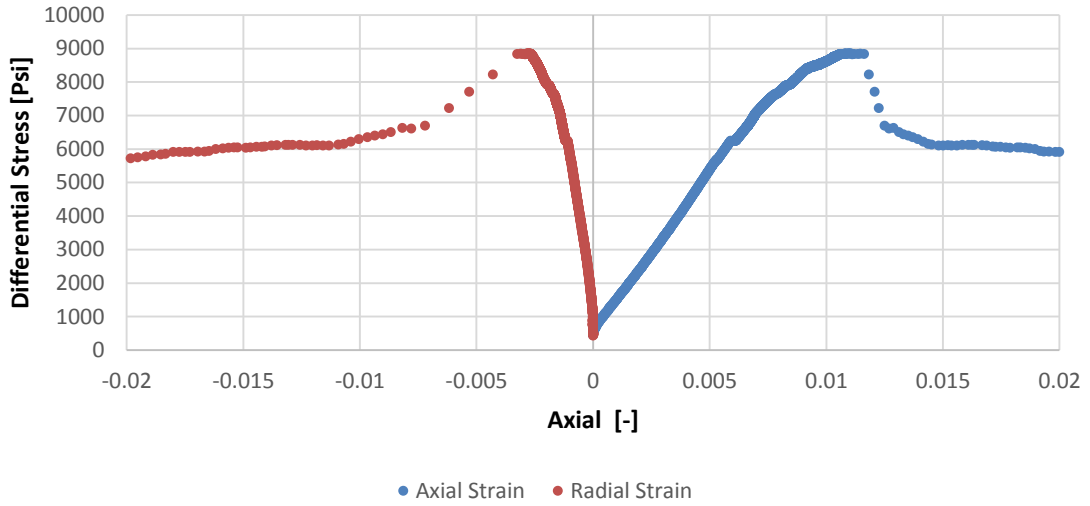




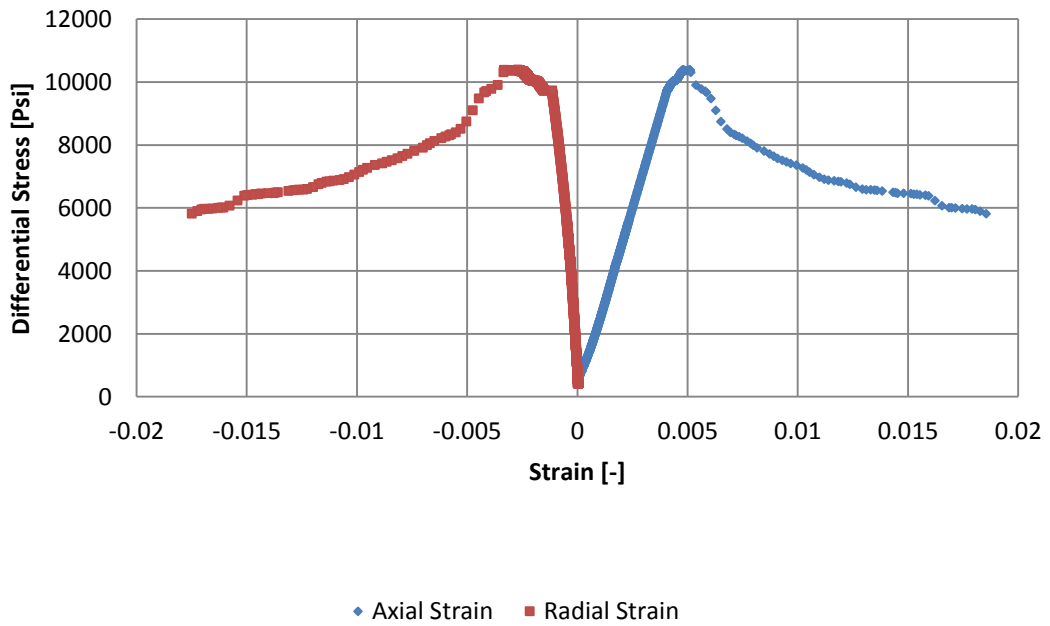




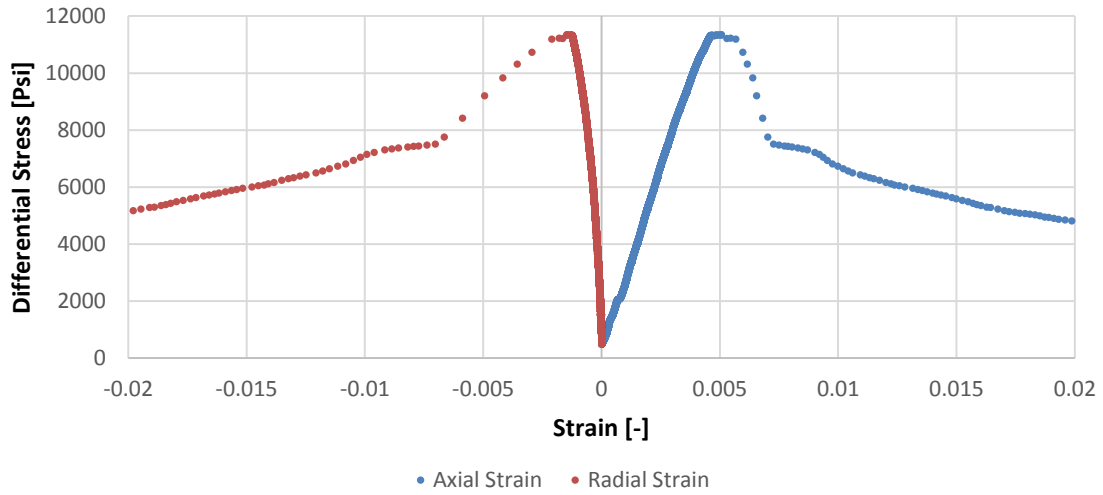
Ultimate Compressive Strength (5) Bed-perpendicular - Elimsport



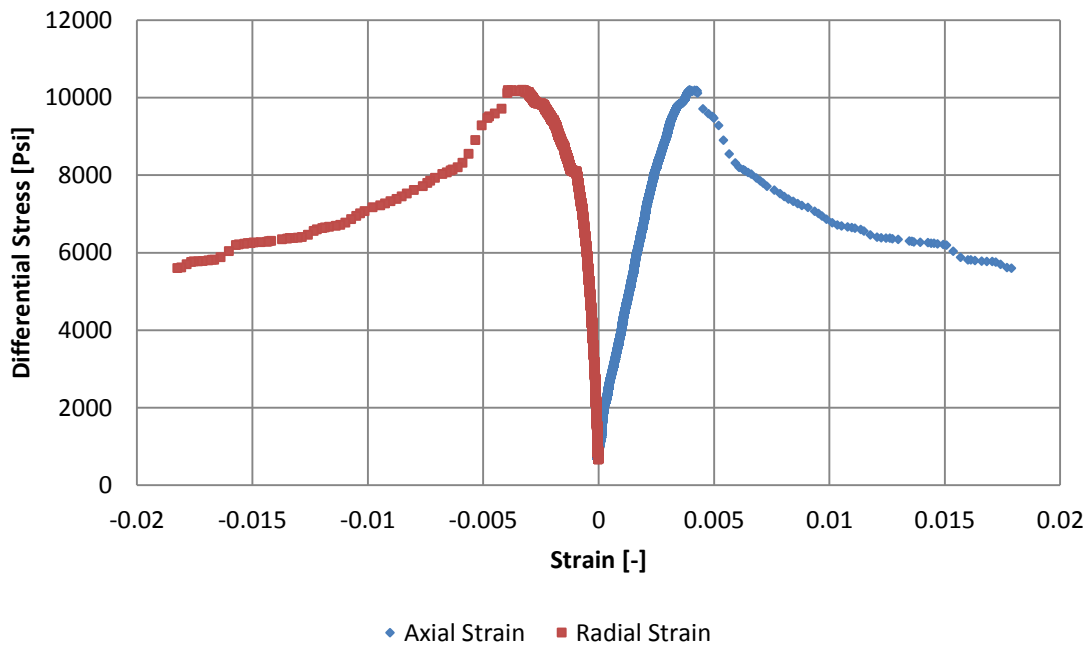
Ultimate compressive Strength (1) Bed-Parallel - Elimsport



Ultimate compressive Strength (2) Bed-parallel - Elimsport

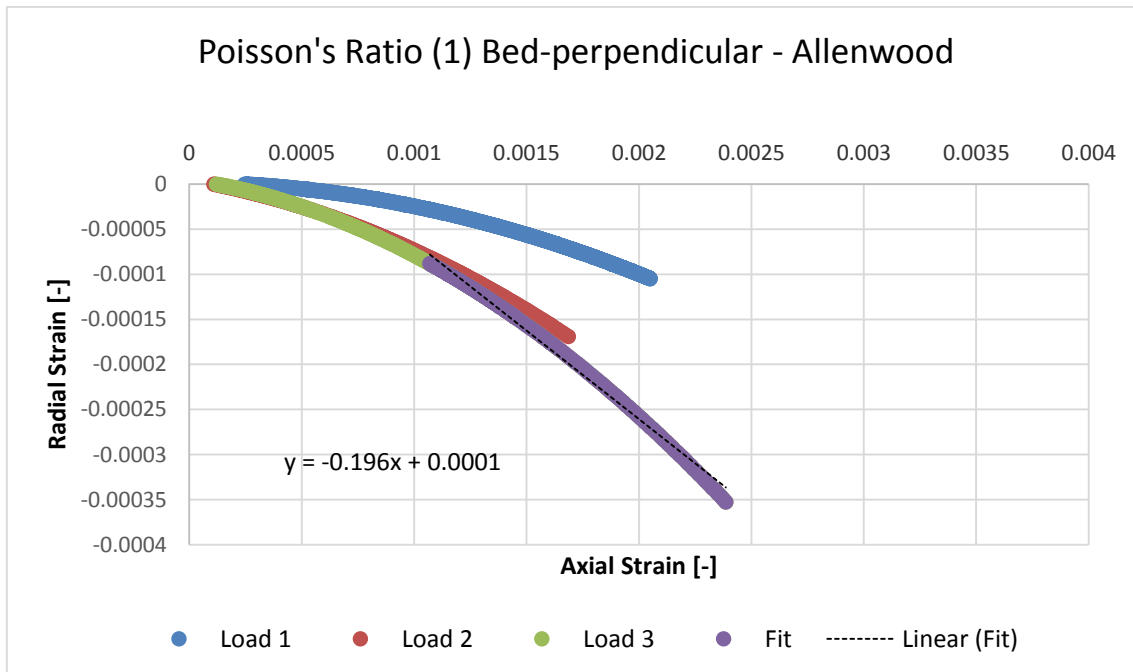
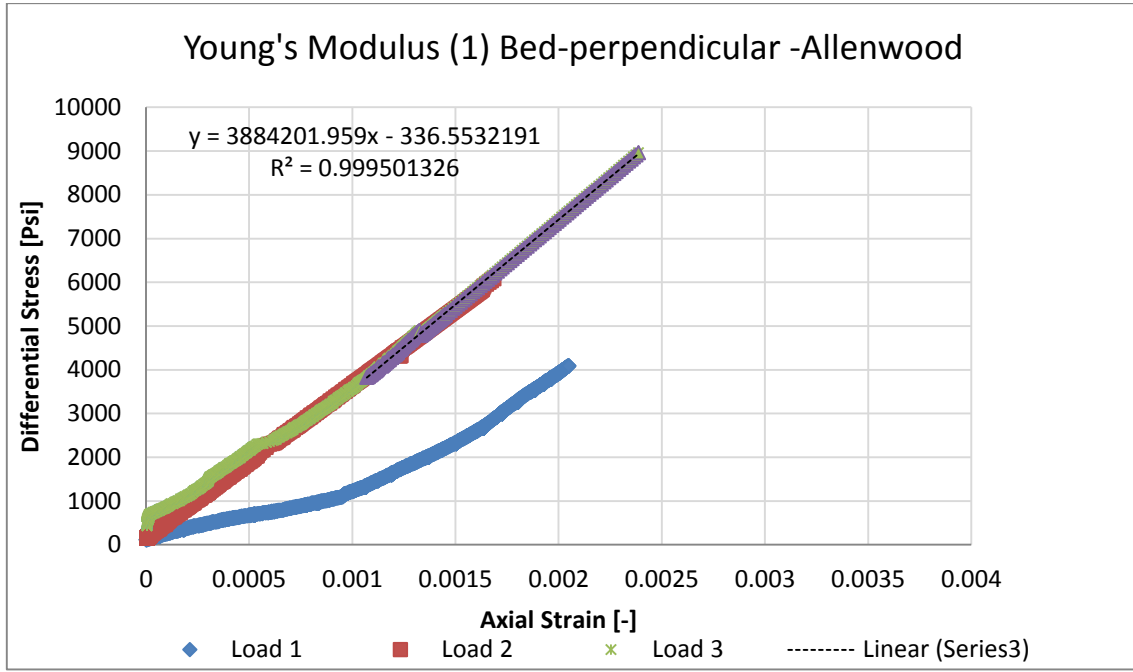


Ultimate compressive Strength (3) Bed-parallel - Elimsport

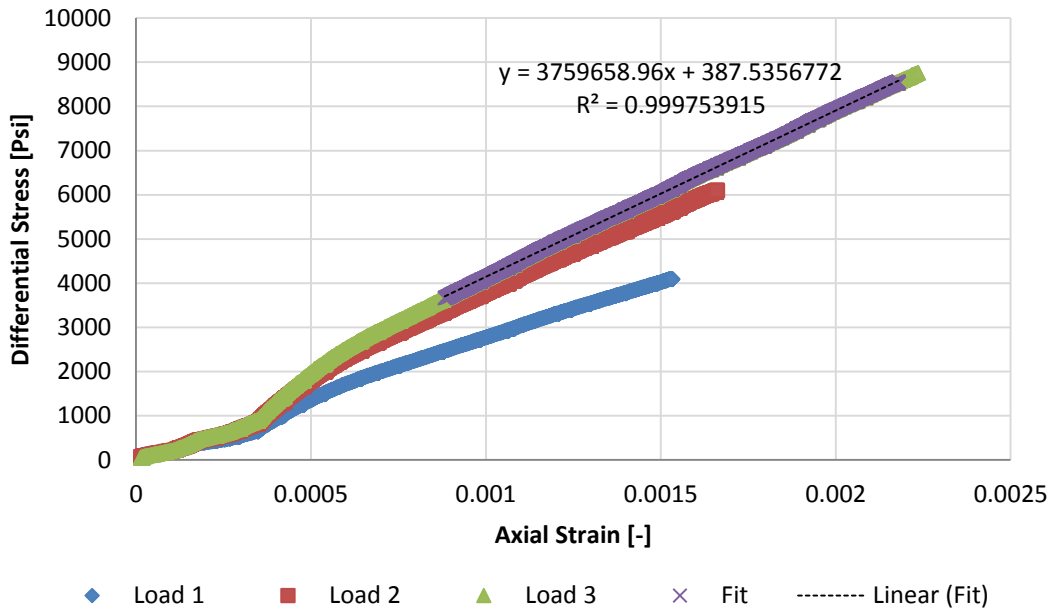


APPENDIX B

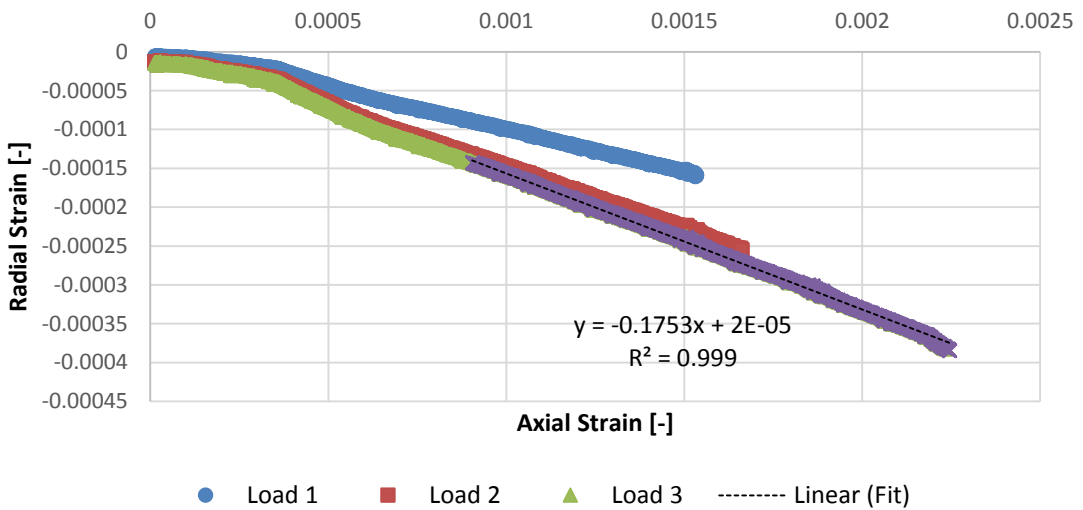
Allenwood Results



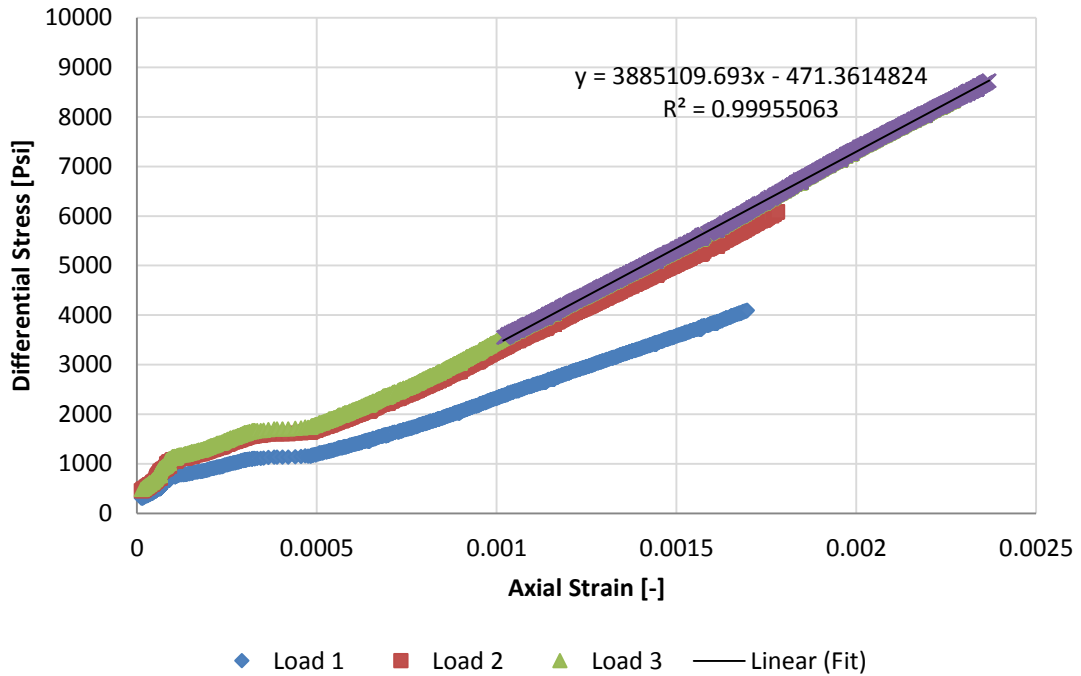
Young's Modulus (2) Bed-perpendicular -Allenwood



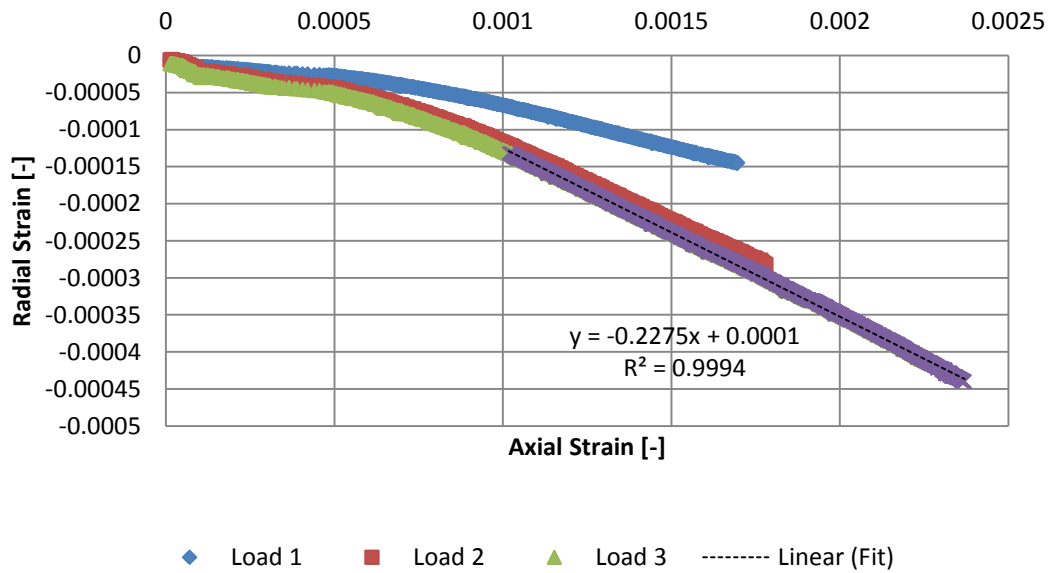
Poisson's Ratio (2) Bed-perpendicular - Allenwood

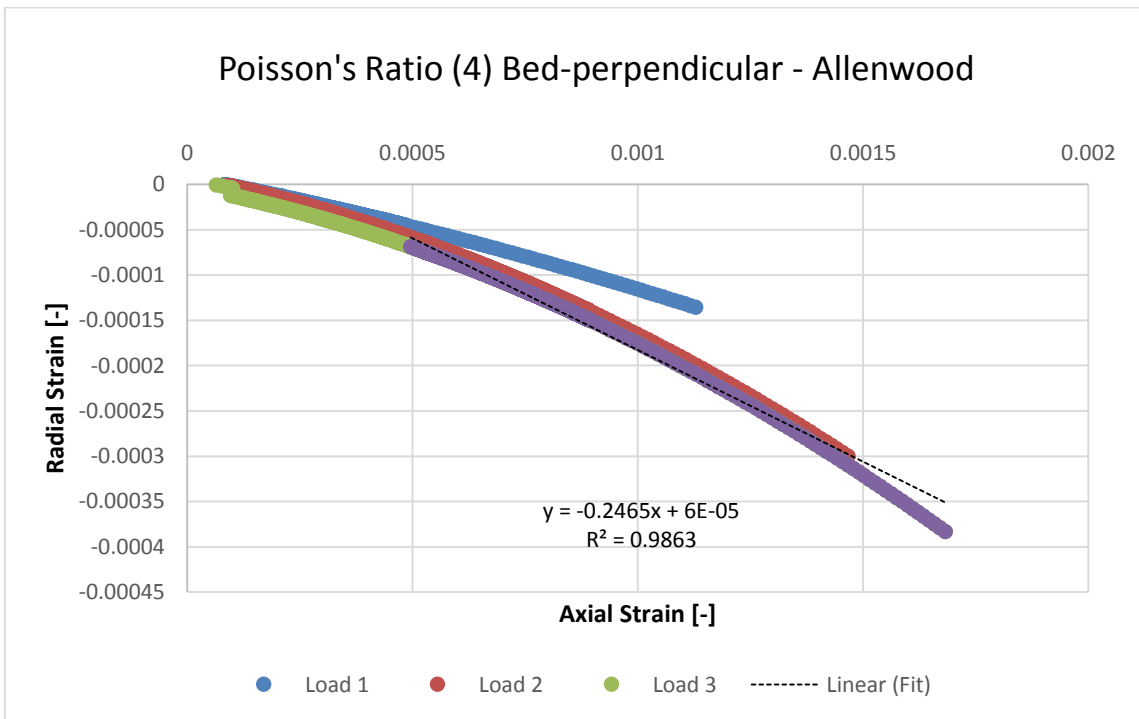
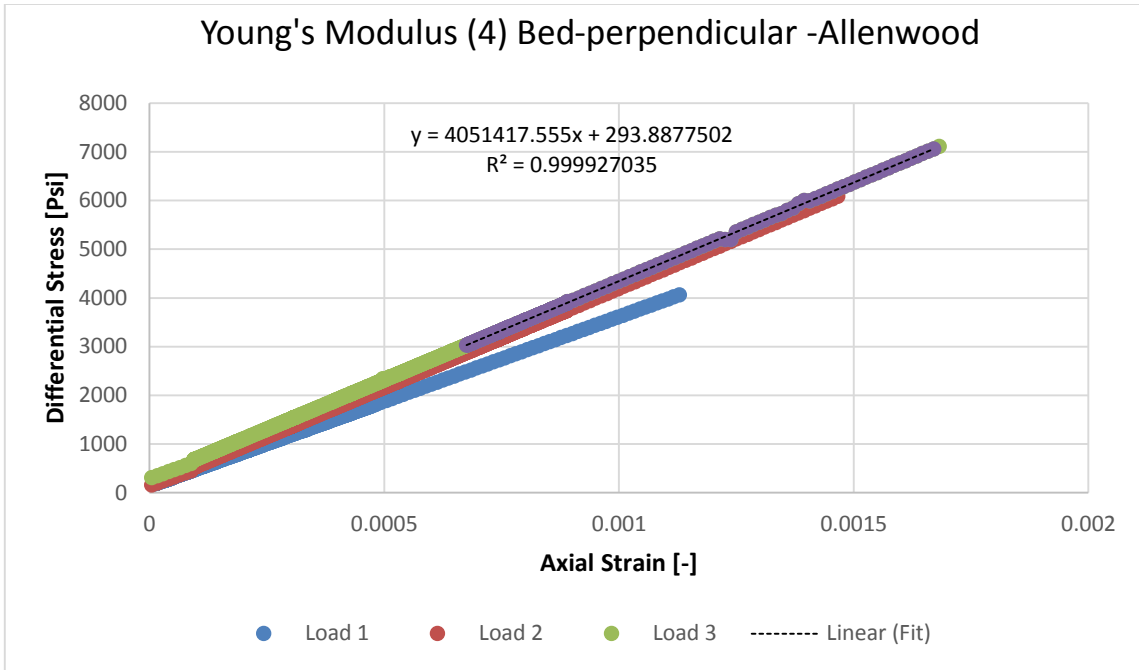


Young's Modulus (3) Bed-perpendicular -Allenwood

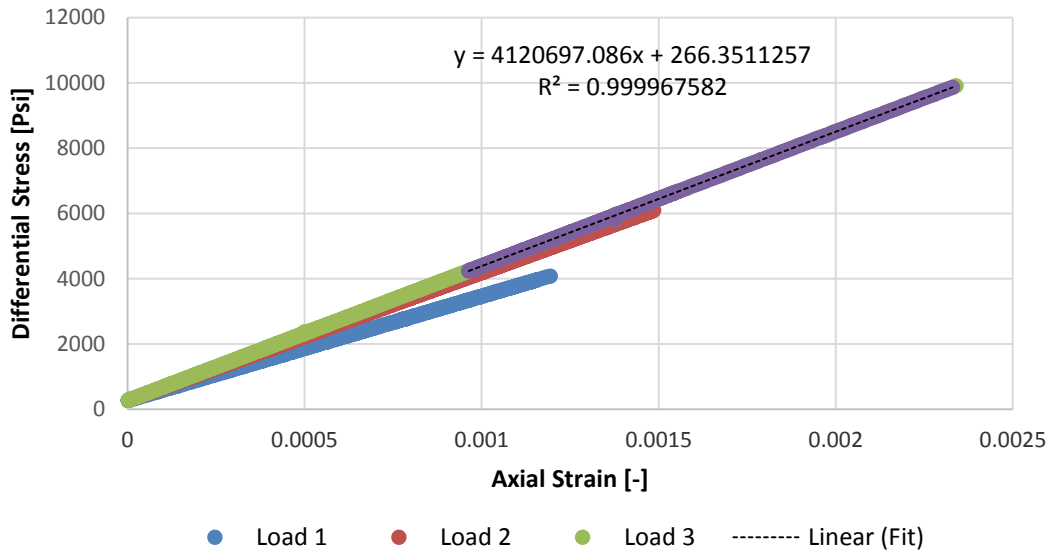


Poisson's Ratio (3) Bed-perpendicular - Allenwood

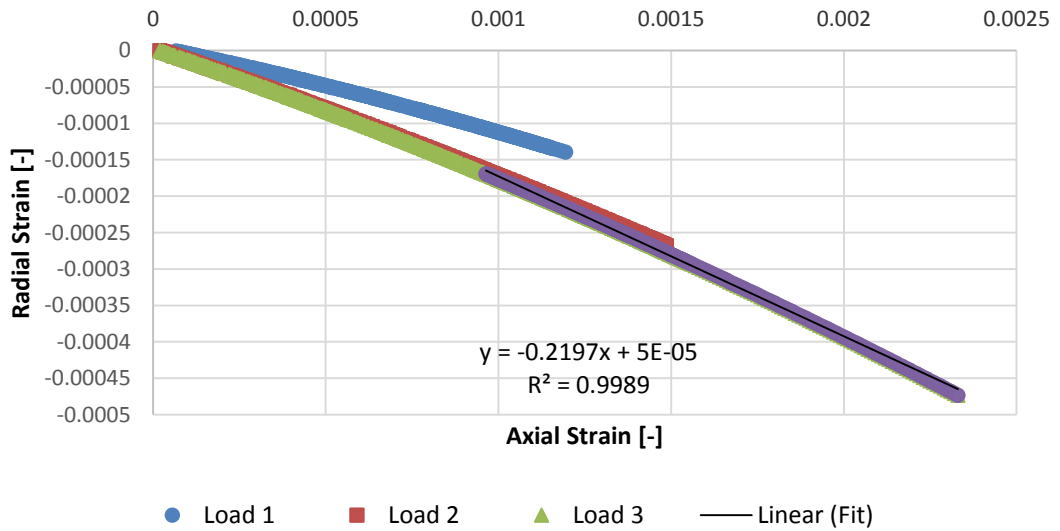


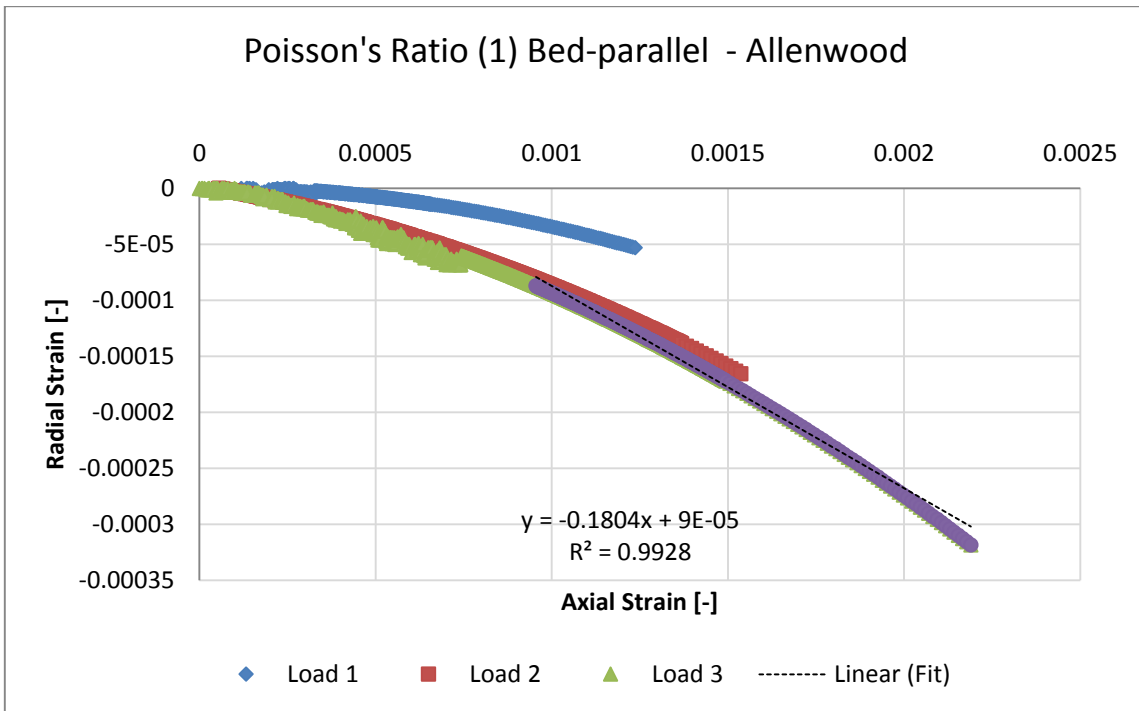
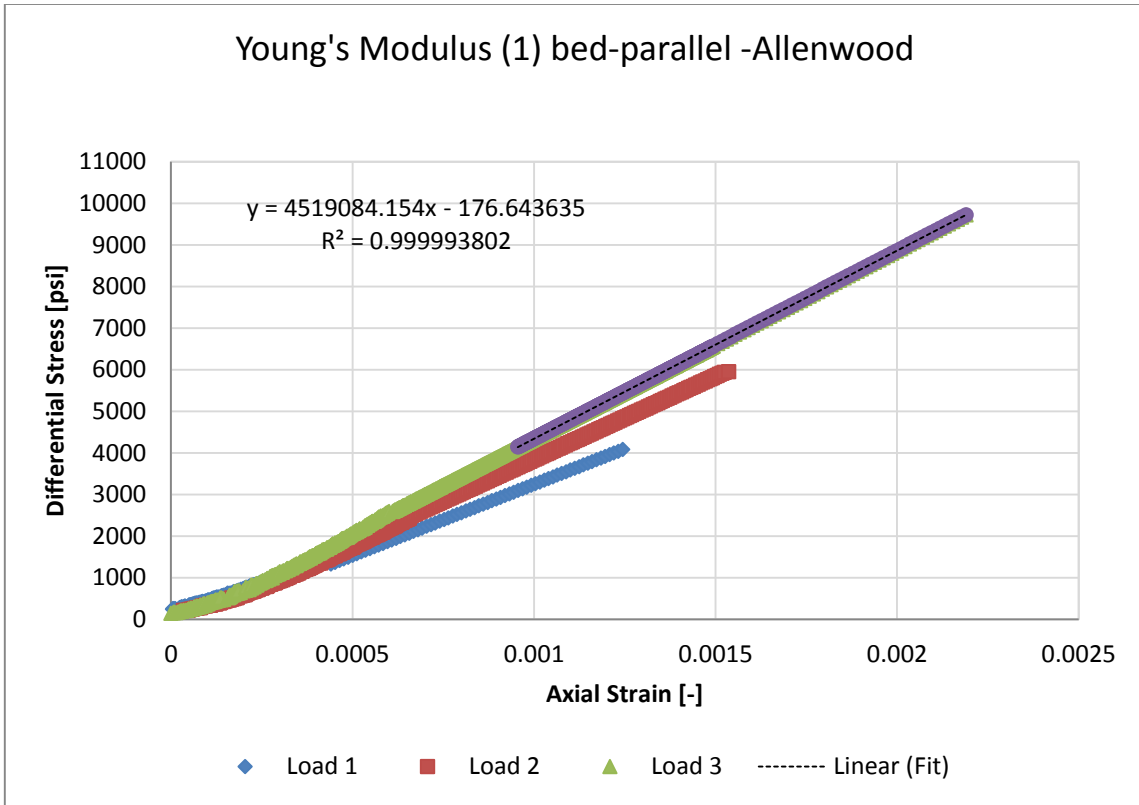


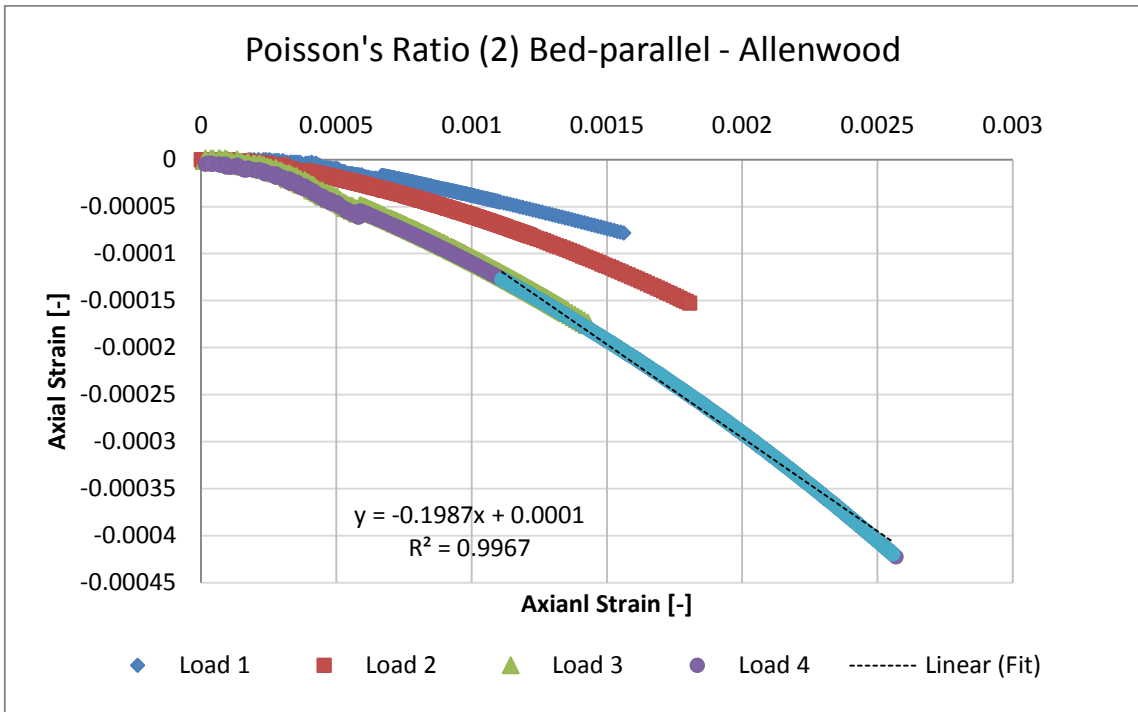
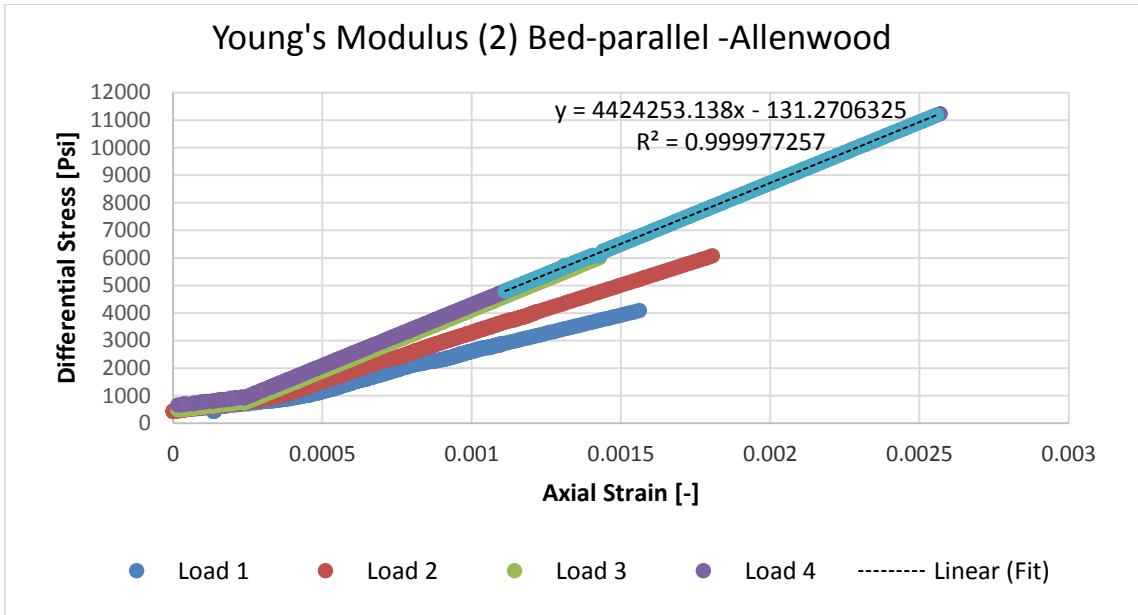
Young's Modulus (5) Bed-perpendicular -Allenwood

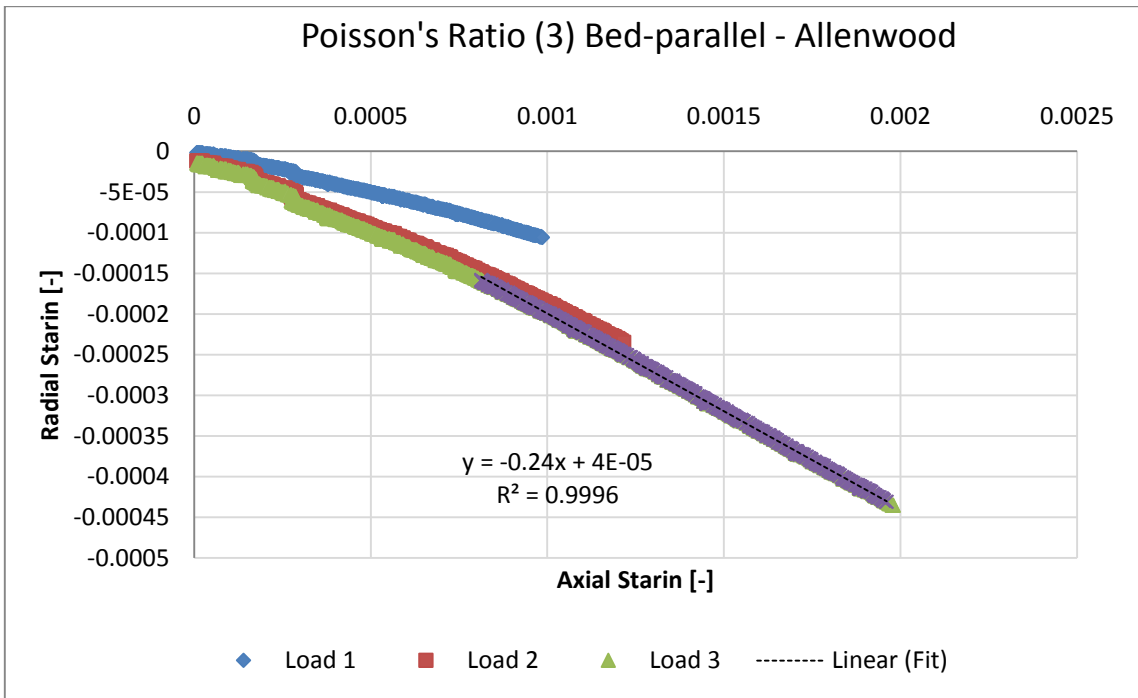
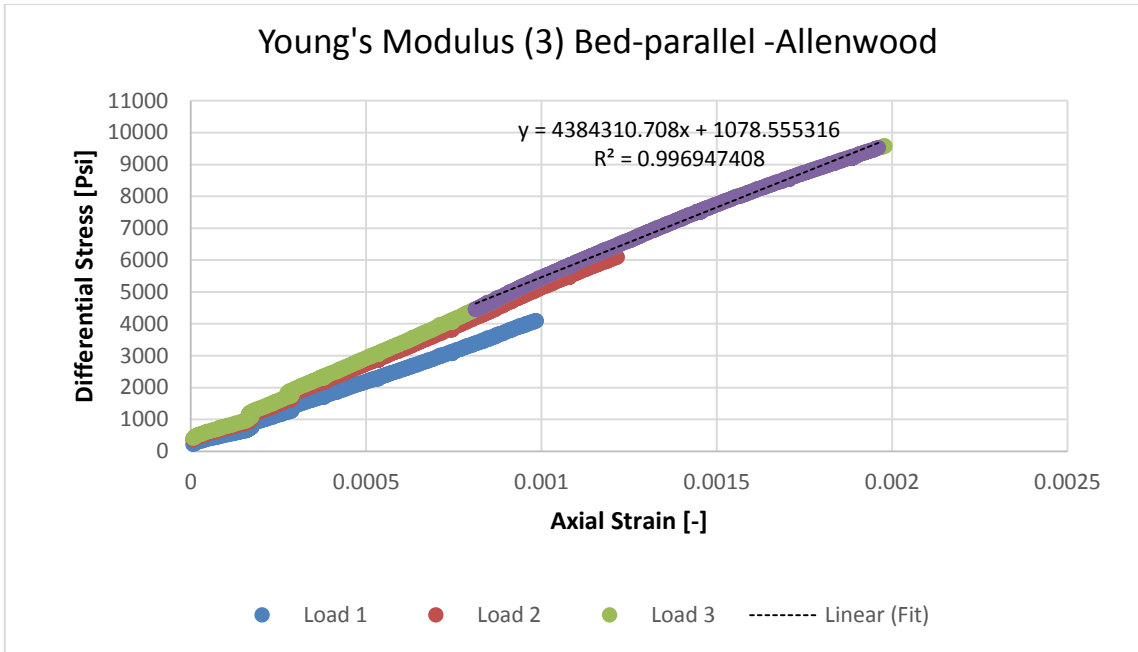


Poisson's Ratio (5) Bed-perpendicular - Allenwood

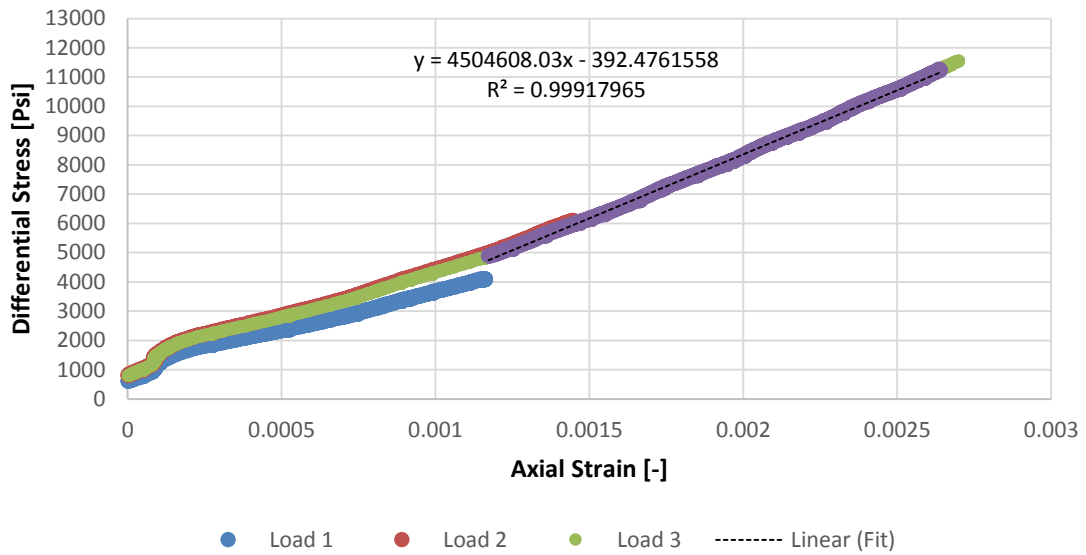




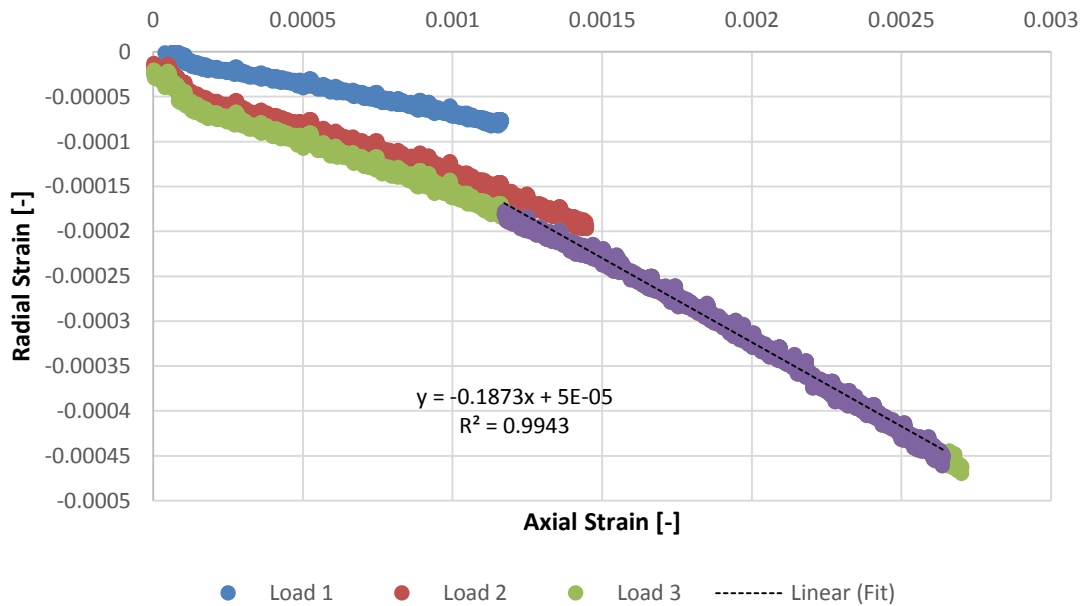




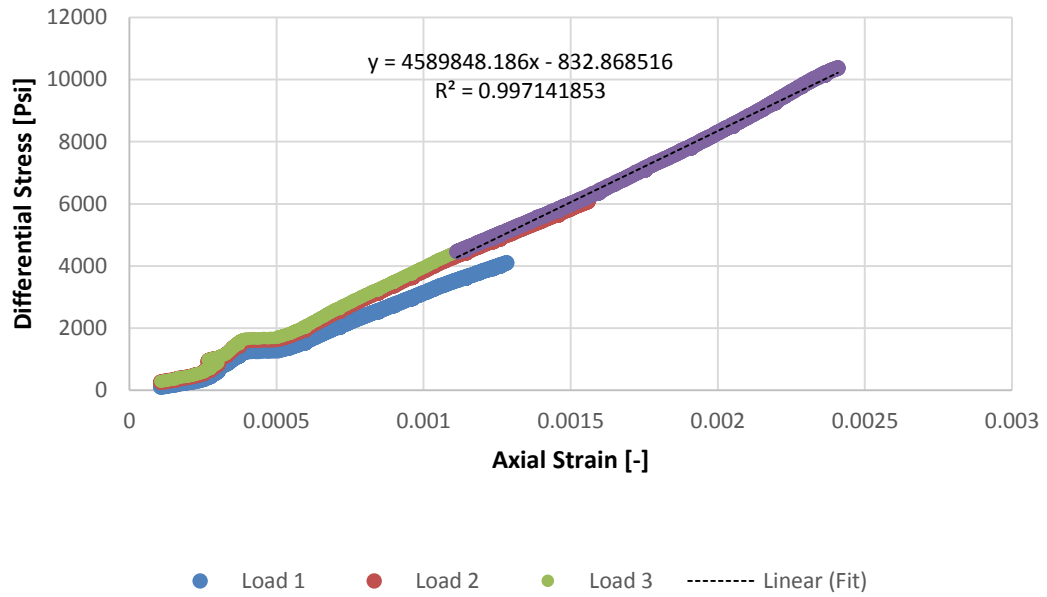
Young's Modulus (4) Bed-parallel -Allenwood



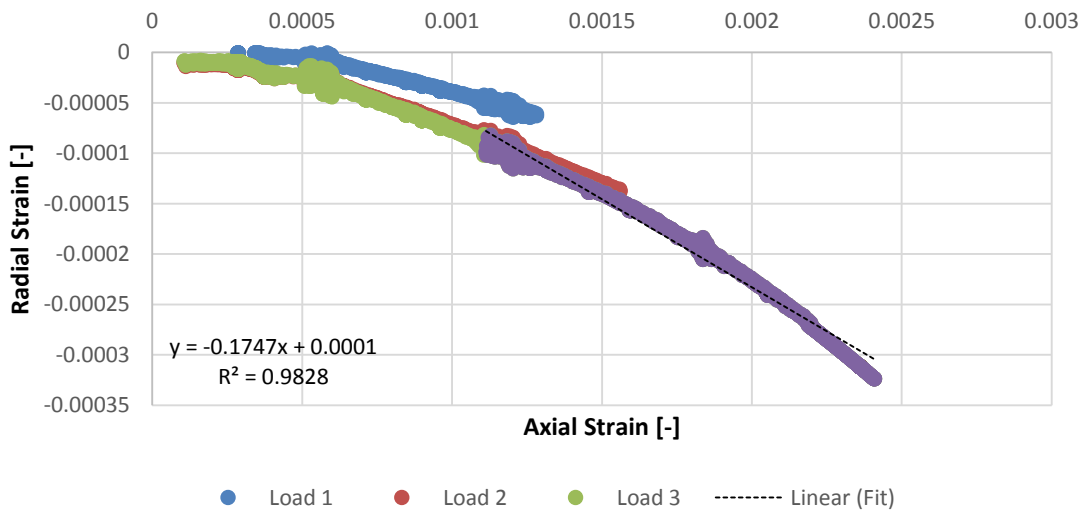
Poisson's Ratio (4) Bed-parallel - Allenwood

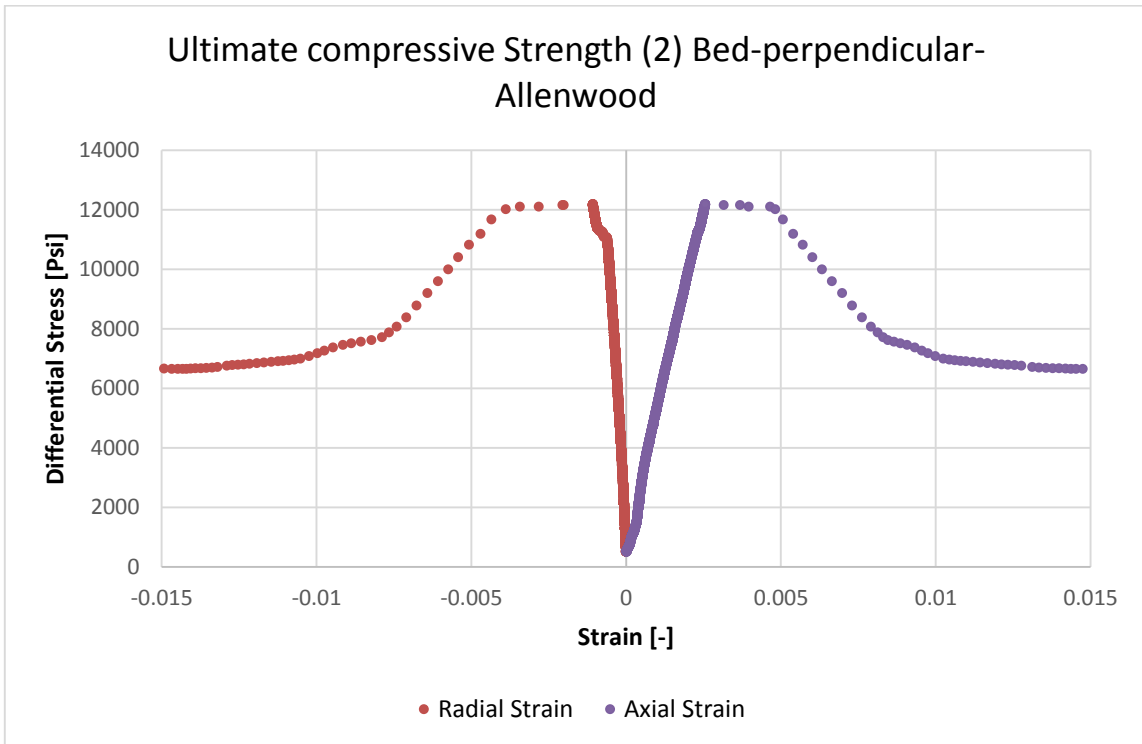
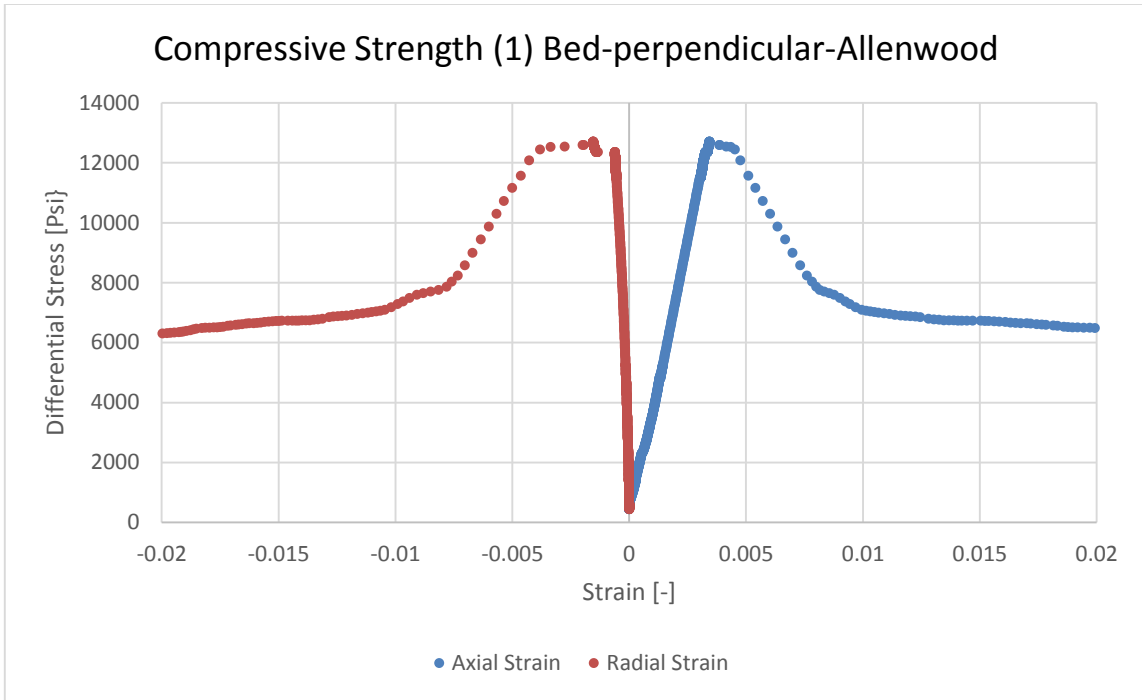


Young's Modulus (5) Bed-parallel -Allenwood

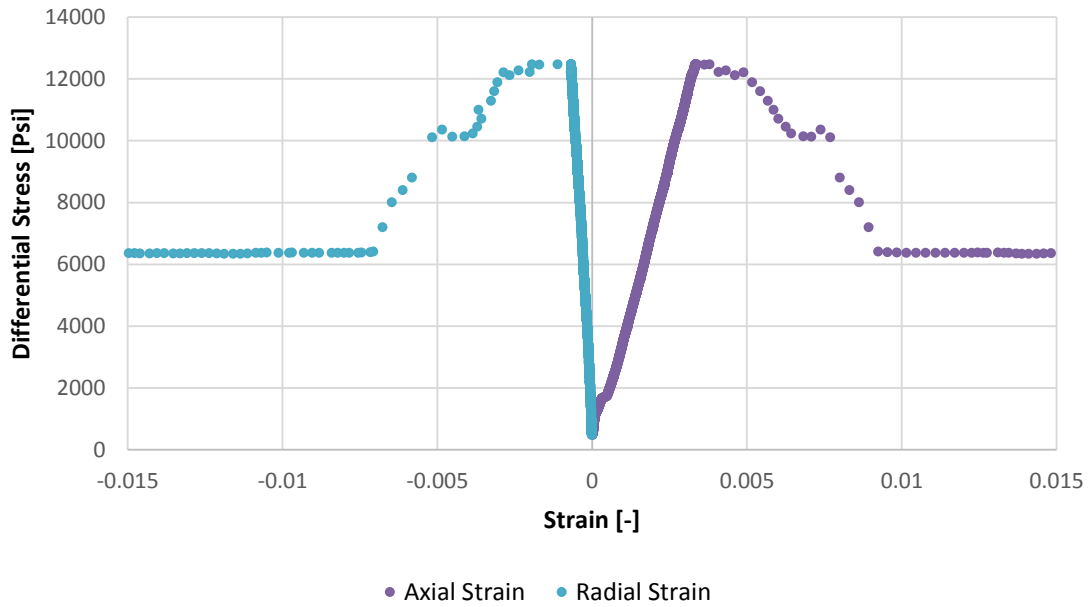


Poisson's Ratio (5) Bed-parallel - Allenwood

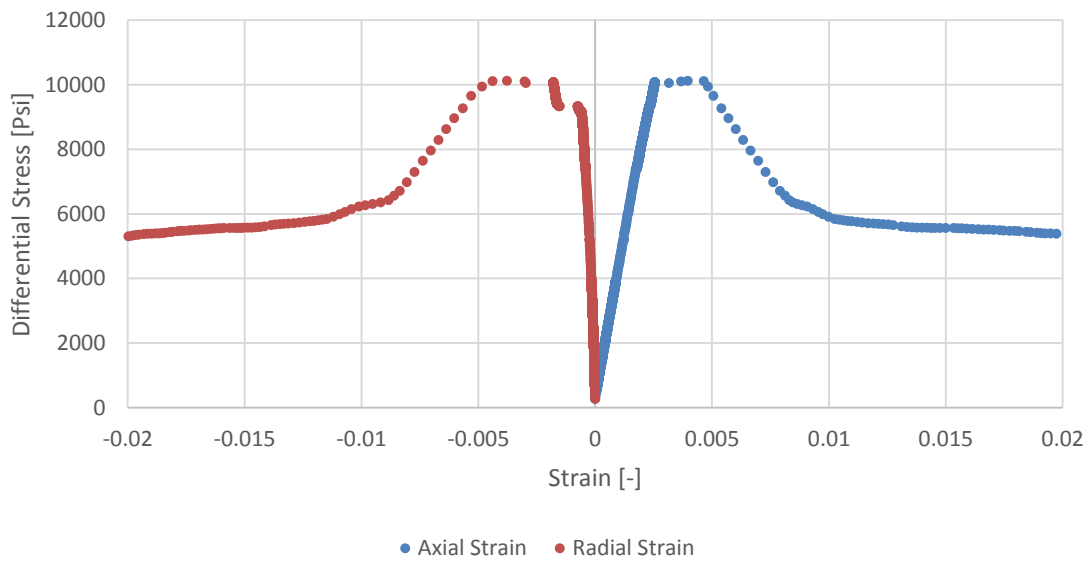


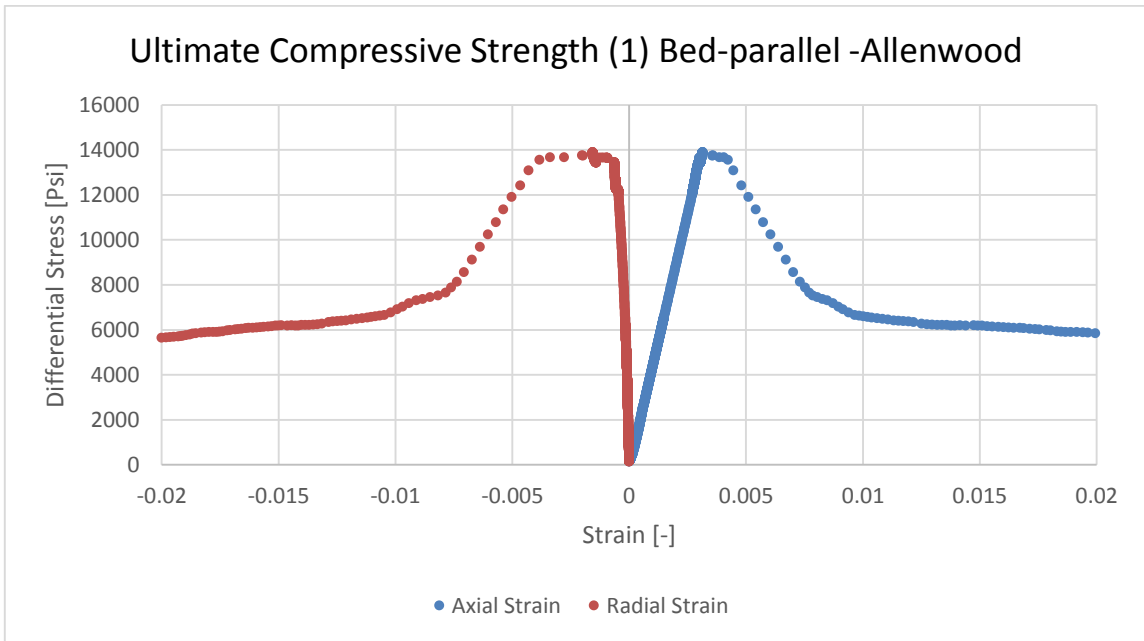
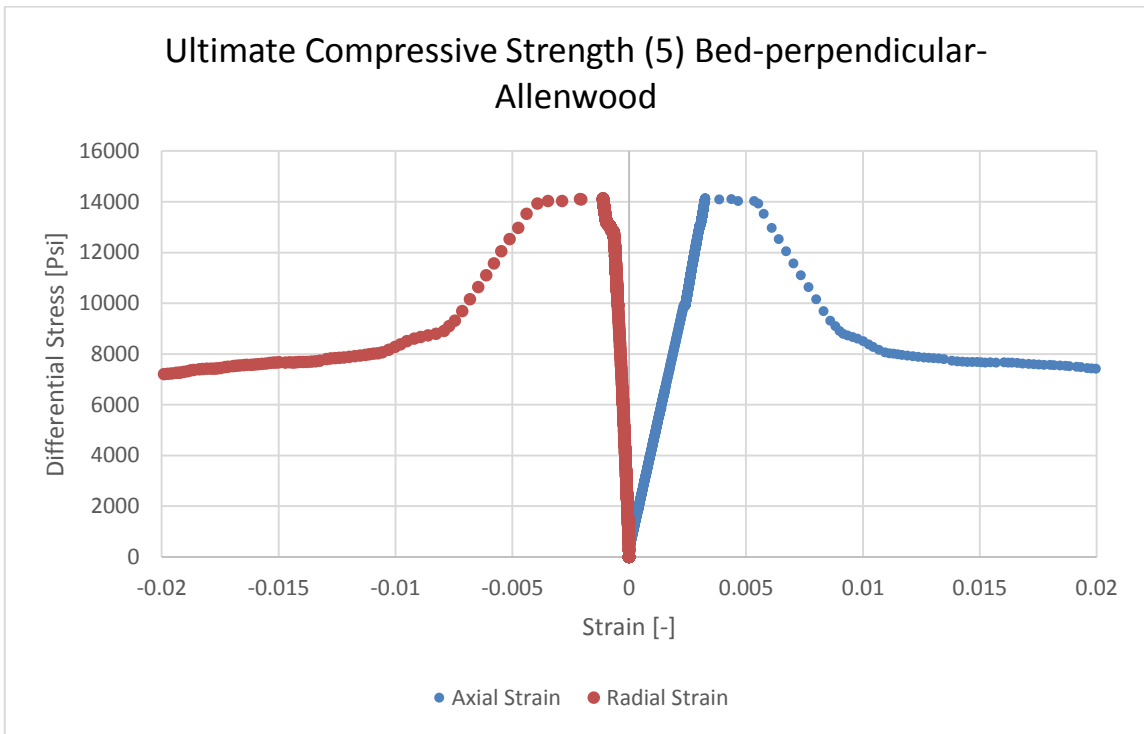


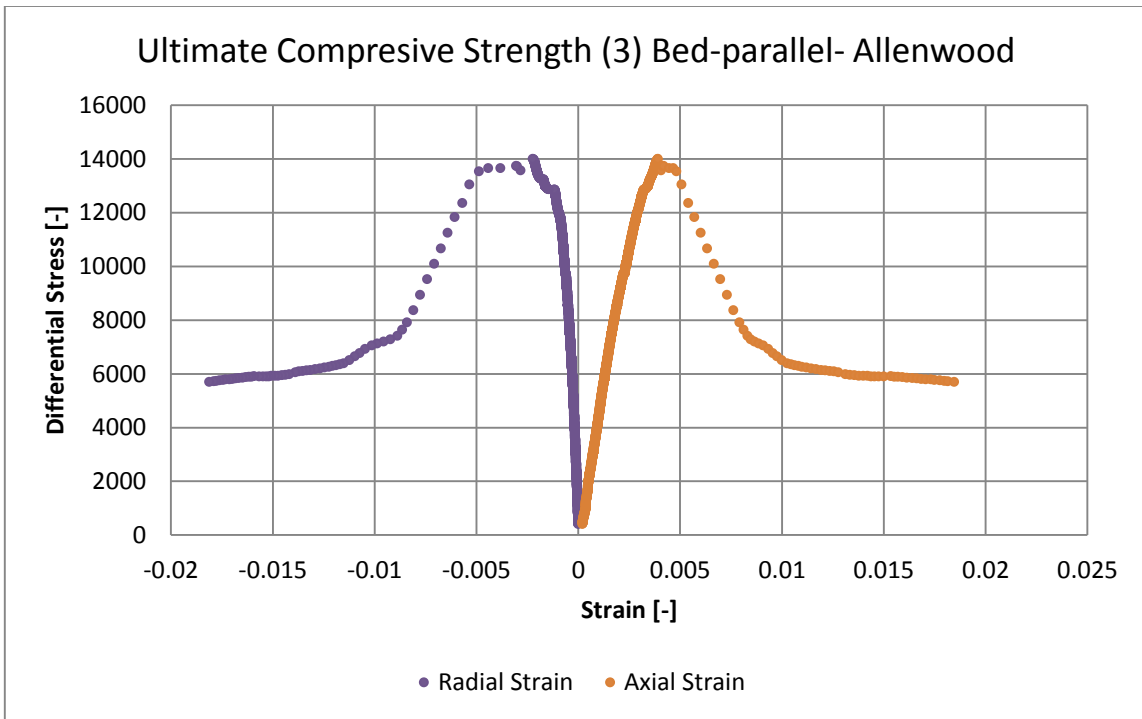
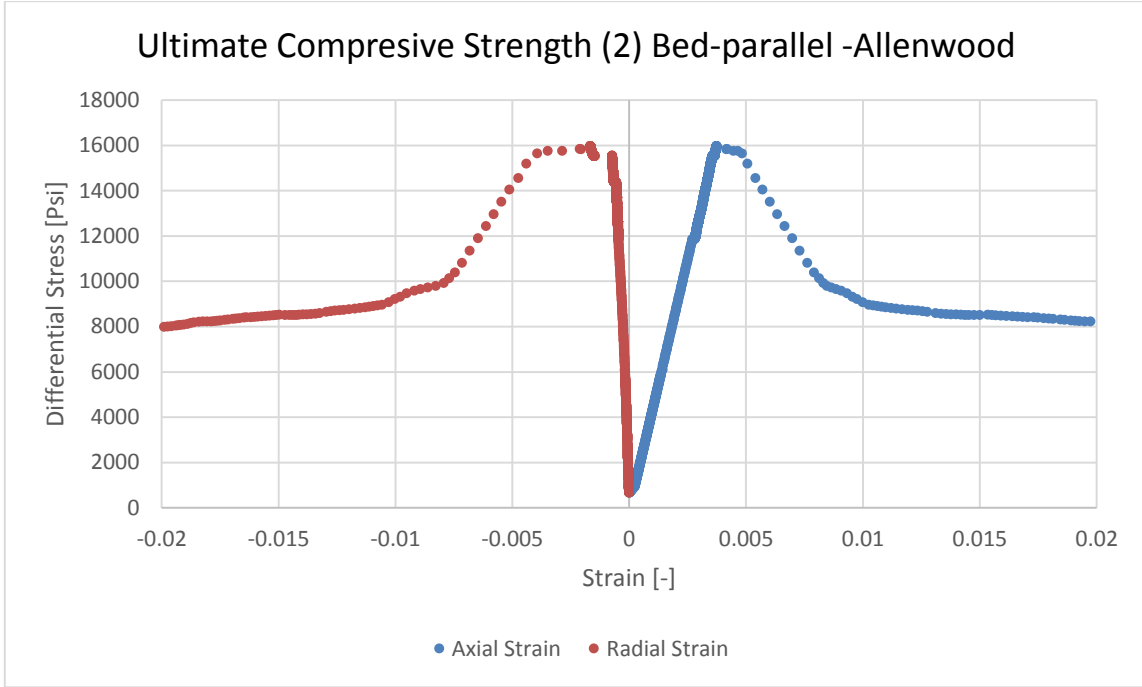
Ultimate compressive Strength (3) bed-perpendicular-Allenwood



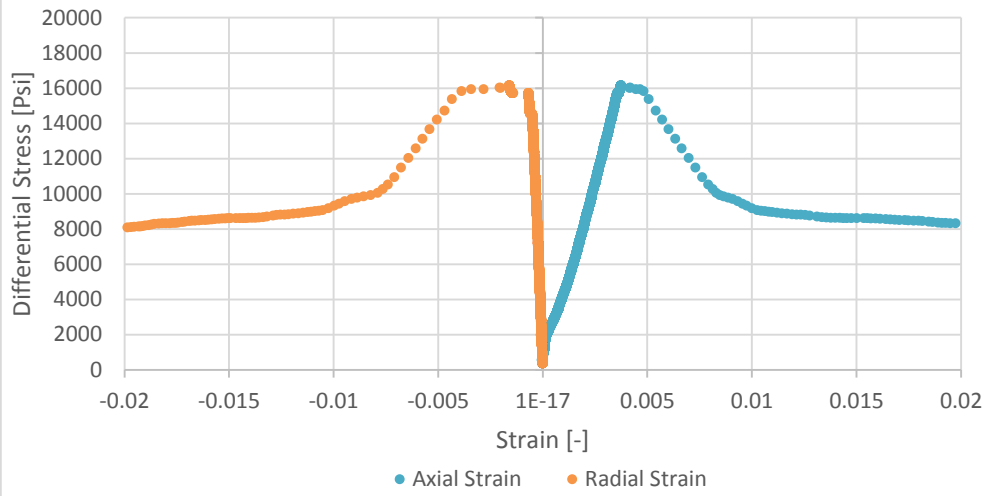
Ultimate Compressive Strength (4) Bed-perpendicular-Allenwood







Ultimate Compressive Strength (4) Bed-parallel- Allenwood



Ultimate compressive strength (5) Bed-parallel -Allenwood

